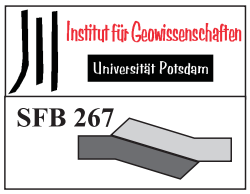

Universität Potsdam
Institut für Geowissenschaften

DISSERTATION

Subduction zone wave guides: Deciphering slab structure using intraslab seismicity at the Chile-Peru subduction zone

von

Sebastian Martin

Betreuer

Prof. Dr. F. Scherbaum

Dr. A. Rietbrock

Jahr 2005

Contents

Zusammenfassung

Subduktionszonen sind bis in große Tiefen von intensiver Erdbebentätigkeit geprägt. Die Erdbebenquellen befinden sich in der subduzierten Lithosphäre (*Slab*), ihr Wellenfeld wird deshalb stark von der internen Slab-Struktur beeinflusst. Eine Schicht mit reduzierter seismischer Geschwindigkeit im oberen Bereich der Platte kann als Wellenleiter für diese Signale fungieren. In der nur wenige Kilometer dicken Schicht entstehen sogenannte *geführte Wellen*, die in Teilen des *Forearc* beobachtet werden. Diese Phasen bergen wertvolle Informationen über die Struktur nahe der Slab-Oberfläche, wie zum Beispiel Dicke der Schichtung, Herdlokationen und vor allem Tiefe und Art mineralogischer Umsetzungen.

Die Beobachtungen stammen von mitteltiefen Beben (70 km - 300 km) im Untersuchungsgebiet in Nord-Chile (23° - 20.5°S) und wurden im Rahmen des Sonderforschungsbereich 267 'Deformationsprozesse in den Anden' aufgezeichnet. Stationen in einem Streifen um 69°W, der sich parallel zum Streichen der Subduktionszone erstreckt, zeigen niederfrequente Ersteinsätze ($\sim$ 2 Hz), denen teilweise höherfrequente Phasen folgen.

Mit Hilfe eines 2-dimensionalen Finite-Differenzen-Algorithmus werden die P-SV Wellenausbreitung simuliert, und die Beobachtungen erklärt. Zentrale Fragestellungen zu Wellenleitern in Subduktionszonen werden untersucht: Es werden zwei Mechanismen, die das Auskoppeln seismischer Energie aus dem Wellenleiter ermöglichen beschrieben - eine Grundvoraussetzung für das Auftreten von geführten Wellen in großen Entfernungen vom Wellenleiter (bis zu 100 km). Des weiteren werden Stärken und Grenzen der Analyse von geführten Wellen erörtert.

Die Spektren der geführten Wellenzüge erweisen sich als robuste Messgröße, um die Charakteristika des Wellenleiters zu bestimmt. Struktur des Wellenleiters und Quellpositionen können so für festgelegte Quell-Empfänger-Geometrien abgeleitet werden. Die Peak-Frequenz der Grundmode wird durch eine Kombination aus Dicke der Schicht und Geschwindigkeitskontrast bestimmt. Die Stärke der Anregung der Grundmode und höherer Moden lässt auf die Lage und Orientierung der Erdbebenquelle relativ zur Schicht schließen. Geschwindigkeitskontrast, Schichtdicke und Quellposition sind von herausragender Bedeutung, um mineralogische Interpretationen des Wellenleiters zu überprüfen.

Aufbauend auf die Simulationen werden die Beobachtungen interpretiert und Auskunft über die Struktur der Chile-Peru Subduktionszone erhalten: Eine dünne Schicht an der Slab-Oberfläche (durchschnittlich 2 km dick) trägt geringere seismische Geschwindigkeiten als der umgebende Mantel und fungiert als Wellenleiter für intra-platten Ereignisse in Tiefen von 100 bis mindestens 160 km. Ereignisse, die geführte Wellen hervorrufen, liegen in dieser Schicht oder direkt darunter im subduzierten Mantel. Um zu den Stationen nahe 69°W in der *Forearc*-Region zu gelangen, entkoppelt ein Teil der geführten Wellen in einer Tiefe von circa 100 km aus der Niedergeschwindigkeitsschicht. Die Krümmung des Slab erlaubt das Austreten der Wellen und nimmt auch Einfluss auf die Pulsformen.

Der Wellenleiter in der Chile-Peru Subduktionszone ergibt sich als unregelmäßige Schicht mit reduzierter seismischer Geschwindigkeit, in der geführte Wellen entstehen, in unterschiedlichen Tiefen wieder austreten, und an die freie Oberfläche gelangen. Die Beobachtungsgebiete befinden sich im *Forearc* und werden durch die Geometrie und Struktur der subduzierten Platte festgelegt.

Die nur wenige Kilometer dicke, seismisch langsame Schicht an der Oberfläche des Chile-Peru Slab legt nahe, dass die Unterkruste der subduzierten Platte bis in große Tiefen besteht und nicht vollständig eklogitisiert ist. Abgeleitete Schichtdicke, Geschwindigkeitskontrast (7 %) und Lage der Quellen sprechen für diese Erklärung.

Summary

Subduction zones are regions of intense earthquake activity up to great depth. Sources are located inside the subducting lithosphere and, as a consequence, seismic radiation from subduction zone earthquakes is strongly affected by the interior slab structure. The wave field of these intraslab events observed in the forearc region is profoundly influenced by a seismically slow layer atop the slab surface. This several kilometer thick low-velocity channel (wave guide) causes the entrapment of seismic energy producing strong guided wave phases that appear in P onsets in certain regions of the forearc. Observations at the Chile-Peru subduction zone presented here, as well as observations at several other circum-pacific subduction zones show such signals. Guided wave analysis contributes details of immense value regarding the processes near the slab surface, such as layering of subducted lithosphere, source locations of intraslab seismicity and most of all, range and manner of mineralogical phase transitions.

Seismological data stem from intermediate depth events (depth range 70 km - 300 km) recorded in northern Chile near 21°S during the collaborative research initiative 'Deformation Processes in the Andes' (SFB 267). A subset of stations - all located within a slab-parallel transect close to 69°W - show low-frequency first arrivals ($\sim$ 2 Hz), sometimes followed by a second high-frequency phase.

We employ 2-dimensional finite-difference simulations of complete P-SV wave propagation to explore the parameter space of subduction zone wave guides and explain the observations. Key processes underlying the guided wave propagation are studied: Two distinct mechanisms of decoupling of trapped energy from the wave

guide are analyzed - a prerequisite to observe the phases at stations located at large distances from the wave guide (up to 100 km). Variations of guided wave effects perpendicular to the strike of the subduction zone are investigated, such as the influence of phases traveling in the fast slab. Further, the merits and limits of guided wave analysis are assessed. Frequency spectra of the guided wave onsets prove to be a robust quantity that captures guided wave characteristics at subduction zones including higher mode excitation. They facilitate the inference of wave guide structure and source positioning: The peak frequency of the guided wave fundamental mode is associated with a certain combination of layer width and velocity contrast. The excitation strength of the guided wave fundamental mode and higher modes is associated with source position and orientation relative to the low-velocity layer.

The guided wave signals at the Chile-Peru subduction zone are caused by energy that leaks from the subduction zone wave guide. On the one hand, the bend shape of the slab allows for leakage at a depth of 100 km. On the other, equalization of velocities between the wave guide and the host rocks causes further energy leakage at the contact zone between continental and oceanic crust ($\sim$ 70 km depth). Guided waves bearing information on deep slab structure can therefore be recorded at specific regions in the forearc. These regions are determined based on slab geometry, and their locations coincide with the observations.

A number of strong constraints on the structure of the Chile-Peru slab are inferred: The deep wave guide for intraslab events is formed by a layer of 2 km average width that remains seismically slow (7 % velocity reduction compared to surrounding mantle). This low-velocity layer at the top of the Chile-Peru slab is imaged from a depth of 100 km down to at least 160 km. Intermediate depth events causing the observed phases are located inside the layer or directly beneath it in the slab mantle. The layer is interpreted as partially eclogized lower oceanic crust persisting to depth beyond the volcanic arc.

Chapter 1
Introduction

1.1 Note to the reader

The core of this thesis is composed of three research papers enveloped by an introductory chapter and a conclusive resume. Chapter 1 gives a short introduction to subduction zone processes followed by a review of the common seismological methods utilized to image subducted crust. The chapter concludes with an overview of the geoscientific setting and the seismic data and method used.

Chapters 2 to 4 originate from stand-alone articles, published or to-be-published in international journals. Each paper is preceded by a short introduction motivating this particular piece of research and putting it in context in this compendium. Each chapter reflects a stage of the investigations undergone in the last three years. Naturally methods and scientific approaches evolve and topics touched in one paper may be revisited in more detail in the sequels. The chapters can easily be read as self-contained works of research and consequently repetitions of contents previously described may occur. Selected paragraphs of chapters 2, 3 and 4 are also included in chapter 1 to give a more concise introduction.

The closing chapter 5 serves to compile the results of the foregoing three chapters and moreover to sum up the knowledge gained on subduction zone wave guides and in particular the Chile-Peru subduction zone through the course of this PhD project. The presented text and figures are partially adjusted in style to ultimately fit more concisely in this compendium and may therefore differ from original publications.

1.2 The fate of subducting slabs

What happens to a lithospheric plate after its subduction is hotly debated since the advent of plate tectonics. The extensive interest arises for example because of a variety of extraordinary geoscientific phenomena connected with the subduction of oceanic lithosphere. The largest earthquakes in the planet are caused by subduction (e.g., the recent $M_w = 9.0$ Sumatra earthquake) and all volcanic arcs are related to subduction of lithospheric plates. Moreover, the topic of subduction points to the future of plate tectonics itself. A complex and ever changing interplay of thermal stresses, bending/unbending and phase transitions influences the state of the slab and subsequently the conditions of slab pull. Ultimately, knowledge on the fate of subducting slabs contributes to uncover the driving forces of plate motion. Imaging of subduction zones to ever greater depth and detail is equivalent to getting to the bottom of plate tectonics.

With the descent of cold lithosphere into the hot mantle, a number of phase transformations in the slab occur until, at great depth, the subducted material partially blends with the surrounding rocks. The plate is not composed of uniform mantle pyrolite, but due to differentiation at the ridge axis, segregated into basaltic/gabbroic ocean crust (approximately 8 km thick) and residual harzburgite underlain by pyrolite. The oceanic crust and sediments contain hydrous phases, carrying bound water down to depth as it subducts. Hydration can be due to the cooling history of the plate near the spreading center of midocean ridges [*Kirby et al.*, 1996], volatile rich mantle plumes beneath the plate [*Seno and Yamanaka*, 1996] and/or bending related faulting systems beneath outer rises [*Kirby et al.*, 1996; *Peacock*, 2001].

Subduction then causes oceanic crust to gradually dehydrate and densify. While the crust advances into the continental mantle, p-T conditions change allowing high-pressure low-temperature transformations of gabbro. The most important process is the gabbro-eclogite transformation that can be triggered starting from depth of 30 - 40 km [*Ahrens and Schubert*, 1975]. This metamorphosis is however predicted

to proceed slowly considering the low temperatures in subduction zones and thus the formation of eclogite may not be completed even at great depth. The detailed processes of the transformation are subject of ongoing discussion [e.g., *Helffrich et al.*, 1989; *Helffrich*, 1996; *Lin et al.*, 1999; *Hacker et al.*, 2003a, b]. The hindrance of eclogite formation does imply the persistence of hydrous phases down to depths of 150 km and further [*Gubbins et al.*, 1994; *Abers*, 2005]. This has far-reaching consequences for subduction zone processes such as the generation of arc magmas [*Davies*, 1999], buoyancy of slabs [e.g., *Helffrich*, 1996], and the cause and location of intermediate depth seismicity itself (for a summary see *Kirby et al.* [1996]). In recent years, seismic measurements are beginning to place direct constraints on the structure of subducted plates contributing restrictions to subduction processes such as *in situ* bounds on dehydration [*Hori et al.*, 1985; *Helffrich and Stein*, 1993; *Bock et al.*, 2000; *Yuan et al.*, 2000; *Abers*, 2005]. Thus, thermal-petrological models can now be tested and enhanced incorporating recent advances in seismology.

Slabs are influencing seismic waves in diverse ways, reflecting thermal structure, layering of the slab as it is subducted, and last but not least mineralogical phase changes of subducted crust as it dehydrates and interacts with the surrounding host rocks [e.g., *Davies and McKenzie*, 1969; *Kirby et al.*, 1996]. In turn, these processes are associated with the triggering of intermediate depth earthquakes (at depth between 70 km and 300 km), possibly by the effects of water liberated by dehydration (*'dehydration embrittlement'*) or through changes in the stress state of the slab [*Kirby et al.*, 1996].

1.3 Seismological methods at subduction zones

Seismic wave anomalies are used to infer seismic velocity structure of subducted lithosphere and ultimately information on slab mineralogy. Velocity contrasts are derived from observations of a variety of seismic signals that are influenced by the subducted plate. Travel times, for example, are easy to measure, but only yield av-

erage velocities along ray paths [e.g., *Fukao et al.*, 1978]. Detailed velocity structure within the slab that gives evidence for mineralogical phase changes can thus not be imaged [*Mitronovas et al.*, 1971].

Another widely used technique employs converted waves caused by the slab surface or layering within the subducted lithosphere. *Helffrich and Abers* [1997], for example, employed converted waves to investigate a low-velocity layer at the eastern Aleutian subduction zone. Studies at the Chile-Peru subduction zone in the western Central Andes inferred a similar layer up to depths of 120 - 160 km from P-S converted waves [*Bock et al.*, 2000; *Yuan et al.*, 2000]. The resulting velocity contrast is 15 % with a thickness of 5 to 10 km. Likewise investigations at the north-east Japanese subduction zone found undulating velocity contrasts between the accretional wedge and subducted crust at various depths which are interpreted as evidence of chemical phase changes of the gabbroic subducted crust [*Snoke et al.*, 1978; *Helffrich*, 1996].

The existence of a layer of reduced seismic velocity atop subducted slabs is postulated at almost all circum-pacific subduction zones [*Hori et al.*, 1985; *Lin et al.*, 1999; *Abers*, 2005; *Martin et al.*, 2003], it may be a common feature of slabs in general provided they are sufficiently cold (i.e. older than $\sim$ 25 Ma) [*Kirby et al.*, 1996]. This comparably thin low-velocity layer (LVL), not only causes converted seismic body waves, but also can act as a seismic wave guide for up-dip and along-strike signals of intraslab events. These signals provide the longest interaction times within the slab and thus yield potentially large slab related signals. The wave guide causes entrapment of guided waves and therefore high amplitudes, distortion in pulse shapes and differences in long- and short-period energy arrival times.

Among the mentioned methods, guided waves is one that is directly linked to the existence of layered structures such as subducted crust. A more or less continuous layering is a prerequisite for the occurrence of guided waves [*Abers and Sarker*, 1996; *Li and Vidale*, 1996; *Abers*, 2000]. Furthermore, studies on fault zones and

subduction zones have shown so far that occurrence, pulse shapes and frequency content of guided waves are directly related to parameters such as layer thickness, length of the wave guide structure and source location in relation to the layer [*Li and Vidale*, 1996; *Igel et al.*, 1997; *Ben-Zion*, 1998; *Fohrmann et al.*, 2004].

The data from the Chile-Peru subduction zone used in this work constitute the first guided wave observations at the Nazca slab.

1.4 Geoscientific setting of the Central Andes and data

The Andes are the worlds longest mountain range (stretching over 5000 km) forming a continuous chain of highland along the western coast of South America reaching from the Caribbean to *Tierra del Fuego*. The Central Andes are the prime example of a cordilleran orogen related to subduction of an oceanic plate beneath a continental plate. It is in fact name-giving to the whole class of oceanic plate subduction beneath continental lithosphere, the Andean- or Cordilleran-type margins.

The lithosphere descending beneath the Central Andes is formed by the eastern limb of the oceanic Nazca plate which is currently subducted beneath South America. The plate is bordered by three more oceanic plates. To the west the East Pacific Rise defines the border to the Pacific plate, to the north the Nazca plate is separated by the Galapagos ridge from the Cocos plate and to the south by the Chile ridge from the Antarctic plate (Figure 1.1). Presently, the Nazca plate moves at a rate of 5.1 cm/yr to the east, while the South American continent overrides it at 3.4 cm/yr westwards with respect to the absolute hot-spot reference frame [*DeMets et al.*, 1990]. This yields a slightly oblique ENE directed convergence between the two plates with a velocity of 8.5 cm/yr (Figure 1.1). The Chile-Peru subduction zone is relatively young and the descending ocean floor is only 40 - 46 Ma old.

Tectonic style of the Chile-Peru subduction zone varies significantly along- and

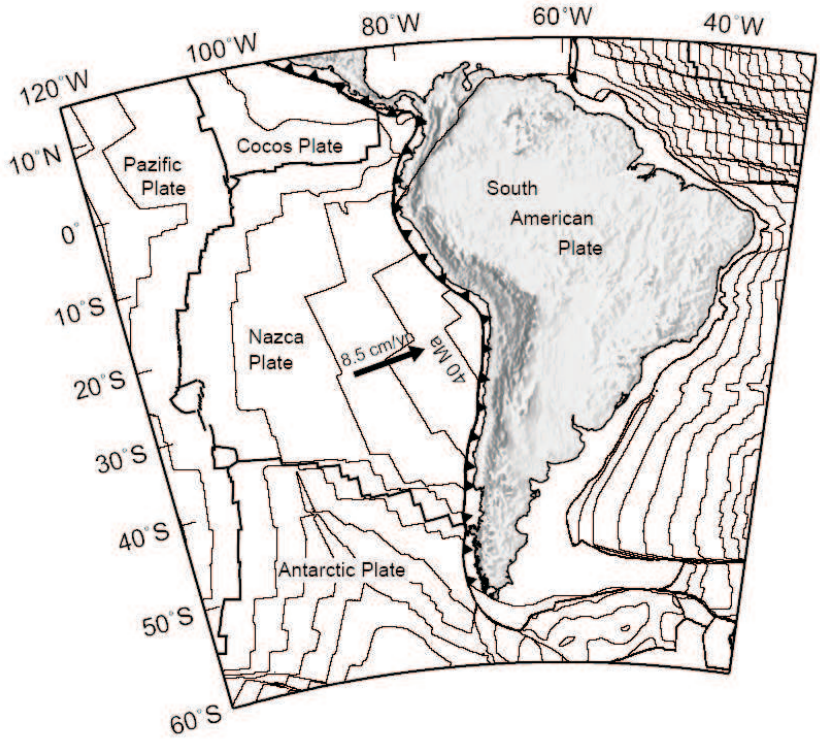

Figure 1.1: The South American continent (Plate-tectonic setting). Convergent margins are indicated by barbed lines, spreading ridges and transform plate boundaries are marked by thick lines. Ocean-age isochrones (thin lines) are shown for every 10 Ma.

across-strike resulting in a changing geometry of the Nazca slab along the South American coast. The study area is situated above a slab segment subducting at an intermediate angle of about 30°, further to the north and south of this segment, the subduction progresses almost flat (Figure 1.2).

In the study area, above the comparatively steep dipping segment of oceanic lithosphere, volcanic activity is abundant, and while the northern and southern Andes form narrow mountain belts, the Central Andes are characterized by a more than 3000 m high and about 300 - 400 km wide plateau. The study area lies between 20°S to 24°S and 66°W to 70°W where the *Cordillera Costal* constitutes the forearc separated from the *Precordillera* by the Longitudinal Valley (Figure 1.2). The *Western Cordillera* forms the present magmatic arc and constrains the Central Andean plateau to the east.

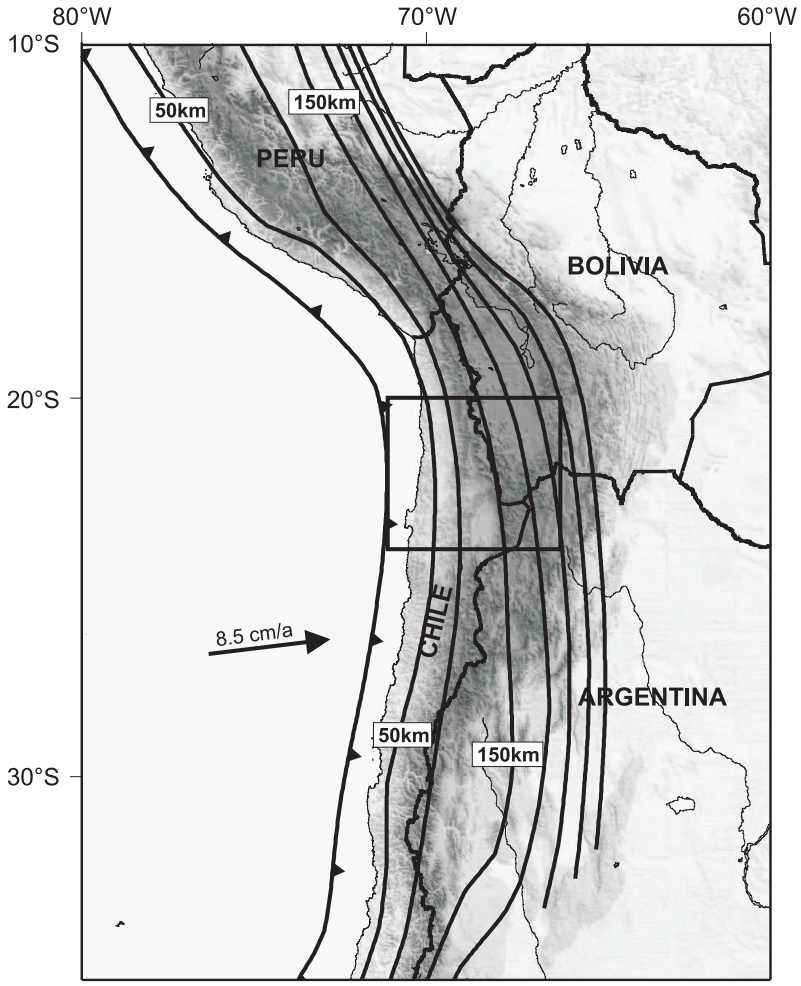

Figure 1.2: Overview of the Central Andean subduction zone. Contour lines show the depth of the Wadati-Benioff-Zone [*Gudmundsson and Sambridge*, 1998], the barbed line marks the convergent plate margin and the rectangle outlines the study area.

To derive subduction zone structure, we use up-dip events recorded at stations located above the slab in the forearc region. Data stem from an extensive interdisciplinary research initiative 'Deformation Processes in the Andes' (SFB 267), established in 1993 operating for twelve years. Three passive seismic experiments were carried out in the Central Andes between 1994 and 1997, deploying portable, mostly short-period seismograph arrays between 20°S and 25°S. The PISCO'94 (Projecto de Investigación Sismológica de la Cordillera Occidental) seismic experiment was centered in the forearc region between 22°S and 24°S. It involved both, an active

part [*Schmitz et al.*, 1999] and a temporary passive array [*Graeber and Asch*, 1999; *Haberland and Rietbrock*, 2001]. The CINCA'95 (Crustal Investigación on- and offshore Nazca plate and Central Andes) campaign was focused on the seismogenic part of the subduction interface in the costal region of Central Chile [*Husen et al.*, 1999]. The following year, the ANCORP'96 (Andean Continental Research Project) passive array [*ANCORP Working Group*, 1999] continued coverage of PISCO to the north, but additionally reached into the Bolivian backarc [*Rietbrock and Haberland*, 1998; *Haberland and Rietbrock*, 2001]. All data used come from the above three passive experiments.

Figure 1.3 shows the study area and selected stations of the SFB 267 networks (gray triangles). At these stations, the majority of P onsets of up-dip intraslab events located deeper than 100 km are distorted or expose later arriving second phases. Pulse shapes of P first arrivals vary dependent on receiver location and source depth. Strong low-frequency arrivals followed by delayed high-frequency energy are observed as well as onsets resembling two phases, the second phase being higher in amplitudes than the first (Figure 1.4). Non of the analyzed stations show a comparable effect or other kinds of systematic frequency distortion for along-strike registrations or source-receiver geometries not sampling the slab surface.

Data are taken from latitude-longitude boxes each approximately forming an up-dip section located near 22°S (see Figure 1.3). Focal depths range from 70 to 300 km and the events are in the narrow magnitude range of $M_l = 2$ to $M_l = 4$ [*Rudloff*, 1998]. Expected fault plane radii are smaller than 1 km [*Brune*, 1970, 1971] and source functions are expected to be sufficiently flat in the analyzed frequency range (1.0 to 5.0 Hz) [*Lay and Wallace*, 1995].

Throughout the course of this PhD project, we were dwelling on different selected observations. The first research work (chapter 2) is focused on an up-dip seismogram section recorded at station AER (dashed line in Figure 1.3. The second study (chapter 3) again contains the seismogram section at station AER and in addition

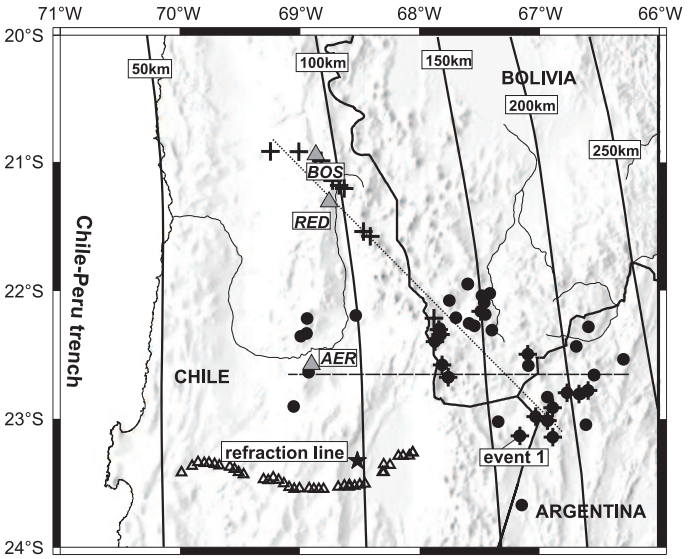

Figure 1.3: Map of the study area. Gray triangles indicate receivers showing distorted onsets. Events analyzed at station AER (solid circles) and BOS (crosses) are approximately located along up-dip profiles (dashed line and dotted line respectively). Open triangles represent receivers of the PISCO refraction profile where a single event (indicated by a star) was recorded ($M_l \sim 5.0$, March 17, 1994, 21:22:49.54 GMT, [*Rudloff*, 1998]). All receivers are equipped with Mark L-4A-3D sensors. Solid lines represent depth contours. The profiles at station AER and BOS are further described in section 2.2.3 and section 3.2.4 respectively, details regarding the registration at the refraction line are found in section 4.2.3.

a further seismogram section recorded at station BOS (dotted line in Figure 1.3). In the final study (chapter 4) a recording of a local earthquake along a temporarily deployed refraction line (star and open triangles in Figure 1.3) to the south of the former sites is analyzed [*Lessel*, 1997; *Schmitz et al.*, 1999].

1.5 The finite difference method

To gain an inside view of the mechanism underlying the observed distorted pulse shapes, a numerical simulation of the wave propagation is best suited. It is a demanding task to simulate body waves with frequencies as high as 8.5 Hz that prop-

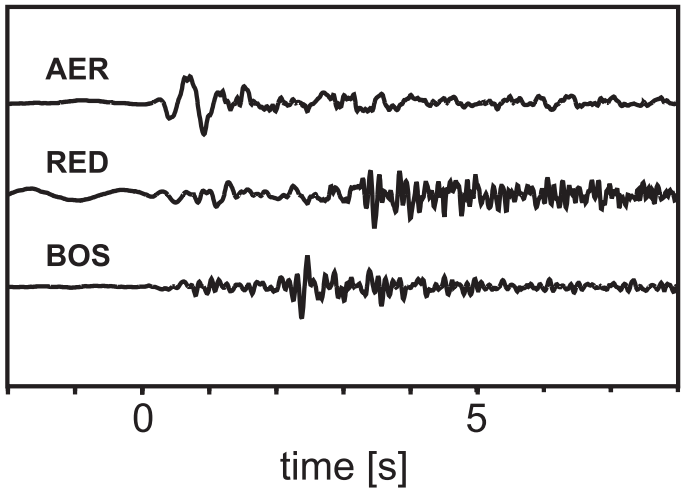

Figure 1.4: Selected seismograms at stations AER (22.58°S, 68.91°W), RED (21.29°S, 68.77°W) and BOS (20.94°S, 68.87°W) (Figure 1.3), the event is labeled 'event 1' in Figure 1.3. Seismograms (vertical component) are aligned on first arrivals and show ground displacement, band-pass-filtered between 0.5 Hz and 12.0 Hz. Representative effects caused by the subduction zone wave guide are displayed: Seismograms at station AER expose low-frequency onsets whereas stations BOS and RED show a second phase following the P first arrival.

agate hundreds of kilometers in a laterally inhomogeneous medium.

Seismological modeling can basically be approached by three different methods, all distinctive in their merits. The first, wavenumber-integration, is suited to calculate the complete seismic response for layered media (e.g., reflectivity method [*Fuchs and Müller*, 1971; *Wang*, 1999]. The high accuracy of this method makes it well suited to gage other methods in respect to layered media. The second technique, the ray tracing method, is comparatively fast, but only accurate if wavelengths and curvatures of the seismic rays are small in comparison to the geological structures considered [*Wang*, 1997]. Third, grid based methods constitute the most flexible approach. The seismological model is mapped on a discrete grid, thus permitting modeling of complete wave propagation in any heterogeneous seismic velocity structure.

To investigate frequency dependent wave form effects in laterally heterogeneous geological structures, such as subduction zones, only these grid based methods are

suitable. They are either based on spectral and pseudo-spectral techniques or the finite difference technique. Spectral and pseudo-spectral methods solve the spatial derivations in the wave equation by applying a fourier transform [*Carcione*, 1993; *Tessmer and Kosloff*, 1994], whereas the finite difference methods are operating in the spatial domain entirely.

We chose an efficient finite difference technique to calculate complete P-SV wave propagation within a 2D depth section of the subduction zone. The elastodynamic equation of motion is expressed in terms of velocity and stress. Our approach uses a 4th-order staggered grid finite difference scheme as proposed by *Virieux* [1984, 1986]. The method is well suited for the challenge of simulating wave propagation up to high frequencies in large media (in our case up to 330 km x 260 km) including complicated boundaries. Furthermore, the model space can easily be distributed on parallel computers. Since we are interested in frequency effects, special care must be taken to prevent numerical dispersion that would distort frequency content of guided waves. The staggered grid method allows a fine discretisation of the model while the cost of computing stays low. In the finite difference calculations, grid spacing is as little as 40 meters, the time increment is only 0,0027 seconds. Thus even the highest frequencies of S waves are covered with 12 points per wavelength and numerical dispersion stays well below 0.5 % [*Levander*, 1988].

The scheme is rounded out using the planar free surface condition given by e.g. *Levander* [1988], which employs a zero stress formulation to produce accurate and numerically stable surface reflections and P-SV conversions. The artificial edges of the model are damped by simple exponential terms [*Randal*, 1989].

Among the options to include DC sources in the 2D staggered grid scheme, the simple and effective approach of *Coutant et al.* [1995] was favored. Explosive sources or DC sources of varying dip angle are implemented by stress excitation and efficiently centered at a single grid point. In the following chapter 2, explosive sources are used in the simulations for simplicity, in the remaining chapters of the

thesis both explosive and DC sources are employed.

In order to excite guided waves within a broad frequency range, we utilize a band-limited delta impulse as source wavelet, the subsequent processing is dependent on the aspect of guided waves we focus on. In the following chapters 2 and 3 we present low-pass-filtered ground displacement seismograms emphasizing frequency effects. The synthetics shown in chapter 4 are furthermore convolved with a 1 Hz Ricker wavelet to underline the coherent registration of a low-frequency guided phase.

The accuracy of the seismograms produced by the finite difference algorithm was verified by comparison with reflectivity synthetics [*Fuchs and Müller*, 1971; *Wang*, 1999] for a layered half-space applying 2D to 3D corrections for amplitudes [*Amundsen and Reitan*, 1994].

Due to hardware limitations, simulations of the given size, were, up to recent years, extremely cost intensive to undertake. Today 2D simulations of a down-dip section (280 km x 220 km) can be run on 16 nodes of a Beowulf cluster (733 MHz Pentium III dual processor) within 10 hours real time.

Chapter 2

Intraslab events causing guided waves in subducted oceanic crust

2.1 Preface

Is a wave guide effect possible at the Chile-Peru subduction zone for an up-dip source-receiver geometry? Can observed P wave distortion be explained by such an effect? These are the basic problems tackled in this chapter.

In this first part of the research work, we focus on explaining the observed distortion in P onsets at station AER at the Chilenian coast by means of a wave guide effect. The data used come from intraslab events associated with up-dip ray path to the recording station (up-dip events). The parameter space of subduction zone wave guides is explored in the laterally varying subduction zone structure using finite difference simulations. We translate the wave guide theory already established at fault zones [*Ben-Zion*, 1998] to the much bigger length scales and different geometry of subduction zone up-dip wave guides and give a short outline of the theoretical background.

The first step consists of developing a velocity model adequate to match the observations while keeping the geological structure, the wave guide geometry, and resulting wave field as simple as possible. We then look at the confinements on width, propagation distance and source location needed to produce a wave guide effect. Rather than modeling the exact waveforms, the FD simulations show that a wave

guide structure facilitates observations of the kind made at the Nazca slab. With the aid of structural and mineralogical information from other sources, the width and velocity contrast of the wave guide is estimated and ultimately the minimum depth extent of a seismically distinct crustal layer can be derived.

2.2 Guided waves propagating in subducted oceanic crust

(**published article:** Martin, S., A. Rietbrock, C. Haberland, and G. Asch, Guided waves propagating in subducted oceanic crust, *J. Geophys. Res.*, 108, 2003, doi: 10.1029/2004GL019610.)

2.2.1 Abstract

We use guided waves traveling up-dip along the surface of the Nazca slab to image subducted oceanic crust at the Chile-Peru subduction zone. Observed P onsets of intermediate depth events near 21°S in northern Chile reveal wave guide behavior: with growing focal depth, low-frequency energy (< 2 Hz) becomes more and more dominant, higher frequencies arrive delayed, sometimes resembling two distinct phases. To explain the observations we employ 2D finite difference (FD) simulations of complete P-SV wave propagation along an up-dip profile of the subduction zone. The FD calculations allow to shed some light on several basic issues regarding crustal wave guides. The development of guided waves dependent on event focal depth is simulated. Further, we show that the observed guided wave energy must decouple from the wave guide near 100 km depth to reach the deployed stations and that the decoupling process is related to variations in subduction angle. Simulations also yield constraints on source locations relative to the low-velocity structure. Finally, the frequency content of P onsets is used to constrain the thickness of the wave guide. The results indicate that a structure of less than 4.5 km average width and

7 % low velocity remains seismically slow compared to the surrounding mantle down to a depth of at least 160 km. The layer is interpreted as the unaltered lower part of the subducted oceanic crust, suggesting that complete eclogite transformation in the Chile-Peru subduction zone is unlikely to take place until beyond the volcanic front.

2.2.2 Introduction

The fate of subducted oceanic crust at intermediate depths is of main contemporary interest for understanding the subduction processes and, in particular, the origin of intermediate depth earthquakes [*Meade and Jeanloz*, 1991; *Abers*, 2000; *Yuan et al.*, 2000]. Seismic waves from intraslab earthquakes that probe the seismic velocity structures of slabs are a valuable source of information on the mineralogical and thermal structure of subducted lithosphere [e.g., *Davies and McKenzie*, 1969; *Kirby et al.*, 1996]. Seismic wave anomalies are used to infer seismic velocity structure of subducted lithosphere and ultimately information on slab mineralogy [*Mitronovas et al.*, 1971].

Velocity contrasts are derived from observations of a variety of seismic signals that are influenced by the subducted plate. Travel times, for example, are easy to measure, but only yield average velocities along ray paths [e.g., *Fukao et al.*, 1978]. Detailed velocity structure within the slab that gives evidence for mineralogical phase changes can thus not be imaged [*Mitronovas et al.*, 1971].

Another widely used technique employs converted waves caused by the slab surface or layering within the subducted lithosphere. *Helffrich and Abers* [1997], for example, employed converted waves to investigate a low-velocity layer at the eastern Aleutian subduction zone. Studies at the Chile-Peru subduction zone in the western Central Andes inferred a similar layer up to depths of 120 - 160 km from P-S converted waves [*Bock et al.*, 2000; *Yuan et al.*, 2000]. The resulting velocity contrast is 15 % with a thickness of 5 to 10 km. Likewise investigations at the

north-east Japanese subduction zone found undulating velocity contrasts between the accretional wedge and subducted crust at various depths which are interpreted as evidence of chemical phase changes of the gabbroic subducted crust [*Snoke et al.*, 1978; *Helffrich*, 1996].

Lastly, subducted lithosphere not only causes converted seismic body waves, but also can act as a seismic wave guide for up-dip and along-strike signals of intraslab events. These signals provide the longest interaction times within the slab and thus yield potentially large slab related signals. The wave guide causes distortion in pulse shape and differences in long- and short-period energy arrival times.

Among the mentioned methods, guided waves is one that is directly linked to the existence of layered structures such as subducted crust. A more or less continuous layering is a prerequisite for the occurrence of guided waves [*Abers and Sarker*, 1996; *Abers*, 2000]. Furthermore, studies on fault zones have shown so far that occurrence, pulse shapes and frequency content of guided waves are directly related to parameters such as layer thickness, length of the wave guide structure and source location in relation to the layer [*Li and Vidale*, 1996; *Igel et al.*, 1997; *Ben-Zion*, 1998; *Fohrmann et al.*, 2004].

The first successful studies in subduction zones were undertaken for high- velocity structures, often modeling the whole slab as a high-velocity layer [e.g., *Barazangi et al.*, 1972]. Observations at the Kermadec subduction zone gave proof that thinner layering also results in frequency effects. High-frequency phases were observed prior to low-frequency onsets at stations in New Zealand. This is explained by introducing a thin (8-10 km) high-velocity layer (5 % faster than surrounding mantle) on top of the Kermadec plate [*Ansell and Gubbins*, 1986; *Van der Hilst and Snieder*, 1996].

In accordance with investigations utilizing converted waves, the Japanese subduction zone, which has so far been investigated the most, features a low-velocity layer that causes guided wave effects. P onsets show low frequencies arriving faster than high frequencies. Studies on the crustal wave guide in the Philippine plate

subducting beneath southwest Japan concluded that the wave guide was less than 10 km thick and that V_p equals 7 km/s for earthquake sources down to focal depth of 50-60 km [*Fukao et al.*, 1983; *Hori*, 1990; *Oda et al.*, 1990]. As these velocities were indistinguishable from those for oceanic crust beneath ocean basins, the wave guide was identified as gabbroic crust that survived untransformed to a depth of 50-60 km. In the Pacific plate subducting beneath northeast Japan, the low-velocity crustal channel persists to depths of 75 to 150 km, and its thickness is estimated to be about 5 km [*Matsuzawa et al.*, 1986; *Hurukawa and Imoto*, 1992; *Iidaka and Obara*, 1993]. Since change in temperature cannot cause the appropriate velocity contrasts [e.g., *Helffrich*, 1996], it is likely, that a layering persists to greater depths than those reached beneath the volcanic arc. Recently, low-velocity layers were postulated for most of the subducted slabs in the north Pacific region down to depths of 100 to 250 km by evidence from guided waves [*Abers*, 2000].

This study is motivated by the mentioned results at other subduction zones and promising observations from Intraslab events at stations of the ANCORP '96 seismic network located between 21° and 24°S in northern Chile [*Rietbrock et al.*, 1997].

Typically, the observation of guided waves is restricted to the case of receivers situated within or close to the wave guide rather than complex geometries including receivers at greater distances to the low-velocity layer [*Ben-Zion et al.*, 2003]. Therefore, we will address simple, but crucial questions regarding the potential of guided waves to examine layering of subducted lithosphere: (1) Under which circumstances does guided wave energy actually leave the wave guide structure and is observable at surface stations? (2) Which restrictions on source locations are required to have guided wave energy enter the low-velocity structure? (3) Do distorted P onsets allow estimates of structural parameters of the low-velocity zone? Ultimately, we infer under which circumstances guided wave energy from a low-velocity layer on top of the Nazca plate at the Chile-Peru subduction zone is observable in P onsets.

We calculate complete P-SV wave propagation for a 2D cross section through

the Chile-Peru subduction zone utilizing finite difference (FD) simulations. This allows us to compare directly pulse shapes and frequency content (up to 8.5 Hz) of collected data with synthetics for different slab geometries and internal structures. The FD calculations allow a much more direct approach to the problem than analytical guided wave solutions which are feasible for SH waves and plain layers only. Furthermore, the FD approach allows to investigate the decoupling process of guided waves from laterally inhomogeneous wave guide structures.

2.2.3 Data and observations - distorted arrivals at the ANCORP station AER

Data used come from the ANCORP '96 campaign that was undertaken during November 1996 to March 1997 in northern Chile between 23° to 20.5°S and 70° to 66.5°W [*Rietbrock et al.*, 1997]. The ANCORP temporary seismic network consisted of 32 short-period stations equipped with Mark L-4A-3D sensors.

A subset of stations (BOS, AER, VOL, CHG; see Figure 2.1) - all located close to 69° +/- 0.2° longitude - show distorted P wave first arrivals, sometimes resembling two distinctive phases. This work focuses on the data recorded at station AER, where the effect is most pronounced and the noise level is low. Events were selected from the latitude-longitude box 23.88° to 21.95°S and 69.05° to 66.29°W. They cover a range of focal depths from 70 to 300 km and form an up-dip section centered around station AER (Figure 2.1).

P waveforms in seismograms recorded at AER can be classified into two groups. A clear, impulsive onset is typical for the recorded shallow earthquakes (focal depth ($<$ 110 km). In contrast, the P onset of earthquakes with greater focal depth ($>$ 140 km) at AER has low frequencies that form the early part of an extended wave train rather than a sharp onset (Figure 2.2).

Offset was removed and the data were band-pass-filtered (0.5 Hz - 8.5 Hz). During the ANCORP '96 campaign, 48 events located deeper than 110 km were recorded

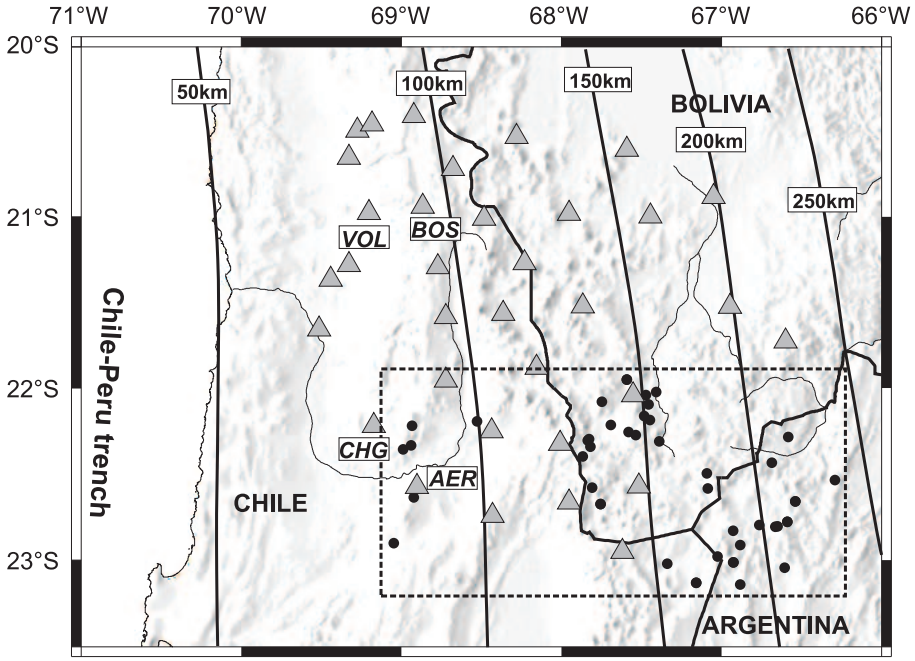

Figure 2.1: Map of the ANCORP '96 temporary seismic network consisting of 32 short-period stations (solid triangles) equipped with Mark L-4A-3D sensors. Solid lines represent depth contours. The dashed line contains events (black dots) recorded at station AER forming an up-dip section centered at 22.58°S. The events were located by *Rietbrock et al.* [1997] using a local earthquake tomographic method.

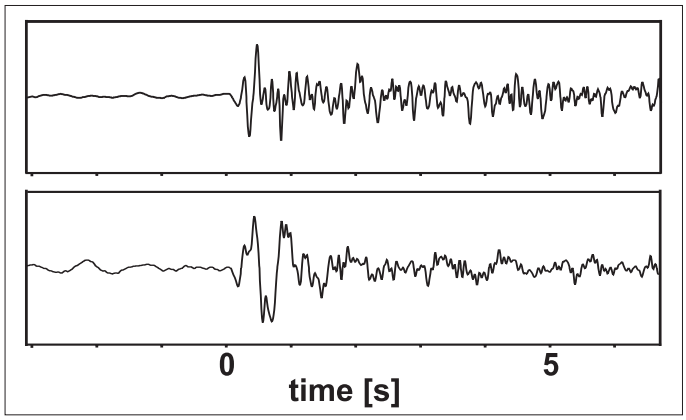

Figure 2.2: P onsets at station AER aligned on first arrivals and plotted proportional to ground displacement. Data is band-pass-filtered between 0.5 Hz and 8.5 Hz, amplitudes are normalized. Above: event at 80 km focal depth (26 km epicentral distance) located close to station AER (see Figure 2.1). Below: distorted P onset (focal depth 190 km, epicentral distance 167 km).

at station AER. 45 of these 48 events show remarkably strong low-frequency energy arriving prior to higher frequencies. The effect is particularly strong for deeper events with larger hypocentral distances. A selected subset of seismograms representing different event depth illustrates the dependency on source location (Figure 2.3a). A relative increase of low-frequency energy with focal depth is evident from

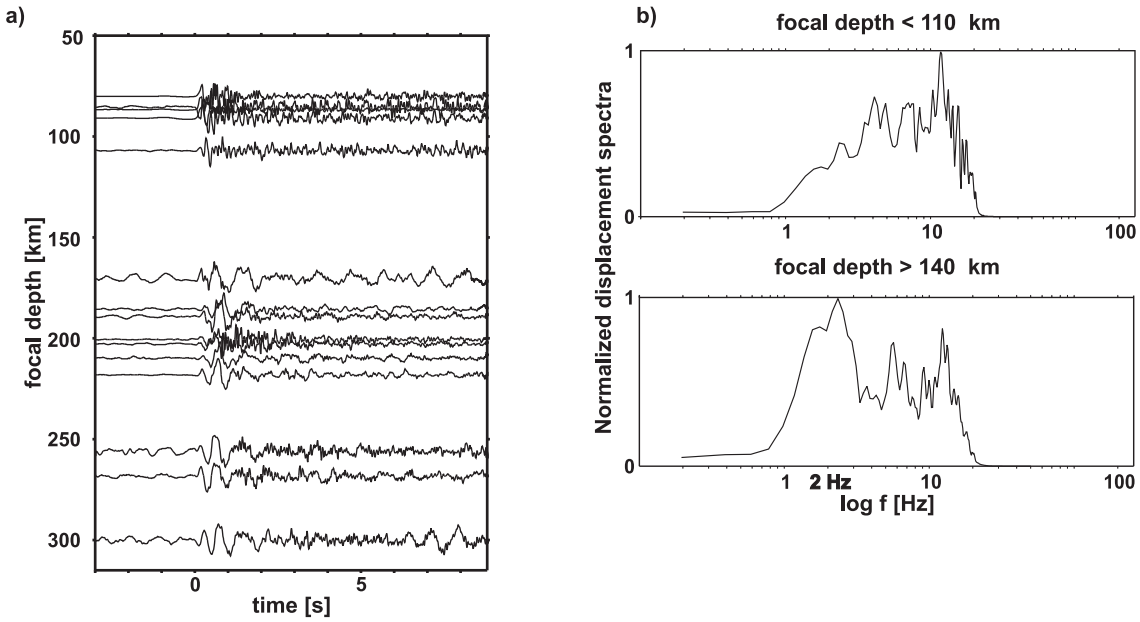

Figure 2.3: a) Aligned P onsets of selected events recorded at station AER plotted by focal depth (for further explanations see Figure 2.2). b) Stacked displacement spectra of onsets (first 2 seconds) of all events contained in the up-dip section (see Figure 2.1) with focal depth < 110 km and > 140 km, respectively.

visual assessment. For one of the deepest events high-frequency energy (> 5 Hz) arrives up to 1.0 second later than energy below 2.5 Hz (compare Figure 2.3a). This suggests that slab structure is responsible for the effect. Figure 2.3b compares the summed up spectra of all events located above 110 km and below 140 km respectively. Only the latter spectrum exposes a clear peak around 2 Hz while sources above 110 km lack this low-frequency energy. At the same time, the peak frequency of low-frequency energy for events located deeper than 140 km does not shift systematically precluding a pure attenuation effect.

2.2.4 Finite difference modeling of wave guide effects

To gain an inside view of the mechanism underlying this systematically distorted pulse shapes, a numerical simulation of the wave propagation seems best suited. It is, however, a demanding task to simulate body waves with frequencies as high as 8.5 Hz that propagate hundreds of kilometers in a laterally inhomogeneous medium. An efficient, easy to parallelize, grid based finite difference technique was chosen to calculate complete P-SV wave propagation within a 2D depth section of the subducting Nazca slab.

The elastodynamic equation of motion is expressed in terms of velocity and stress. Our approach uses a 4th-order staggered grid finite difference scheme as proposed by *Virieux* [1984, 1986]. The method is well suited for the challenge of simulating wave propagation up to high frequencies in large media (330 km x 260 km) including complicated boundaries. Furthermore, the model space can easily be distributed on parallel computers. Since we are interested in frequency effects, special care must be taken to prevent numerical dispersion that would distort frequency content of guided waves. The efficient staggered grid method allows a fine discretisation of the model while the cost of computing stays low. In the finite difference calculations, grid spacing is as little as 40 meters, the time increment is only 0,0027 seconds. Thus even the highest frequencies of S waves are covered with 12 points per wavelength and numerical dispersion stays well below 0.5 % [*Levander*, 1988].

The scheme is rounded out using the planar free surface condition given by e.g. *Levander* [1988], that employs a zero stress formulation to produce accurate and numerically stable surface reflections and P-SV conversions. In order to excite guided waves within a broad frequency range, we use a band-limited delta impulse as source wavelet in conjunction with subsequent low-pass-filtering (8.5 Hz). The artificial edges of the model are damped by simple exponential terms [*Randal*, 1989]. Due to hardware limitations, simulations of the given size, were, up to now, extremely cost intensive if not impossible to undertake. Today the scheme can be run on a LINUX

cluster with 16 nodes (1 GHz Pentium III) within 16 hours real time.

2.2.5 Excitation of guided waves and dependencies on structural parameters

Guided waves: Effects and prerequisites

Understanding and using the available data require a basic knowledge of wave guide phenomena. Any continuous layered structure that is slow compared to bounding media can act as a wave guide provided no large heterogenities are present. Scales of layer thickness range from meters to tens of kilometers, dependent on the frequency range under observation. This structure causes - for certain source-receiver configurations - internally reflected waves that produce prominent interference Patterns called guided waves. The effect is most pronounced for shear energy, but does also occur for P waves. In this case, trapping of energy is less efficient and energy is leaking into the surrounding host rocks (P-SV converted waves originating at the interfaces of the low-velocity structure). The first studies to utilize the effect for P and S waves in the context of tectonic faults are probably those of *Fukao et al.* [1983] and *Hori et al.* [1985].

The dispersion properties of guided waves are such that the lowest frequencies propagate along the structure with velocities similar to P velocities of surrounding host rocks, while higher frequency energy arrives later, dependent on structural parameters [*Li and Leary*, 1990]. The pulse shape and the frequency content of the resulting wave train is ultimately dependent on the material parameters and geometry of the wave guide structure. The interference pattern controlling the waveform character changes with the number of times the waves are reflected internally in the wave guide structure [*Ben-Zion*, 1998]. In particular, a minimum number of internal reflections is a prerequisite to perceive the interference pattern as a continuous dispersive wave train rather than separate phases. For given velocity contrasts, the number of reflections increases with propagation distance along the structure and it

decreases with the thickness of the structure.

Thus, occurrence of guided waves is restricted by a lower limit of propagation distance and an upper limit of wave guide thickness. In addition, observed motion is a strong function of relative lateral position of the source and lateral receiver coordinates. Finally low quality factors modify the dominant period and overall duration of the guided waves considerably [*Ben-Zion*, 1998].

Within the context of the Chile-Peru subduction zone, we are able to utilize mineralogical interpretations to constrain velocity contrasts and studies of attenuation tomography give information on average quality factors. Thus, geometry of the subducting slab along with receiver position, propagation length of signals along the layer (i.e. focal depth), thickness of subducted crust and the source position relative to the layer will be the parameters investigated.

Results

Slab structure and occurrence of guided waves: We aim to reproduce the observed effect in principle, utilizing a velocity model that only contains the basic features common along the extent of the subduction zone from surface to intermediate depth. The basis is a simplified sketch of the subducted slab, deduced from refraction seismic studies [*Lessel*, 1997; *Patzwahl*, 1998] and works of *Bock et al.* [2000] and *Yuan et al.* [2000] using P-S converted waves. Seismic velocity contrasts between continental mantle and slab surface in North Chile could be traced down to depth of 160 km, while the oceanic Moho that delineates the subducted crust is visible down to 120 km. Continental crust is assumed to extend down to 60 km with an average P velocity of 6.0 km/s. Mantle P velocities at depth greater than 60 km are averaged to be 8.0 km/s, the subducted material of the relatively young Nazca plate appears only slightly faster (8.1 km/s). If subducted crust persists as a partially eclogized layer on top of the slab surface, P velocities of 7.5 km/s are expected [*Helffrich et al.*, 1989; *Hacker et al.*, 2003a, b]. The average subduction

angle at latitude 21°S down to 300 km depth was inferred from the works of *Graeber* [1997] and *Rietbrock et al.* [1997] to be 30°. In our simulations we inserted a simple, if unrealistic explosive source. The simulation of complete P-SV wave propagation within a laterally inhomogeneous velocity model results in complicated seismogram sections. We therefore find it helpful to exclude influences of source functions and mechanisms from our investigations, allowing an unobstructed look at structural parameters of the wave guide.

In advance of simulations that include a low-velocity layer, the wave field resulting from an unstructured subducted slab was inspected. The reference model includes a homogeneous slab of 1.25 % higher velocity than the host rocks. The seismogram section of an event at 200 km focal depth located 5 km below the slab surface is depicted in Figure 2.4. No low-frequency energy emerges.

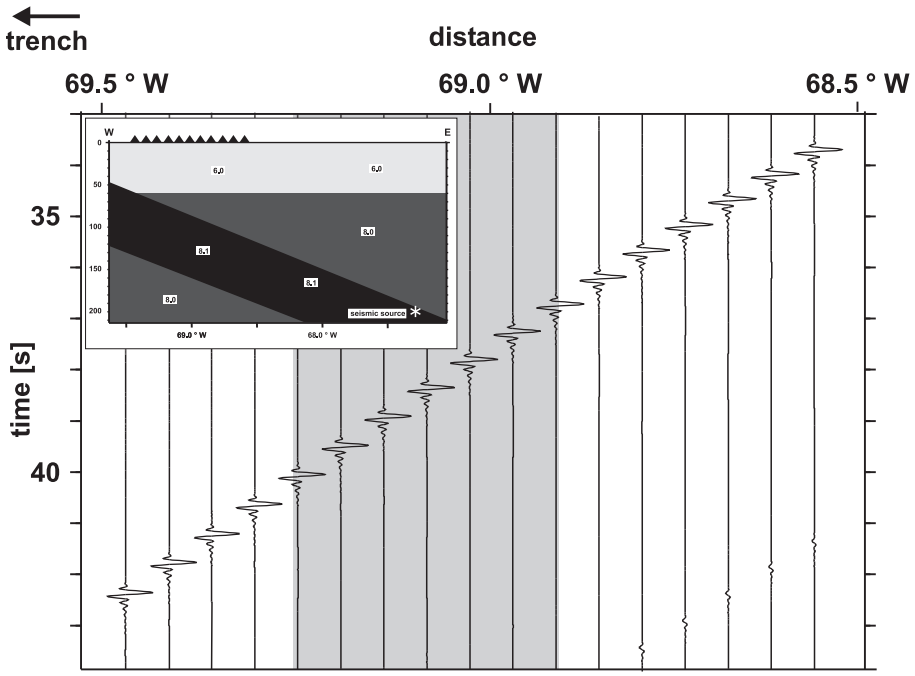

Figure 2.4: Velocity model (Insert) and resulting seismogram section for an homogeneous slab of 1.25 % increased velocity compared to continental mantle. Labels in the insert indicate P velocities. Synthetics are impulse responses proportional to ground displacement and low-pass-filtered with 8.5 Hz. The shaded area in the seismogram section marks the longitude range of ANCORP stations exposing distorted onsets.

The simplest structure to produce the observed low-frequency onsets is a planar low-velocity layer in an otherwise homogeneous medium such as slow subducted crust surrounded by faster mantle rocks. Therefore the first approach uses a model that is reduced to these three components. While guided waves begin to develop right from the start of their journey through the slab, the point of occurrence of guided wave energy at the surface is assumed to be determined mainly by the velocity structure above 100 km depth. Various studies on fault zone waves were already dedicated to the issue. Under which circumstances do guided waves leave the wave guide and can be observed outside of it? It has been shown, that a maximum of guided wave energy is observed within and directly above a vertical low-velocity layer. With increasing distance from the layer, amplitudes decay rapidly [*Igel et al.*, 1997].

A zone of transition below the receiver line in the continental mantle was assigned the same seismic velocities as the low-velocity layer. The transition zone was placed at a depth of 80 km, where studies suggest the same velocities for subducted lithosphere and mantle [*ANCORP Working Group*, 1999] (model see insert of Figure 2.5).

To restrict the range of layer thickness and source location to those values that produce a maximum in guided wave energy within the desired frequency range ($<$ 5 Hz), spot checks were undertaken for a range of layer thicknesses (1 to 10 km) and source locations relative to the low-velocity layer (ranging from 10 km below the subducted crust to sources located in the center of the subducted crust). Focal depth was 200 km, the seismic velocity contrast toward continental mantle was kept at a constant of 7 %. The strength of guided wave energy at a receiver located in the center of the layer was used as a criterion to estimate an upper limit for the layr thickness and ideal values for source location. In accordance with studies carried out for planar, vertical low-velocity layers [*Igel et al.*, 1997], the wave guide effect was most pronounced for sources located within the layer. A closer look at the effects of source positioning will be taken in section 2.2.5. The tests also indicated, that -

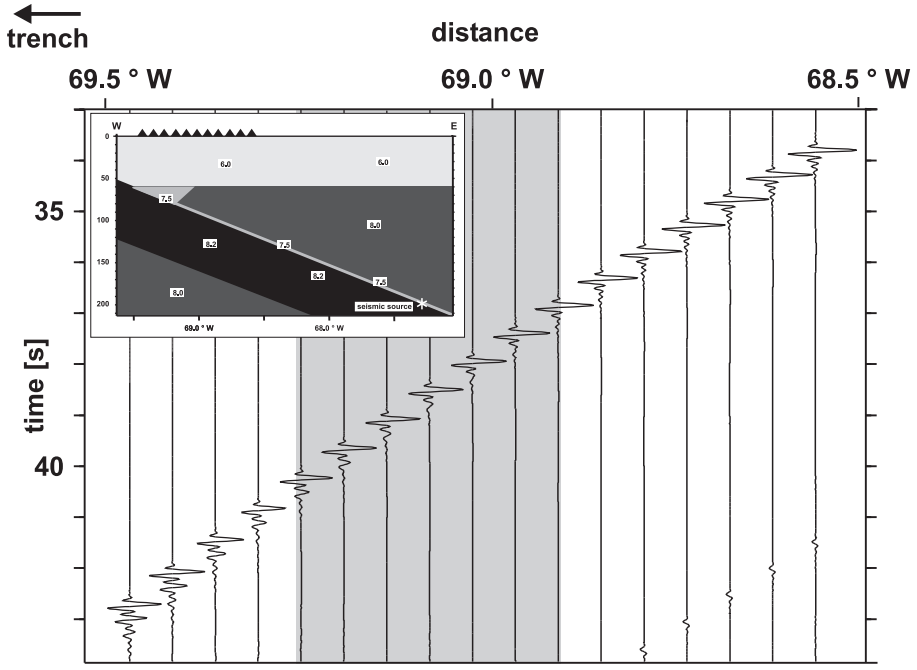

Figure 2.5: Velocity model (Insert) and resulting seismogram section for a straight slab structure with a layer of 7 % low velocity relative to continental mantle and 3 km width at its top. The shaded area marks the longitude range of ANCORP stations exposing distorted onsets. For further explanations see Figure 2.4.

for velocity contrasts less than 10 % and the given focal depth - low-velocity layers thicker than 5 km do not cause sufficient internal reflections for the development of a guided wave train.

Using maximum amplitudes and frequency content of guided waves as a measure [*Igel et al.*, 1997; *Ben-Zion*, 1998], the starting parameters for further simulations were set to 3 km layer thickness for a contiguous layer of 7 % reduced velocity. The source at 200 km depth was located at 0.3 km distance from the oceanic Moho inside the low-velocity layer.

The receiver line of Figure 2.5 shows displacement seismograms starting roughly 90 km inland from the coast line. Guided wave energy does not appear anywhere near the stations of the ANCORP network at the free surface. However, snapshots of the wave field show the development of a guided wave train with strong amplitudes propagating upwards along the slab surface (Figure 2.6). Considerable guided

wave energy builds up, but the waves continue to travel trenchwards with the same slowness originally formed by the direction of the layer. Despite the opening of the layer, guided waves in this context would only be observable at stations off shore.

Since the initial slab structure appears oversimplified and unsuited to explain the observations, the slab geometry was adjusted. The modified slab is now smoothly bending downward in the depth range of 90 to 150 km (hypocenters derived by *Graeber* [1997] and *Rietbrock et al.* [1997]) (see Figure 2.7). The subduction angle varies from 16° to 35°. A series of snapshots resulting from this enhanced model reveals that the waves are not strictly '*guided*' by the low-velocity layer, but are in fact partially transmitted toward the bounding rocks if the structure is not planar (Figure 2.8). At depth around 100 km, where bending is most severe, part of the energy leaves the low-velocity layer. After the decoupling process, this low-frequency energy proceeds with the same slowness as defined by the lower portion of the slab and same direction through the continental mantle and to the surface.

The slab geometry and alterations in subduction angle - not the local velocity structure of the slab - thus defines the point of appearance of guided wave energy at the surface. Within a small stripe around 140 km inland from the coastline (69.2°W - 68.8°W) guided waves are observed as P first arrivals (Figure 2.7). This is in accordance with the locations of stations AER, BOS and CHG of the ANCORP network (compare Figure 2.1).

A receiver at 69.0°W where guided wave energy is strongest (see above simulation), illustrates the typical pulse shape of guided waves for down-dip events (Figure 2.9a). The guided wave forms the low-frequency first arrival that lasts for 1 to 2 seconds. The energy trapping effect of the wave guide results in very large amplitudes compared to the higher frequency body waves which begin to dominate the wave field after around 1 second. The center frequency of the guided wave for the simulated layer thickness comes out to be 2 Hz, pulse shapes of the synthetics bear similarity to those observed for a focal depth of 200 km (Figure 2.9b).

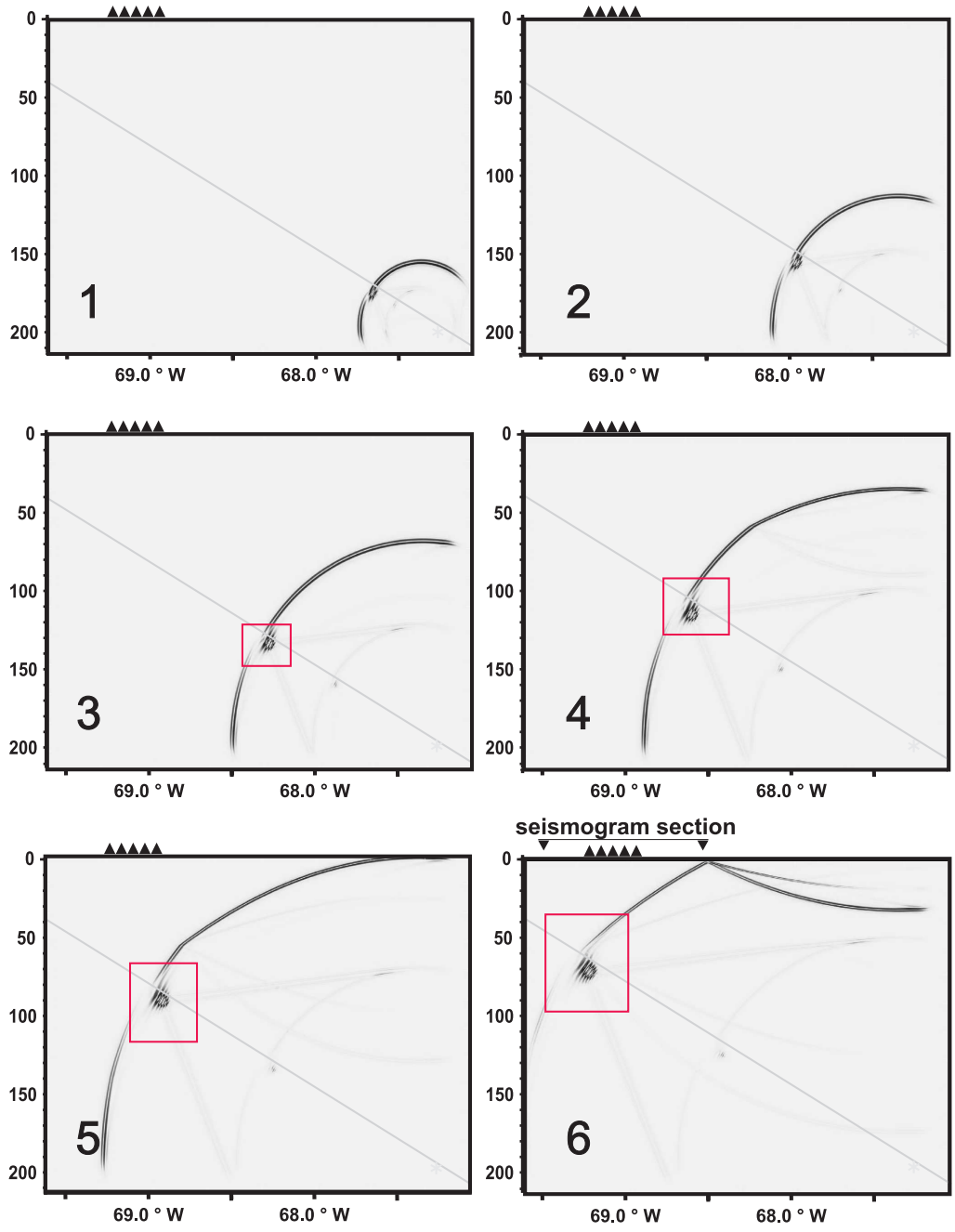

Figure 2.6: Snapshots of root mean squared ground velocity of 2D P-SV wave propagation (velocity model see Figure 2.5). The gray line marks the slab surface, the black frame highlights the guided waves traveling along the slab surface. Solid triangles indicate receiver positions, source position is indicated by a solid asterisk.

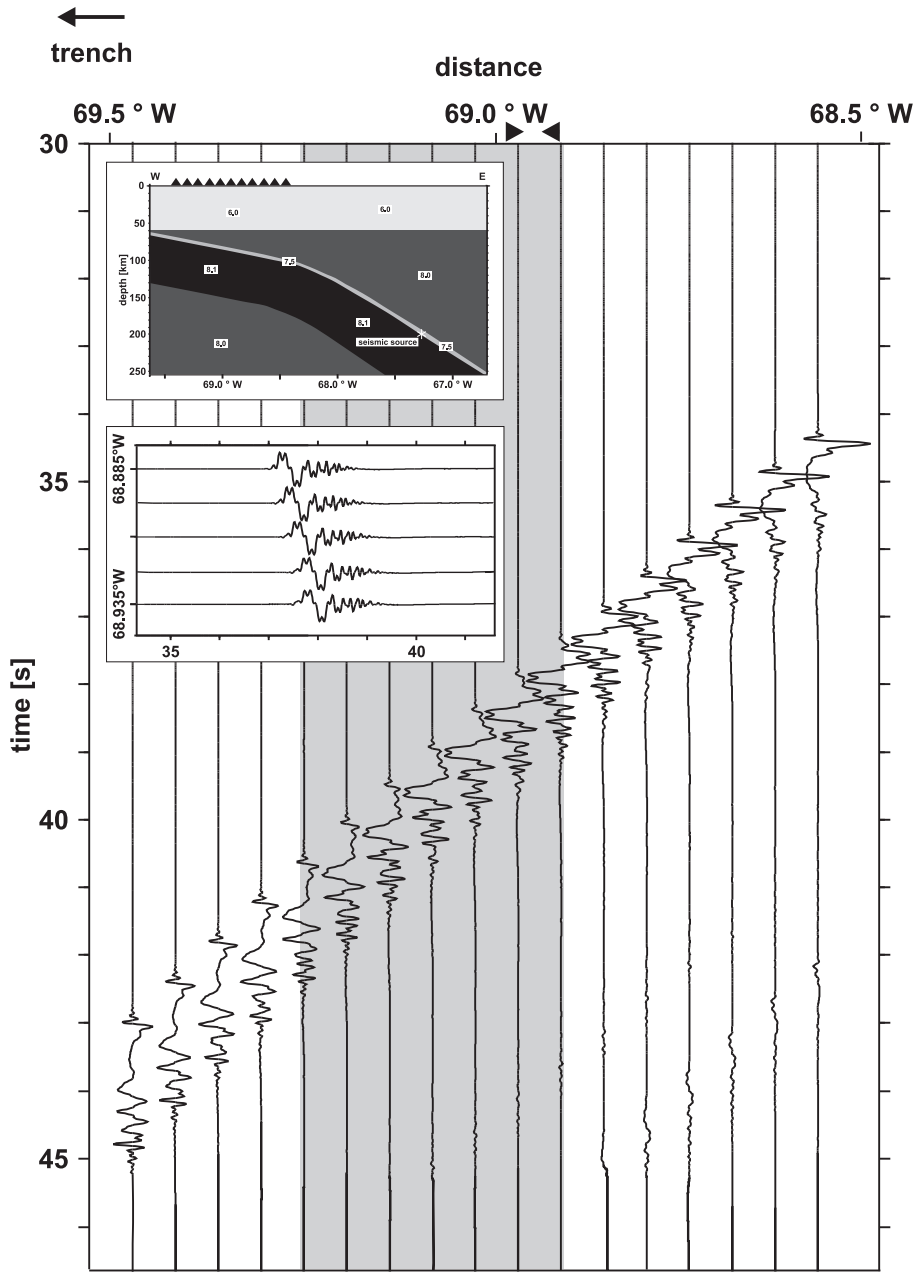

Figure 2.7: Seismogram section (displacement) for a bend slab structure with a layer of 7 % low velocity and 2 km width at its top. The shaded area marks the longitude range of ANCORP stations exposing distorted onsets. Insert 1: Velocity model. Insert 2: Enlargement on receivers located around 68.91°W (station AER).

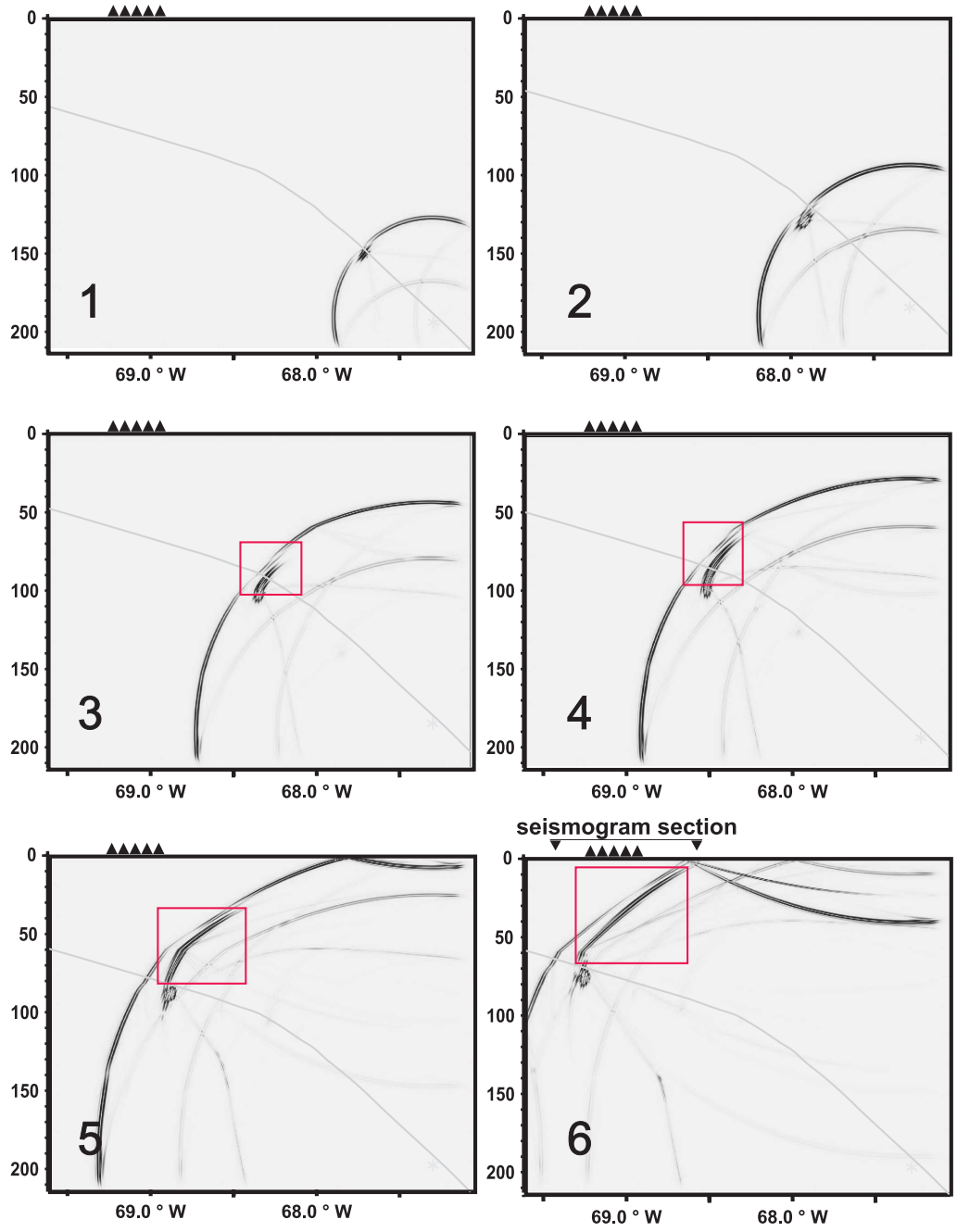

Figure 2.8: Snapshots of root mean squared ground velocity of 2D P-SV wave propagation (velocity model see Figure 2.7). The gray line marks the slab surface, the black frame highlights the parts of guided wave energy decoupling from the low-velocity layer. Solid triangles indicate receiver positions, source position is indicated by a solid asterisk.

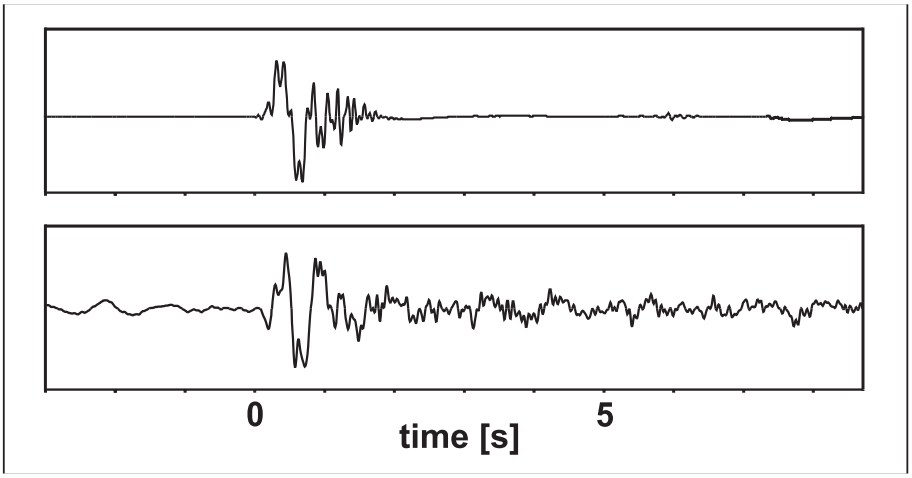

Figure 2.9: Aligned P onsets (displacement seismograms, low-pass-filtered with 8.5 Hz). a) Synthetic signal resulting from the bent slab model (see insert of Figure 2.7) (receiver position: 68.9°W). b) Observed signal for comparable hypocentral distance and receiver position (station AER).

Source depth and development of guided waves: The development of guided waves is controlled by the distance traveled within the low-velocity layer and thus by source depth. To shed some light on the '*birth*' of a guided wave train, synthetics for different source depths were calculated using the above model (Figure 2.7). Each synthetic seismogram is displayed together with a recorded signal of the corresponding source depth.

The seismic source is again located within the low-velocity structure to allow an efficient excitation of guided waves. A 7 % slow layer as proposed by *Bock et al.* [2000] is assumed. The layer thickness was changed from 3 km in the above tests using the straight slab model to 2 km for the bending slab model. This thickness resulted in the best fits taking into account the reduced propagation distance within the LVL due to the bend in the slab structure and decoupling of guided waves. The source depth varies between 110 and 250 km, accordingly hypocentral distances range from 140 to 350 km (Figure 2.10). The receiver remains at 69°W, where maximum wave amplitudes are observed.

Each of the synthetic seismograms in Figure 2.10 represents a characteristic pulse

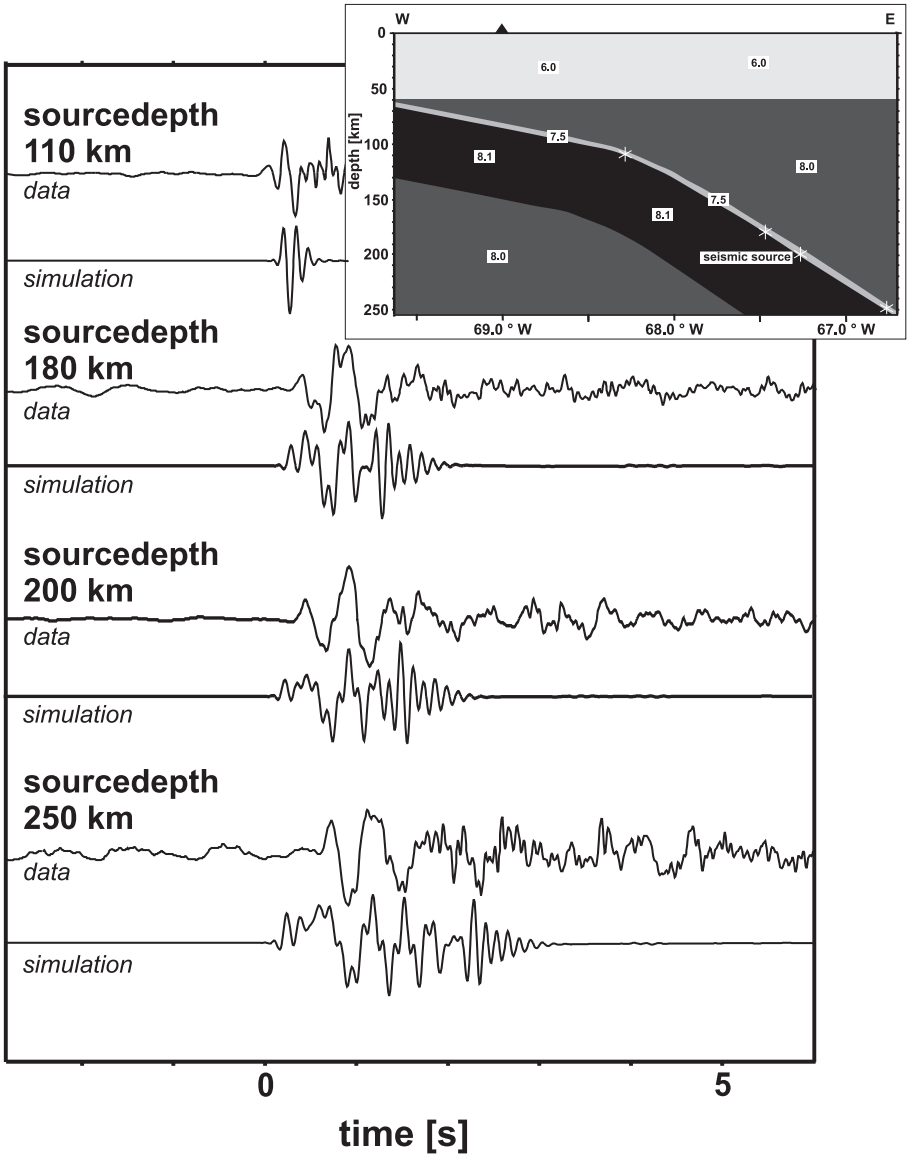

Figure 2.10: Synthetics (receiver at 69°W) for sources located inside the low-velocity layer (at 0.3 km perpendicular distance to subducted oceanic Moho) at various depths and ANCORP data (recorded at station AER) for the corresponding depths. Displacement seismograms are are aligned using a cross-correlation algorithm. Insert: Velocity model and source positions.

form matching the corresponding trace on the observed depth section:

For 110 km focal depth, virtually no guided wave energy is present. Signals travel only a few kilometers within the layer and then decouple when the kink at 100 km depth is reached, therefore no guided waves are excited. Accordingly, no low-frequency peaks are present in spectra of signals originating from source depth less than 110 km. Pulses of synthetics at 200 km focal depth travel along the low-velocity layer for approximately 150 km. The presence of low-frequency guided waves is evident, but at this depth only one to two cycles of the guided wave emerge. Higher frequency energy of phases traversing the lower slab and continental mantle contribute considerably to the waveform. The majority of the observed seismograms at around 200 km source depth bear resemblance to this pattern. Finally, the simulation for 250 km source depth exposes strong low-frequency guided wave energy (Figure 2.3 bottom). The growing ray path within the layer (230 km) causes more cycles to develop, much like in the observed data for source depth greater than 250 km.

The observations at different source depth fit well into the scheme of a developing guided wave. As expected, no effect is visible for focal depth above 110 km. Below that depth, guided waves form slowly and become more and more prominent with growing depth.

Wave guide thickness and frequency content of guided waves: The model of Figure 2.7 now serves as a basis for simulations with varying thickness of the low-velocity layer. Source depth is kept constant at 200 km resulting in hypocentral distances comparable to those of observed intermediate depth events (275 km). The layer thickness varies between 1.5 and 7.0 km. Waveforms differ slightly in number of cycles and amplitudes, but the major differences are in frequency content (Figure 2.11). Spectra of the first 2 seconds of the signals underline the tendency toward higher frequencies for thinner layers. Layers of average width greater than 4.5 km do not yield strong low-frequency guided wave energy in the relevant frequency region.

The spectrum of the 7 km thick LVL for example is clearly dominated by a high-frequency peak resulting from direct P waves arriving in the same time window as the guided waves. Thus, there is evidence that only a fraction of the former crust functions as a low-velocity wave guide. This is in accordance with studies at comparable depth for other slabs [*Helffrich*, 1996].

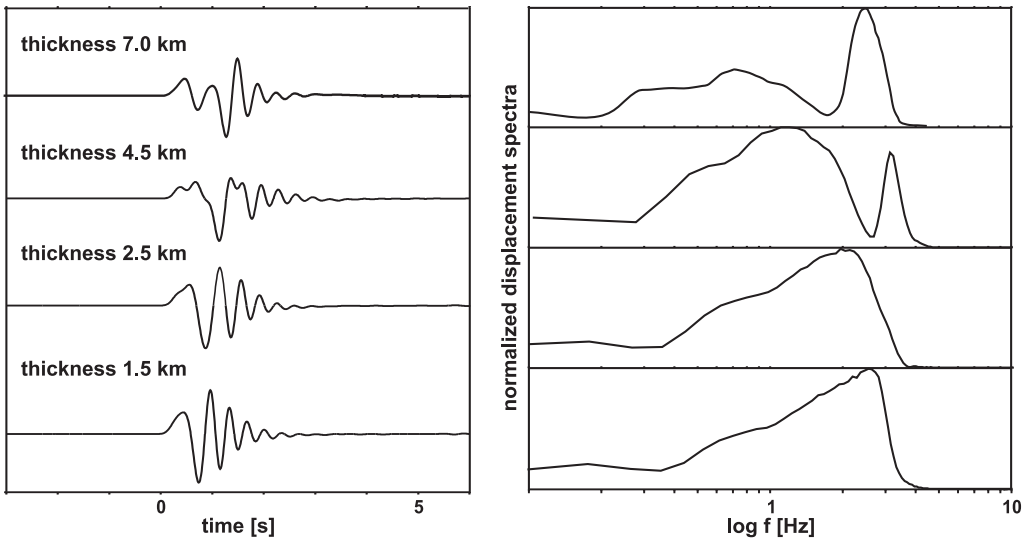

Figure 2.11: Synthetics and spectra for low-velocity layers of varying thickness (velocity model see insert of Figure 2.7). Source depth is 200 km, displacement seismograms are low-pass-filtered (3 Hz) to emphasize the low-frequency guided waves.

Layer thickness is coupled more than any other wave guide parameter with frequency content of the guided waves. On the other hand, estimation of thickness of subducted low-velocity crust is by no means straight forward. A number of other factors is known to produces frequency shift of the waves, namely propagation distance within the layer, velocity contrasts and attenuation effects [*Ben-Zion*, 1998].

Taking into account constraints given by the possible mineralogical regimes, the variation in velocity is restricted to 5 % to 15 % (untransformed gabbro) [e.g., *Helffrich and Stein*, 1993]. Variations within this range yield only marginal changes in the spectral content of the signals. Quality factors within the cold subducted crust are higher than 400 as imaged by *Haberland and Rietbrock* [2001], however dehydration processes may locally cause high attenuation.

Guided waves and source location: The appearance of guided waves is of course dependent on the source location relative to the wave guide [e.g., *Li and Vidale*, 1996]. Thus, the wave guide effect may constrain two major aspects of the subduction process. The guided wave observations 1) have potential to put constraints on localization of hypocenters on a much smaller scale than possible even by 3D location algorithms so far and 2) may help to determine up to which depth range oceanic crust persists and whether a complete eclogite transformation takes places. The following tests throw light on the sensitivity of the observed waveform to source location relative to the low-velocity layer.

Unlike assumed until recently, guided waves may, under certain conditions, also be excited by sources located outside the low-velocity layer [*Abers*, 2000; *Fohrmann et al.*, 2004]. A first exemplary test was carried out for a source at 200 km focal depth located below the low-velocity layer at a perpendicular distance of 7 km. Apparently, only little energy enters the layer (Figure 2.12), the wave guide effect is much less intense for sources located outside the structure. Moreover, emergent body wave phases now mask the guided wave energy, P onsets are dominated by rather high frequencies and do not resemble the observations. Considering attenuation and scattering present in the data, the low-frequency energy would probably be drowned out by the coda of P waves traveling within the faster slab.

The second issue connected to source location to be addressed here is the compatibility of our interpretation of the low-frequency onsets with a possible breakdown and transformation of the oceanic crust at depths in the range of 80 to 200 km [*Fukao et al.*, 1983; *Hori et al.*, 1985; *Helffrich et al.*, 1989]. If a complete transformation of gabbroic crust into eclogite at intermediate depth takes place, the layer of reduced velocity would be transformed into a high-velocity channel. Sources of deep events would then be situated in the continuation of the low-velocity subducted crust, but at several tens of kilometers distance beneath it. It is thus of special interest, whether the observed guided waves for focal depth greater than 160 km

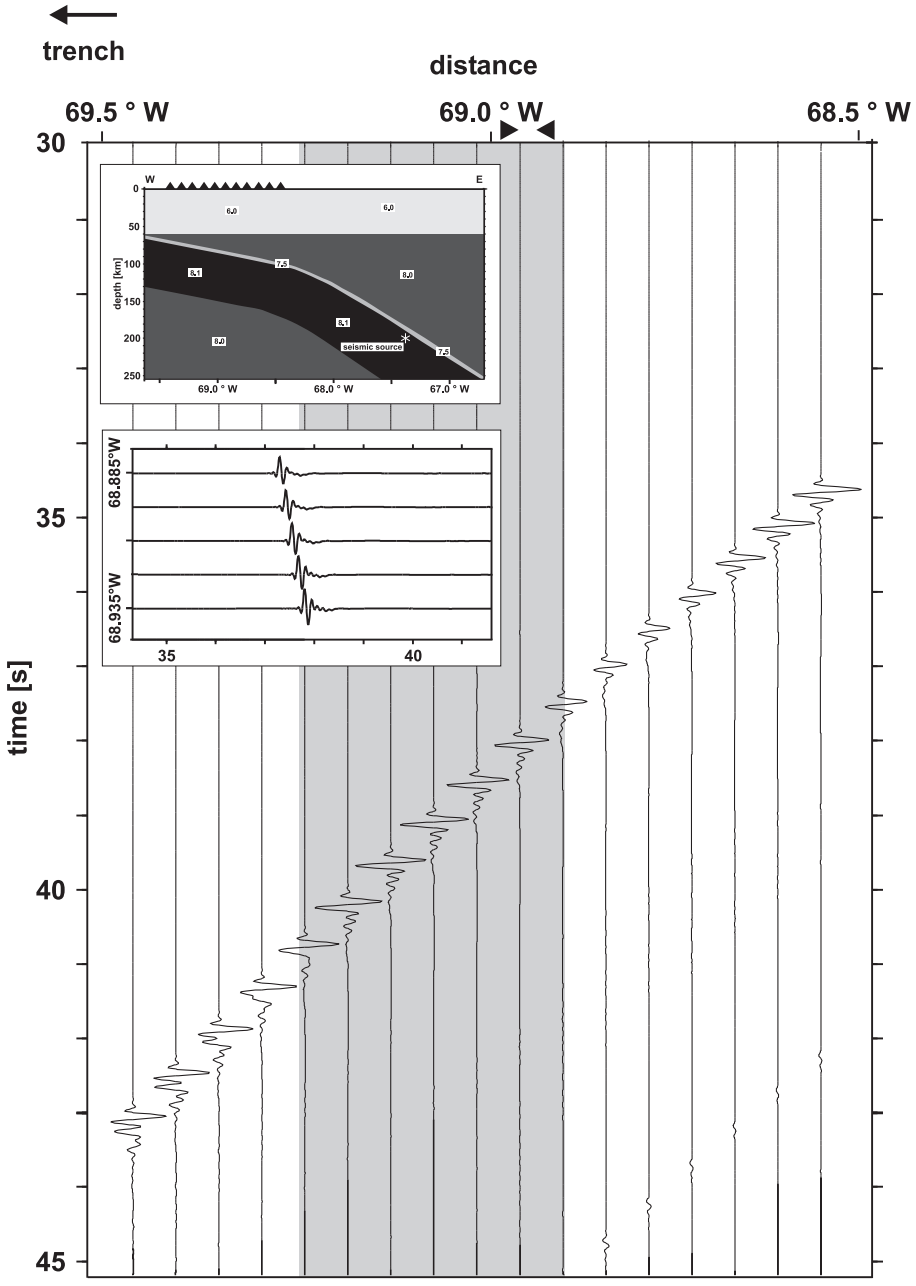

Figure 2.12: Seismogram section (displacement) for a source located 7 km below the subducted crust. Source depth is 200 km. Insert 1: Velocity model. Insert 2: Enlargement on receivers located around 68.9°W (station AER).

can be caused by a low velocity layer that exists only down to depth of 160 km (the maximum extent of layering inferred so far for the Chile-Peru subduction zone [*Bock et al.*, 2000]). The modified model in Figure 2.13 depicts this situation.

Synthetics for different focal depths for a layer that diminishes below 160 km depth are displayed in Figure 2.13 (receiver position is 69°W). The simulated P onsets are in accordance with the observations, high amplitude low-frequency energy arrives prior to higher frequencies (Figure 2.13). This means that the wave guide also influences signals from sources located near the slab surface in continuation of the former low-velocity subducted crust. Simulations with sources located more than 10 km away from the slab surface fail to produce guided wave energy (not shown). This possibly indicates that deep sources registered in the ANCORP campaign are located in continuation of the already transformed low-velocity structure, while events at intermediate depth are located inside the layer.

2.2.6 Conclusion

We summarize our results on the basic issues of (1) slab geometry and decoupling of guided waves, (2) source position and excitation of guided waves and (3) layer thickness and frequency content.

Decoupling of guided waves

Remarkably, we are able to observe guided waves at receivers well outside of the wave guide (distances around 100 km) and are thus provided with information on wave guide structures located at greater depth. In contrast, most wave guide studies for the Japanese slab and works on fault zones investigate primarily more or less shallow wave guides where receivers are situated directly above the structure [*Fukao et al.*, 1983; *Hori*, 1990; *Ben-Zion et al.*, 2003]. We focus on up-dip events, studies at other subduction zones reported similar waves using along-strike data [*Ansell and Gubbins*, 1986; *Matsuzawa et al.*, 1987; *Abers*, 2000]. The up-dip geometry provides

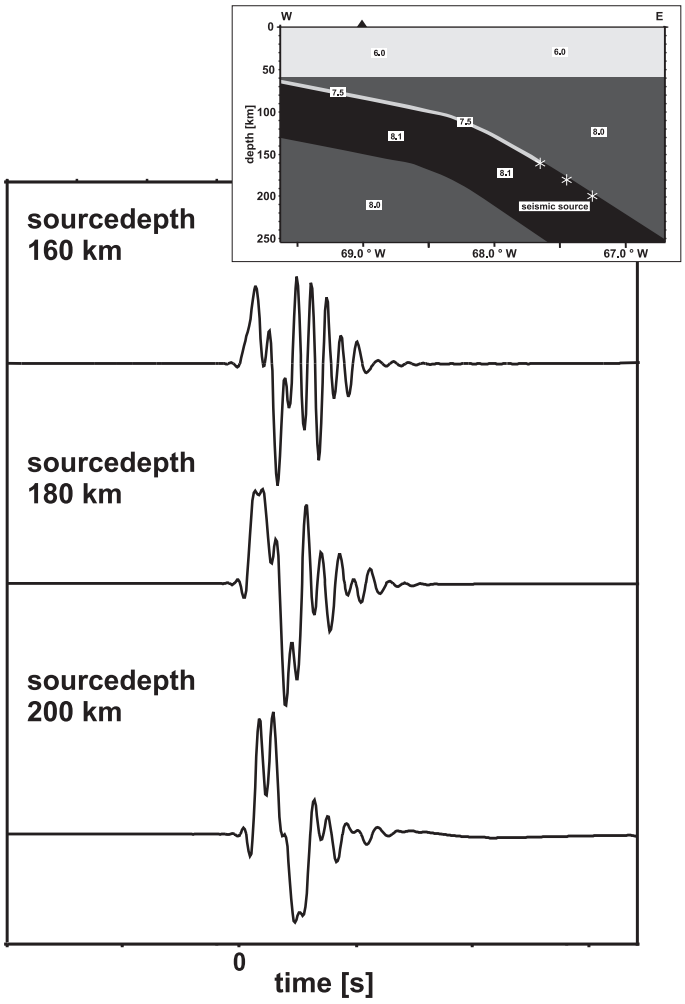

Figure 2.13: Displacement seismograms for sources located beneath the low-velocity subducted crust. The Low-velocity layer ends at 160 km depth. Sources are at 1.2 km perpendicular distance to the slab surface. Insert: Velocity model.

unique information on the decoupling process of the guided waves.

Within the subduction zone context, guided waves are observed only at certain receiver locations and not necessarily close to the coast line. Their point of occurrence is determined by the shape and geometry of the surface of subducted lithosphere. The average dip of the low-velocity layer determines the slowness and ultimately the point of occurrence of guided waves at the free surface. At the Chile-Peru subduction zone, the dip angle of approximately 36° at intermediate depth defines the point of appearance of guided waves at 68.9°W.

This restricts fast guided energy causing distorted P onsets at the investigated site to a small stripe centered around 69,8°W paralleling the strike of the subducted slab. Data of the PISCO '94 network located further south (24°S) also exposes low-frequency onsets for receiver locations in accordance with our model. We are confident to observe and utilize similar effects at other subduction zones, provided that data from sections with small receiver spacing perpendicular to the strike are available.

Source location

The observed wave guide effect constrains source locations relative to the layer. Our study confirmed that the effect does virtually not occur for sources located in the subducted slab outside a continuous low-velocity layer. Thus, there is evidence that intraslab events with focal depth down to approximately 160 km are located within a few kilometers of the layer, a finding already proposed at other subduction zones so far [*Matsuzawa et al.*, 1986; *Abers*, 2000].

However, our results do not imply that all source locations are restricted to within such a thin layer at the top of the slab surface. Simulations indicate that sources situated beneath a finite low-velocity layer can still produce the effect, if they are located in continuation of the structure (i.e. near the slab surface). To draw sound conclusions, however, further detailed investigations are needed. In particular, source mechanisms other than explosive sources have to be tested. Then source locations relative to the slab surface can potentially be restricted for given event depths and ultimately, inferences on the depth of breakdown of the low-velocity layer will be possible.

Wave guide thickness

The frequency content of observed guided waves is a strong function of the average thickness of the structure. Comparison of finite difference simulations with the data

recorded at station AER of the ANCORP network show that velocity contrasts of metastable gabbro (7 % low velocity) result in very promising pulse shapes for a layer thickness of 2 km (compare Figure 2.10). Damping effects that were not considered in the elastic simulations may influence the layer thickness [*Ben-Zion*, 1998]. However attenuation leads to an overestimation of the layer thickness. Thus our estimates are representing upper limits for layer thickness. Simulations give strong evidence that below 100 km depth a layer of 7 km average thickness (i.e. the width of the subducted oceanic crust) can not be reconciled with the data, even a layer of 5 km width can neither match the 2 Hz frequency peak present in the data nor excite sufficient guided waves (see Figure 2.11).

Consequences for the subducting Nazca plate

Our findings show that the observed frequency effect is caused by guided waves developing in a thin low-velocity layer located in the continental mantle beneath northern Chile at 21°S. The part of the low-velocity structure illuminated by guided waves is situated at depth greater than 100 km. It resembles a rather thin layer ($<$ 4.5 km) of 7 % low velocity at the slab surface reaching down to depth of 160 km, probably further. We therefore conclude that we do not image an untransformed basaltic oceanic crust (which we expect to be thicker) but a low-velocity layer that results from mineralogical phase changes taking place within or in the vicinity of the former subducted crust at the interface between continental mantle and subducted lithosphere. For comparable depth, studies at other subduction zones have so far found evidence for a similar low-velocity region [*Matsuzawa et al.*, 1987; *Abers and Sarker*, 1996; *Helffrich and Abers*, 1997; *Abers*, 2000]. Possible compositions for such a layer have been suggested e. g. by *Helffrich* [1996],*Peacock* [1996] and *Hacker et al.* [2003a, b].

Our results regarding the Chile-Peru subduction zone seem to agree with the latest mineralogical model proposed by *Hacker et al.* [2003a, b]. In this scheme,

subducted crust in the depth range of interest is depicted as a coarse grained, partially eclogized low-velocity layer (the lower crust) topped by dehydrated upper crust. From the simulated layer width for the Chile-Peru slab, we deduce that the guided waves image the slow, lower part of subducted crust at intermediate depth. Whether or not this interpretation is to be favored among the other possible mineral assemblages requires further research. In any case, the wave guide is a persistent feature of the subducted Nazca slab and the Chile-Peru subduction zone is one more example within the Pacific subduction zones that features a low-velocity layer at the top of the slab surface extending to depths of 100 to 160 km.

Chapter 3

Exploring fundamental parameters of the subduction zone wave guide

3.1 Preface

The up-dip observations made at the Chile-Peru subduction zone presented in the foregoing chapter, confirm the hypothesis of a wave guide for intraslab events at the Nazca slab.

Commencing by looking at guided waves as a wave field phenomenon, we now clarify geometrical aspects regarding the distribution of guided waves as well as lateral changes in the wave field. Slab geometry, i.e. the variation of the wave guide from a straight layer, is revisited and subsequently effects of decoupling on the observed guided wave are analyzed on an advanced level.

In this section we primarily seek to determine the strength of coupling between observed pulse shapes and fundamental wave guide parameters in the context of subduction zones. We refrain from simultaneous inversion of parameters such as wave guide width and velocity contrast leaving this to faster, but less flexible methods [e.g., *Abers*, 2000, 2005], and use the advantages of the P-SV finite difference method to specifically investigate on a number of parameters relevant for P guided waves at subduction zones.

First, the topic of double couple (DC) sources is of major interest in the context of subduction zone guided waves because of the variations in source mechanisms of

intermediate depth earthquakes and the related issues of energy leakage and P-SV conversion. Second, the topic of bending of the low-velocity layer following the slab surface and subsequent decoupling of guided energy is addressed in detail. This points to one of the basic differences of subduction zones compared to observations at fault zones and the associated analytical solutions for wave propagation [e.g., *Hough et al.*, 1994; *Michael and Ben-Zion*, 1998; *Peng et al.*, 2000]. In the present case, the signal is not recorded within the wave guide but several tens of kilometers far from it. We seek to clarify to which degree the two cases are compatible.

The addressed issues are most relevant not only for the Chile-Peru observations, but as well for investigations at other subduction zones [e.g., *Fukao et al.*, 1983; *Hori et al.*, 1985; *Oda et al.*, 1990; *Lin et al.*, 1999; *Abers*, 2005]. Therefore the slab model introduced in this chapter is designed to describe typical up-dip slab geometries using parameters explicitly connected to the wave guide effect. A gradual change of slope with depth is a common feature of subducted slabs, more precisely the majority of slabs expose a marked change in subduction angle at the depth range of intermediate depth events [*Kirby et al.*, 1996; *England et al.*, 2004]. We divide the slab in two depth regions of different subduction angle connected by a circle segment and show that guided wave observations originating from deep sources are directly linked to this geometrical feature.

Finally we consider that processes in the subducted crust are probably kinetically hindered and in addition oceanic lithosphere is flawed principally by normal faulting causing heterogeneities in the subduction zone wave guide [*Christensen and Ruff*, 1988; *Ranero et al.*, 2003]. Therefore the effects of velocity undulations within the wave guide as well as changes of velocity contrasts along the slab surface are incorporated in a number of advanced velocity models presented at the end of this chapter.

3.2 Guided waves at subduction zones: Dependencies on slab geometry, receiver locations and earthquake sources

(**article in revision:** Martin, S., and A. Rietbrock, Guided waves at subduction zones: Dependencies on slab geometry, receiver locations and earthquake sources, *Geophys. J. Int.*, 2004.)

3.2.1 Abstract

We investigate the geometry of deep subduction zone wave guides (depth > 100 km). The wave field characteristics for up-dip profiles are described and compared with data recorded at the Chile-Peru subduction zone. Observed distorted P onsets at stations in northern Chile near 21°S can be matched by 2D finite difference simulations of a thin low-velocity layer atop the slab in an IASP91 velocity model. The replacement of the low-velocity layer by simple random velocity undulations in the slab in the same model cannot explain the observations.

Varying slab geometries are investigated and the distribution of guided wave onsets originating in deep wave guides is predicted relative to the slab surface. Further, double couple source position and orientation is explored and found to be closely limited by the guided wave observations. Sources situated above the layer and at distances more than 2 layer widths below the subducted Moho are not suitable. For the remaining favorable source locations a strong link between pulse shapes and fault plane dip angle is evident.

We conclude that up-dip guided wave observations at subduction zones follow a simple pattern given by slab geometry and modified by source position. The resulting onsets are shaped by layer thickness and velocity contrast and further influenced by the shape of the slab surface.

3.2.2 Introduction

Subduction zones are regions of intense earthquake activity up to great depth. Sources are located inside the cool subducting lithosphere and as a consequence, seismic radiation from subduction zone earthquakes is strongly affected by the interior slab structure. In particular by basaltic oceanic crust remaining seismically distinct from mantle rocks until transformed at greater depth. Recent seismic measurements utilizing waves reflected or converted at the slab surface [e.g., *Snoke et al.*, 1978; *Fukao et al.*, 1983; *Helffrich and Abers*, 1997; *Bock et al.*, 2000] as well as guided waves [e.g., *Ansell and Gubbins*, 1986; *Hori*, 1990; *Abers*, 2000; *Martin et al.*, 2003] provide the first direct constraints on the structure of subducted crust at that depth. Early models assuming uniform slab structure [*Ringwood*, 1972] and subducted crust transforming and dehydrating completely at shallow depth have to be refined according to these observations. Reduced seismic velocities near the surface of the subducted slab have been detected at depths where eclogite transformation should long be completed, primarily for the Japanese subduction zone [*Matsuzawa et al.*, 1987; *Hori*, 1990; *Hurukawa and Imoto*, 1992; *Iidaka and Obara*, 1993; *Oda and Douzen*, 2001] and subsequently for several more, e.g. the Alaskan [*Abers and Sarker*, 1996; *Helffrich and Abers*, 1997], the Philippines [*Lin et al.*, 1999], and Chile-Peruvian [*Bock et al.*, 2000; *Yuan et al.*, 2000; *Martin et al.*, 2003].

Consequently the depth and type of phase transformations and dehydration processes during the course of subduction is subject of considerable debate [*Fukao et al.*, 1983; *Tatsumi et al.*, 1994; *Schmidt and Poli*, 1998; *Hacker et al.*, 2003a, b; *England et al.*, 2004].

The mechanisms of intermediate depth seismicity and possible connection to devolatisation processes can only be explored backed by precise knowledge of internal slab structure. At the moment refined crustal models including a separation into distinct bands of seismicity [*Hacker et al.*, 2003b; *Cassidy and Waldhauser*, 2003; *Rietbrock and Waldhauser*, 2004] are proposed and could be constrained by knowl-

edge of internal velocity structure. Further, the state of subducted crust may play a role in the composition of geochemical tracers found in arc lavas. Differences in the amount of tracers may possibly be explained by variations in the hydration of the down-going plate or by processes that transmit fluid from slab to arc [*Abers et al.*, 2003]. In addition, the role of the basalt eclogite transformation in driving lithospheric plate motion [*Ringwood*, 1972] is currently being reconsidered accounting for kinetical hindrance of dehydration and eclogitization [*Fukao et al.*, 1983].

To detect slow crustal material in subduction zones, we employ the unique properties of guided waves. Slow layers at the top of subducting slabs promote the entrapment of seismic energy, resulting in guided waves with high amplitudes and low-frequency onsets. Observations have been reported aplenty in recent years. There is seismological evidence for circum-pacific subduction zones featuring low-velocity layers (LVLs) at various depths sometimes in excess of 150 km. Although the existence of a LVL down to intermediate depth is by now well established, mineralogical interpretations are still speculative due to lack of constraints regarding the state of this crustal layer. E.g., whether seismic sources are located inside, above or below the layer and in turn if the layer is located above the slab surface or represents part of the subducted crust.

In the following pages we tackle a number of issues in conjunction with the low-velocity structure by analyzing guided waves originating in the layer. Up to now only little consideration has been given to structural details such as lateral and vertical variations of the layer and the resulting complex wave field including guided waves as well as direct and refracted P waves. A number of recent studies employed high-frequency approximations or analytical solutions for plain low-velocity structures to deduce inferences on subducted crust, either technique being insufficient to accurately take into account dispersive effects and varying geometry, respectively.

The presented finite difference (FD) simulations aim to bridge two gaps in the current research on guided waves at subduction zones. (1) Test the reliability of

estimates from plain layer analytical solutions and reflectivity calculations by exploring the complicated source-receiver geometry at a subduction zone setting. (2) Shed light on possible high-frequency effects caused by double couple (DC) sources in the fine structure (2.0 km width) that most 3D modeling approaches [e.g., *Igel et al.*, 2002] and seismic methods such as tomography fail to resolve so far.

We investigate guided waves caused by intermediate depth events in the Chile-Peru slab at 21°S, addressing excitement, propagation and observation of guided waves in respect to DC source position and slab geometry. Guided wave amplitude distribution is predicted for up-dip events with a special focus on energy partitioning. Further, guided waves are used to categorize source position relative to the subducted oceanic Moho. Finally, the IASP91 velocity model is incorporated in the simulations to test the effect of velocity gradients on the excitation of guided waves.

3.2.3 2D finite difference modeling of subduction zones and observations at the Chile-Peru slab

Finite difference algorithm

We employ 2D FD simulations to model wave guide effects as well as internally reflected and converted phases caused by low-velocity structures at subduction zones. The FD algorithm run on a cluster computer holds two advantages: (1) the high spatial resolution permits to resolve structures even smaller than 1 km with ease. (2) synthetics are computed up to 7.5 Hz, i.e. simulated seismogram data cover the full frequency range of most dispersive onsets currently observed at subduction zones [*Abers*, 2005].

In the 4th-order staggered grid FD scheme the elastodynamic equation of motion is expressed in terms of velocity and stress [*Virieux*, 1984, 1986]. Since guided waves cause frequency effects, special care was taken to prevent numerical dispersion that would distort the frequency content of guided waves. The small grid spacing guarantees that numerical dispersion is less than 1.0 % even for the highest frequencies

of S waves and propagation distances up to 300 km.

Among the options to include DC sources in the 2D staggered grid scheme, the simple and effective approach of *Coutant et al.* [1995] was favored. DC sources of varying dip angle are implemented by stress excitation, efficiently centered at a single grid point. The scheme is rounded out using the planar free surface condition given by *Levander* [1988] employing a zero stress formulation to produce accurate and numerically stable surface reflections. The artificial edges of the model are damped by simple exponential terms [*Randal*, 1989].

The accuracy of the seismograms produced by the scheme was verified by comparison with reflectivity synthetics [*Fuchs and Müller*, 1971; *Wang*, 1999] for a layered half-space applying 2D to 3D corrections for amplitudes [*Amundsen and Reitan*, 1994]. The model space is distributed on parallel computers and 2D simulations of a down-dip section (280 km x 220 km) are now run on 16 nodes of a Beowulf cluster (733 MHz Pentium III dual processor) within 10 hours real time.

2D model of the Chile-Peru slab and data

Data of the ANCORP'96 campaign and first tests on guided wave propagation in the Nazca slab are described in detail in *Martin et al.* [2003]. A map of the area including source locations is depicted in Figure 3.1a, the Chile-Peru observations are presented in Figure 3.2. ?? Events are in the narrow magnitude range of Ml = 2 to Ml = 4 [*Rudloff*, 1998]. Expected fault plane radii are smaller than 1 km [*Brune*, 1970, 1971] and source functions are expected to be sufficiently flat in the analyzed frequency range (1.0 to 5.0 Hz) [*Lay and Wallace*, 1995]. The source mechanisms are predominantly down-dip extensional [*Rudloff*, 1998] and there are no systematic changes with depth.

Selected seismograms and stacked spectra illustrate the systematic effects of frequency distortion at ANCORP'96 receivers. Among the 32 stations of the network, station AER is located ideally to observe low-frequency guided wave onsets for an

up-dip geometry (Figure 3.2a). At AER the guided wave forms the first arrival and onsets contain increasing quantities of low-frequency energy for increasing source depths. Spectra of the onsets at AER show strong low-frequency energy indicating the presence of guided waves for sources deeper than 110 km only (Figure 3.2b).

In the following tests, basic model geometry and parameters such as layer width and velocity contrasts are based on the findings of the preceding study [*Martin et al.*, 2003]. A simplified 2D seismic velocity model of the dipping slab at 21°S serves to investigate the effects of a LVL atop the slab surface (Figure 3.1b). The wave guide is modeled as a uniform layer of 2.0 km thickness and 7 % velocity reduction, the slab surface is parameterized by an upper and lower section of constant subduction angle joined by a circle segment. The shape of the slab surface at 21°S is based on the studies of *Graeber and Asch* [1999] and *Schurr et al.* [2003]. Both tomographies show a pronounced bend near 100 km depth. The change of subduction angle at intermediate depth is a common feature to many subduction zones [*England et al.*, 2004].

Quality factors in the low-velocity layer are assumed to be higher than 400. No areas of high attenuation were imaged in the Chile-Peru, or other subducted slabs [*Hashida*, 1989; *Haberland and Rietbrock*, 2001], and temperatures in the slab are low such that Q values are expected to be comparatively high. Therefore the influence of attenuation is neglected, noting that the issue can not ultimately be discussed since Q factors at such small spatial scales can up to now not be resolved. We also point out?? that Q factors would have to be as small as 100 to affect guided wave characteristics [*Ben-Zion*, 1998].

The model space covers 280 x 220 km (5900 x 7400 points), the receiver position is at 68.9°W. The varying source positions will be referred to by source depth and perpendicular distance to the oceanic Moho (positive sign for sources above, negative sign for sources below). The DC source orientation is expressed relative to the subducted slab at 200 km depth (subduction angle at 200 km depth is 42°), e.g.

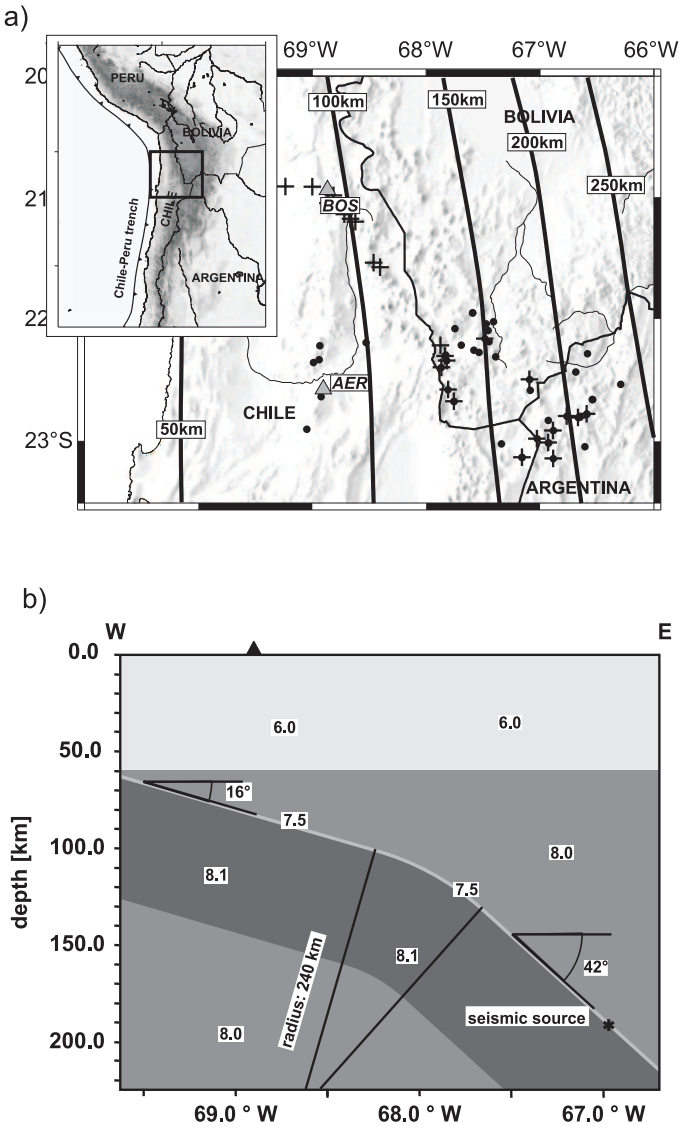

Figure 3.1: a) ANCORP'96 temporary seismic network and events recorded at stations AER (22.58°S, 68.91°W) and BOS (20.94°S, 68.87°W). Stations are equipped with Mark L-4A-3D sensors. Solid lines represent depth contours. Events are indicated by dots (recorded at AER) and crosses (recorded at BOS). The 43 events at station AER form an up-dip section centered at 22.6°S, the 23 events at station BOS form a slightly rotated up-dip section centered at 22.0°S. b) 2D section displaying the standard up-dip model used for station AER. The triangle marks the receiver position, the asterisk indicates the source position, labels and shades indicate P velocities.

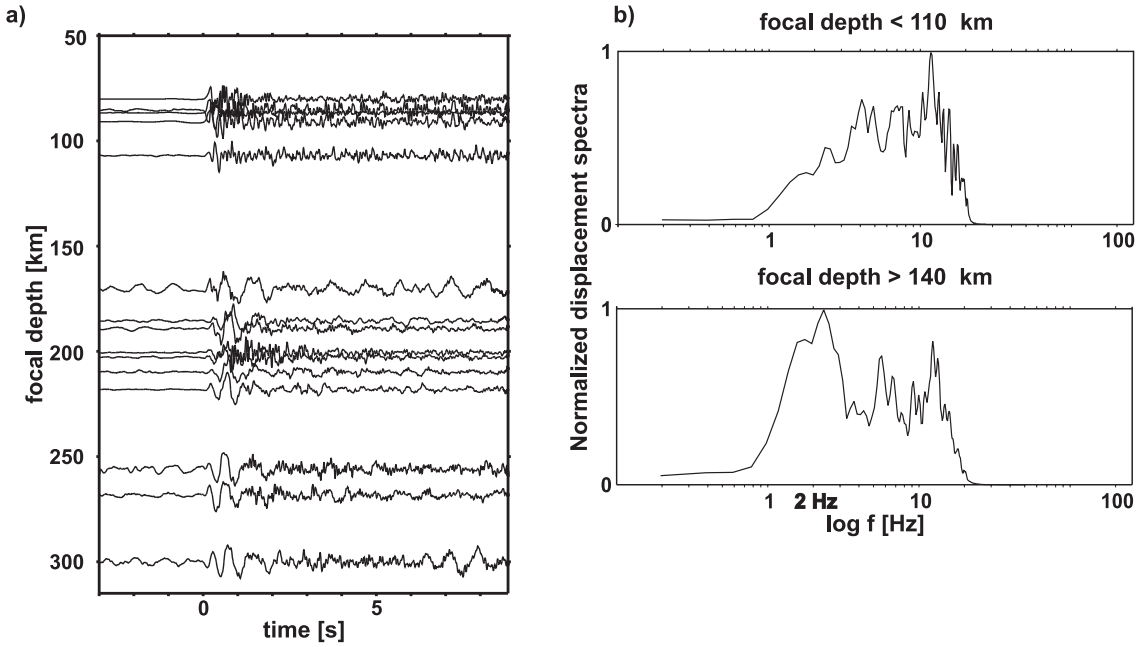

Figure 3.2: a) Seismograms at station AER. P onsets are aligned on first arrivals and plotted by focal depth. Seismograms show ground displacement, band-pass-filtered between 0.5 Hz and 8.5 Hz, amplitudes are normalized. b) Stacked displacement spectra of onsets (first 2 seconds) of all events contained in the up-dip section (Figure 3.1a) with focal depth < 110 km and > 140 km, respectively.

fault plane solutions paralleling the slab surface are assigned a dip angle of 0°. All presented synthetics and data are vertical component recordings, synthetics are band-passed between 0.5 Hz and 7.5 Hz, spectra show the frequency content of a 2 second time window of the arrivals.

3.2.4 Observing guided waves - influence of geometry of the slab surface and receiver position

Almost all reports on subduction zone guided waves state that only particular stations of seismic networks show the low-frequency effect [*Oda et al.*, 1990; *Lin et al.*, 1999; *Martin et al.*, 2003]. Observations originate in general from near coastal stations but no clear pattern regarding the occurrence of guided energy has yet been established.

Naturally, guided wave amplitudes are highly focused around the wave guide [e.g., *Ben-Zion*, 1998]. Dependent on slab geometry, energy must leak from the slab at depth to reach the surface at the deployed stations and the bending of the slab was found to be responsible for the decoupling [*Martin et al.*, 2003]. Subsequently, the point of decoupling is destining the further ray path and therefore the impingement of guided wave energy at the free surface. Since data are recorded at a distance from the wave guide, inferred layer properties may be biased. Therefore it is essential to examine effects of slab geometry on guided wave observability and pulse shapes.

Receiver geometry

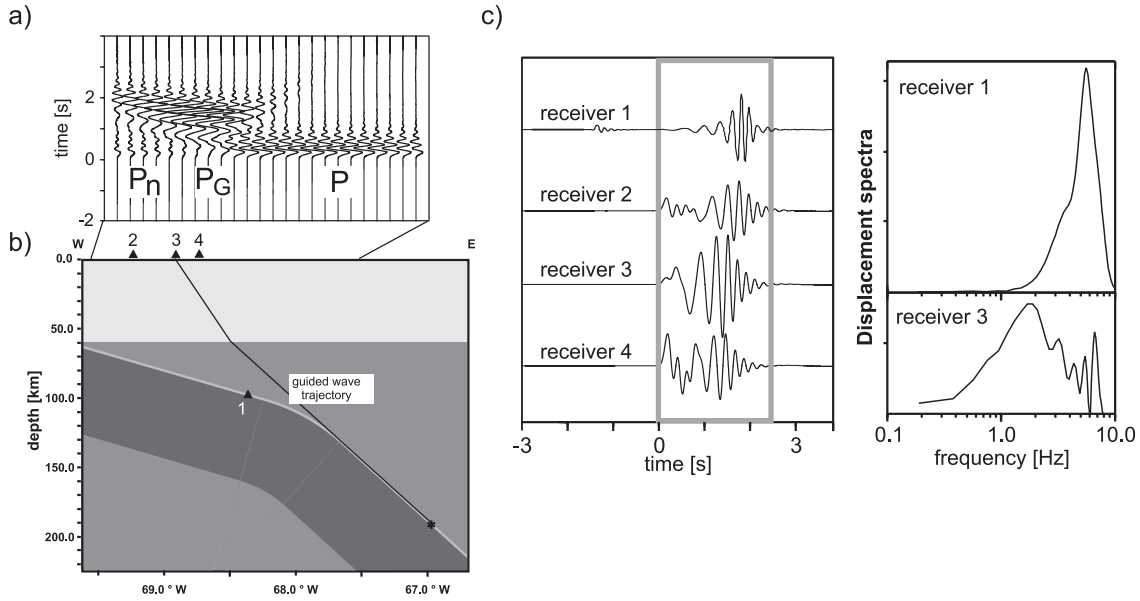

Figure 3.3: 2D velocity model and seismogram section. a) and c) Synthetic displacement seismograms (low-pass-filtered with 7.5 Hz) and spectra. Labels indicate refracted (P_n), guided (P_G) and direct wave (P). DC source depth is 200 km, source distance to the oceanic Moho is 0.5 layer width, dip angle is 45°. Receiver 1 is located in the middle of the LVL at 85 km depth, receiver 2 is at 69.2°W, receiver 3 is at 68.9°W (impingement point) and receiver 4 is at 68.75°W. b) Seismic velocity model (for velocities compare Figure 3.1b). Triangles represent receivers, the asterisk marks the source position, the solid line indicates the guided wave ray trajectory, shades represent p velocity (compare Figure 3.1b).

The first FD simulation illustrates the difference in observations inside, and

at various positions outside of a low-velocity structure (Figure 3.3), an important factor to be taken into account when analyzing guided waves recorded at the earth's surface.

The difference in appearance of the guided wave inside and outside of the wave guide is due to its dispersive character. Dependent on frequency, guided wave energy propagates partially with near mantle velocities and partially with the velocity of the LVL or slower. Effectively, receivers situated in the mantle are picking up more energy of frequencies traveling with high velocities, whereas receivers in the LVL (slow medium) are picking up more energy traveling with lower velocities. The pulse shapes of receiver 1 and 3 therefore show two characteristic types of guided wave observations. Inside the layer (receiver 1), the wave train has maximum amplitudes for energy propagating with velocities smaller than that of the LVL. In contrast, outside of the LVL, the pulse has its highest amplitudes for the energy arriving faster than the velocity of the LVL. The pulse seen outside of the layer will therefore be dominated by the fast low-frequency energy of the normal mode and the fast energy of higher modes. Correspondingly the monofrequent frequency peak near 7.0 Hz in the spectrum of receiver 3 results from a higher mode and is characteristic for the given layer width, velocity contrast and geometry.

As a consequence, guided wave observations at subduction zones potentially consist of separate phases: a) A dispersive normal-mode guided wave that travels at the most with the slowest velocity of the host rock, b) higher modes of guided waves contributing fast high-frequency energy to the dispersion pattern, and c) a direct or refracted phase propagating with velocities of subducted mantle.

Receivers 2 to 4 of Figure 3.3 stand for three distinct regions of the resulting wave field: Near the trench the onset is formed by a fast P wave traversing the slab followed by a guided wave (receiver 2), further inland, low-frequency guided wave onsets are predominant (receiver 3). Finally, at stations located even closer to the source, again a direct P wave appears in onsets (receiver 4). Observations at slabs often show an

onset with relatively small amplitudes, followed by a strong high-frequency phase [e.g., *Hori*, 1990; *Helffrich and Abers*, 1997; *Abers et al.*, 2003]. These observations may either consist of a guided wave including late high amplitudes (receiver 3, station AER in Figure 3.2) or a fast P wave followed by a guided wave (receiver 2). The latter type of onset can be observed at receiver BOS where the slab geometry causes a separate direct phase to reach the station before the guided arrival (Figure 3.4). The first arrivals do not expose the striking low-frequency onsets seen at AER, but instead the guided wave maximum energy constitutes a second delayed arrival for source depth greater than 140 km.

To avoid misinterpretation, it is crucial to define the position of the recording station in the laterally varying wave field and hence account for slab geometry and the depth of decoupling of the wave from the slab. In the following simulations, the seismograms are recorded at position of receiver 3, where the elongation of the lower slab surface intersects with the free surface and guided energy forms the onset. This receiver position will be referred to as IP (impingement point of the ray trajectory with the free surface) and is almost identical with the position of station AER of the ANCORP network.

Slab geometry

Partitioning of energy due to bending is one important mechanism causing leakage of guided energy from the slab surface [*Martin et al.*, 2003], which could explain many guided wave observations at circum-pacific subduction zones, especially for deep sources. The following two test sets investigate on influences of bending on pulse shapes and frequencies in comparison to guided waves propagating in plain LVLs.

Figure 3.5 compares pulses registered at station IP for variations in subduction angle. The lower portion of the slab remains identical to make sure that excitation and propagation distance of guided waves is not influenced. The subduction angle

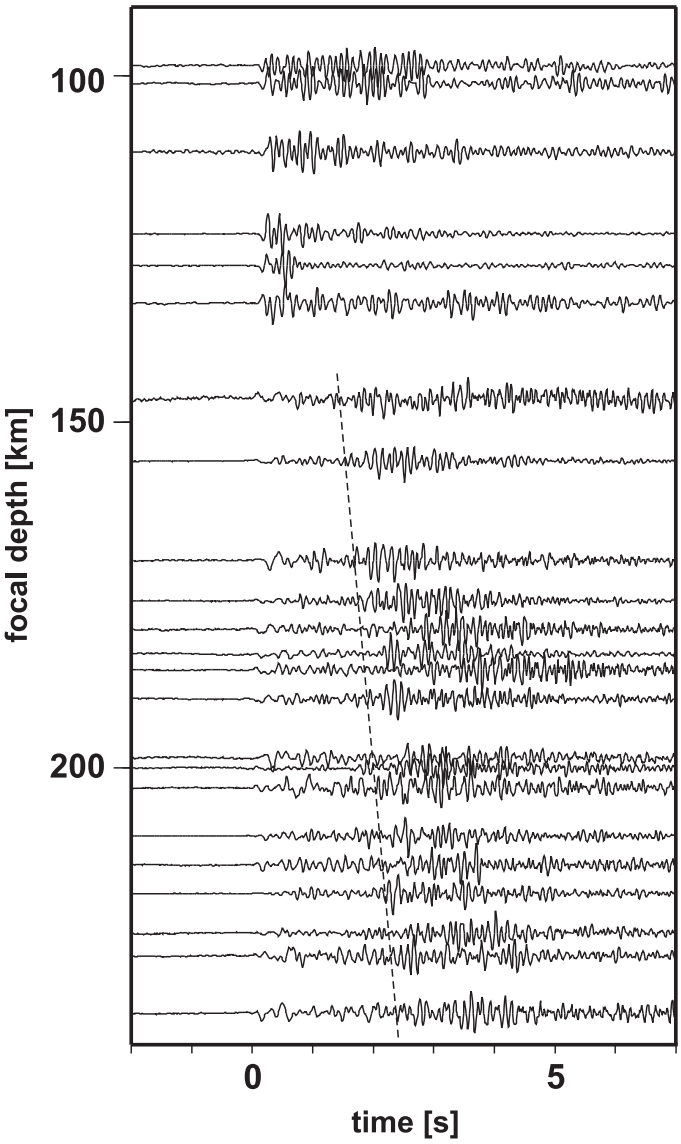

Figure 3.4: Seismograms at station BOS (see Figure 3.1 for location). P onsets are aligned on first arrivals and plotted by focal depth. Velocity seismograms are band-pass-filtered between 0.5 Hz and 12.0 Hz, amplitudes are normalized. The dashed line indicates a second arrival for source depth > 140 km.

of the upper part of the slab varies between 30° and 10° resulting in more and more severe bending of the LVL. The varying slab geometries may be compared to those published by *England et al.* [2004], i.e. the almost plain slab standing for rather shallow subduction zones like the Alaskan and the bend slab resembling the Central Aleutian or Marianas subduction zones.

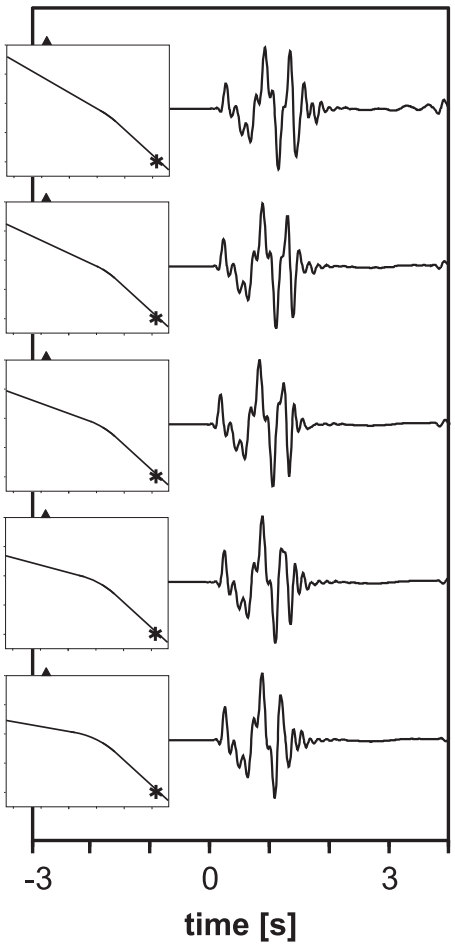

Figure 3.5: Bending of slab surface: Displacement seismograms for varying subduction angles (DC source dip angle is 45°). Source depth is 200 km, distance to subducted Moho is 0.5 layer width. Synthetics are low-pass-filtered with 7.5 Hz. Subduction angle at depth $>$ 110 km is 42°, subduction angle at depth $<$ 110 km is (top to bottom): 30°, 25°, 20°, 15°, 10°. Inserts: Sketch of slab geometry. Asterisks mark source position, triangles indicate receiver position.

The simulated P arrivals remain almost unchanged regardless of the markedness of the kink in the subducted crust (Figure 3.5). The tests proof that decoupling

takes place whether the slab is bending severely or slightly. Amplitudes of guided waves are not influenced, nor is the frequency content at station IP. Even a rather small change of direction of the wave guide (12°) permits part of the trapped energy to escape and reach IP. It is therefore misleading to presume that waves always sample the whole of the wave guide up to directly below the receiver. Equally, fault zone waves may originate from deep structures and reach the surface at distances from the fault zone structure due to decoupling at a bend.

A second test set examines the influence of curvature on decoupling of guided wave energy. We assume different curvature ranging from 10 km radius to 240 km radius, while subduction angles stay fixed. Figure 3.6a displays the dependency of frequency content on radius at station IP. All waveforms feature a low-frequency onset, but only the spectra for the sharp curved slab (radius 10 km and 20 km) contain nearly equal levels of energy throughout the frequency range of the spectrum. With increasing radius of curvature the later arriving high frequencies of the guided wave normal mode are damped. Seismograms recorded in the center of the layer (Figure 3.6b) show that the energy at IP parts from within the wave guide: High-frequency amplitudes of the guided wave in the layer decrease while amplitudes and energy spectra at IP rise. The sharper the curvature of the slab at a particular depth, the more normal-mode energy leaks from that point. Low-frequency energy is present even when slabs are bending only marginally, but higher frequencies of the normal mode are reduced.

The spectra for radius 140 km resemble those observed in the Chile-Peru data. A strong low-frequency onset at 2.0 Hz, a gap in the spectra at 3.0 - 5.0 Hz and almost monofrequent higher-mode energy (6.0 - 7.0 Hz) of varying strength was observed at a number of stations of the ANCORP network. A number of along-strike observations at other subduction zones [*Hori*, 1990; *Abers et al.*, 2003] carry more high frequencies. We predict a rather sharp kink in the low-velocity structure for those slab geometries or parting of guided wave energy due to other mechanisms

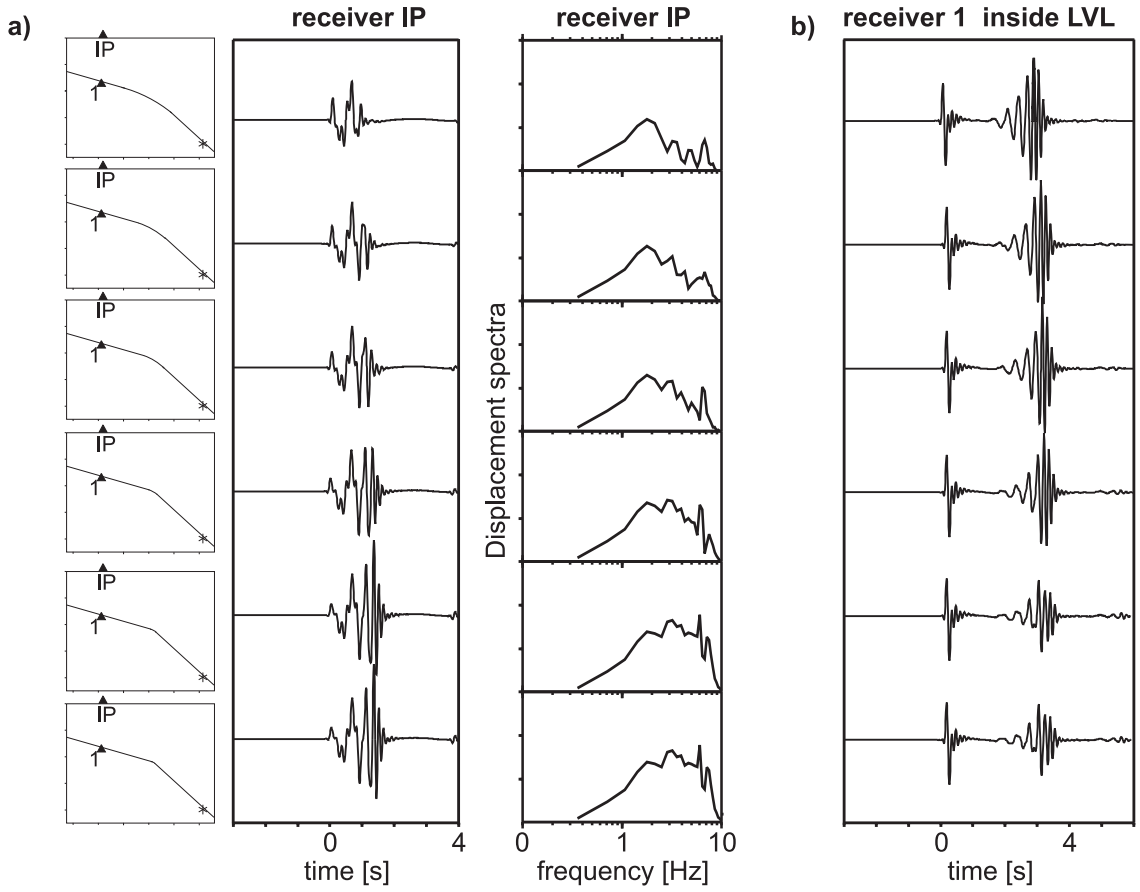

Figure 3.6: Curvature of slab surface: Displacement seismograms and spectra for varying slab curvature. DC source dip angle is 45°, source depth is 200 km, distance to subducted Moho is 0.5 layer width. Synthetics are low-pass-filtered with 7.5 Hz. Radius of curvature of the slab surface (top to bottom): 240 km, 140 km, 100 km, 50 km, 20 km, 10 km. a) Seismograms and displacement spectra at receiver IP. Inserts: Sketch of slab geometry. Asterisks mark source position, triangles indicate receiver position. b) Seismograms at receiver 1 located in the center of the LVL at 85 km depth (the guided wave is preceded by a faster P wave traveling in the slab).

such as reduced velocity contrasts at shallow depth [*Fukao et al.*, 1983; *Hori*, 1990].

Additional receivers at the free surface provide information on the maximum and extent of guided energy perpendicular to the strike of the subduction zone (Figure 3.7). Note that the point of appearance of maximum guided energy at the free surface is ultimately determined by the dip of the LVL at depth [*Martin et al.*, 2003]. When decoupling from the wave guide, the guided phase carries an impressed

slowness and ray paths are determined by its value (compare Figure 3.3a). Figure 3.7 confirms the predicted maximum of guided energy at 68.9°W. Within ten times of the layer width to either side of this point, guided wave amplitudes are larger than direct P onsets. In addition, the slab geometry is such that guided wave energy arrives within the first two seconds following the onset. Only within this small area low-frequency onsets such as observed at the Chile-Peru slab are possible. Changes in radius of curvature or shallow subduction angle have surprisingly little influence on the lateral extent of guided wave energy at the free surface (solid and dashed lines in Figure 3.7).

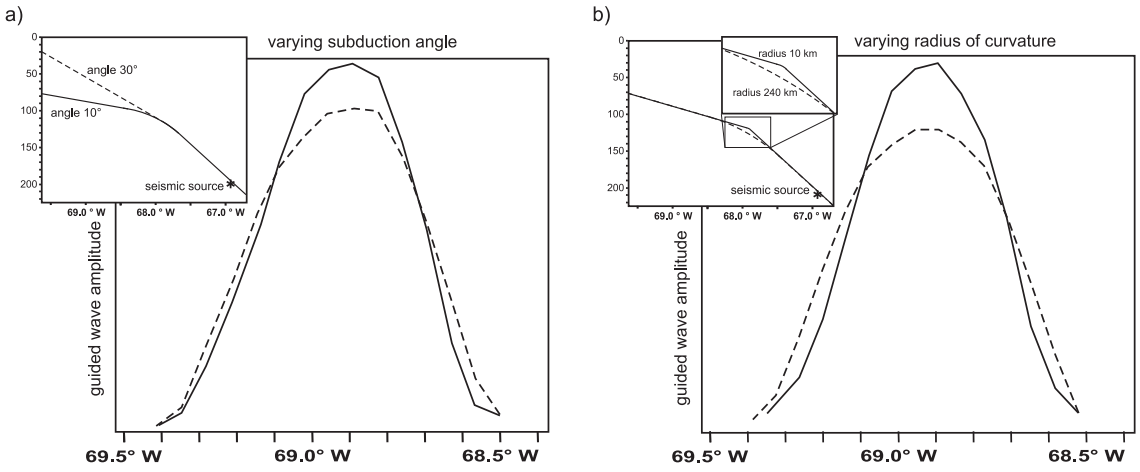

Figure 3.7: Lateral extent of guided wave energy. DC source dip angle is 45°, source depth is 200 km, distance to subducted Moho is 0.5 layer width. a) Lateral extent of low-frequency energy for subduction angle of 10° and 30° (constant radius of 140 km). b) Lateral extent of low-frequency energy for radius 10 km and 240 km (constant subduction angle of 16°). Inserts: Sketch of slab geometry.

3.2.5 Constraints on source position and orientation relative to subducted crust

Source position is the one parameter strongly linked to excitation of guided waves in subducted oceanic crust as well as fault zones [*Igel et al.*, 1997; *Ben-Zion*, 1998; *Jahnke et al.*, 2002; *Martin et al.*, 2003]. At subduction zones source position and

orientation relative to the LVL is most relevant to provide constraints on mineralogical interpretations [*Kirby et al.*, 1996; *Hacker et al.*, 2003a, b]. The following tests are designed to classify wave forms into simple categories with respect to DC source position and orientation relative to the LVL for the Chile-Peru slab at 21°.

As shown in section 3.2.4, amplitude spectra of onsets recorded at the earth's surface consist of two separate low- and high-frequency peaks that originate from different modes of the guided wave. The energy arriving in these two particular frequency slots will be used to classify source orientation and position relative to the layer.

The frequency bands are - for the given receiver geometry, layer width and velocity contrasts - 0.5 Hz - 3.0 Hz and 5.0 Hz - 7.5 Hz, representing the low-frequency arrival and the higher-mode frequency peak at receiver IP, respectively (Figure 3.8). The following tests show the links between source position and excitation of these frequencies.

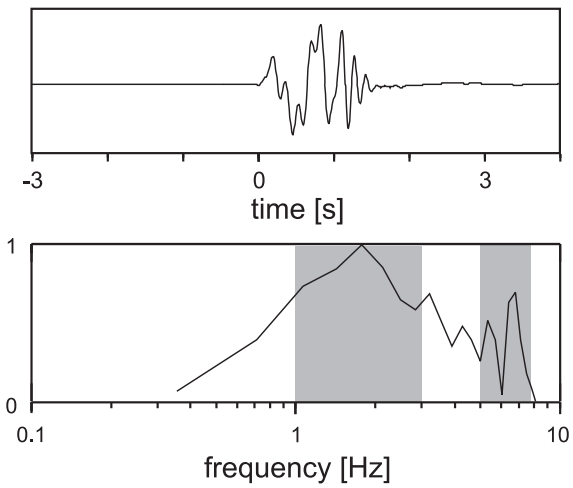

Figure 3.8: P onset and spectrum (displacement seismogram, low-pass-filtered with 7.5 Hz) of synthetic signal at receiver IP resulting from the model of Figure 3.1b (receiver position: 68.9°W). The shaded areas in the spectrum highlight the frequency slots for the peak energy of low- and high-frequency first arrivals.

Explosion source position and guided wave energy

Basic tests on the sensitivity of the guided wave to the position of explosive sources relative to the layer are displayed in Figure 3.9. The 2.0 Hz peak energy is biggest for sources in the middle of the layer and diminishes with growing distance to the layer (see thick lines in Figure 3.9). Sources located at distances further than 2 times the width of the layer produce a sharp direct first onset rather than a stretched out guided wave (see thin lines in Figure 3.9). Notice that although sources are situated inside the LVL, high-frequency energy may contribute in the very first seconds and mask dispersion.

Plots of peak energy at 2.0 Hz and 7.0 Hz versus source position (Figure 3.10a) help to exclude sources that do not match the observed low-frequency onsets. Explosive sources within the layer always result in low-frequency energy, whereas sources outside of the layer cannot produce equal amounts. However, P onsets tend to contain high-frequency phases that mask the low-frequency portion of the onset (dashed line in Figure 3.10a). If high-frequency energy values are larger than 1.5 times the low-frequency energy values, normal distortion is not visible in pulse shapes and we classify the corresponding source position and orientation as unsuitable to produce the Chile-Peru observations at receiver IP. The excitation of high frequencies is sensitive to source location and particularly strong for sources near the layer boundaries and above the slab.

A supplementary test for a layer of 4.0 km width (Figure 3.10b) validates the method of frequency slots. Low and high peak-frequencies for 4.0 km width are 1.0 Hz and 3.0 Hz respectively, as increasing width results in decreasing peak frequencies [e.g., *Ben-Zion*, 1998]. The correlation of peak energy and source position is nearly identical to Figure 3.10a, i.e. the tests are valid independent of layer width.

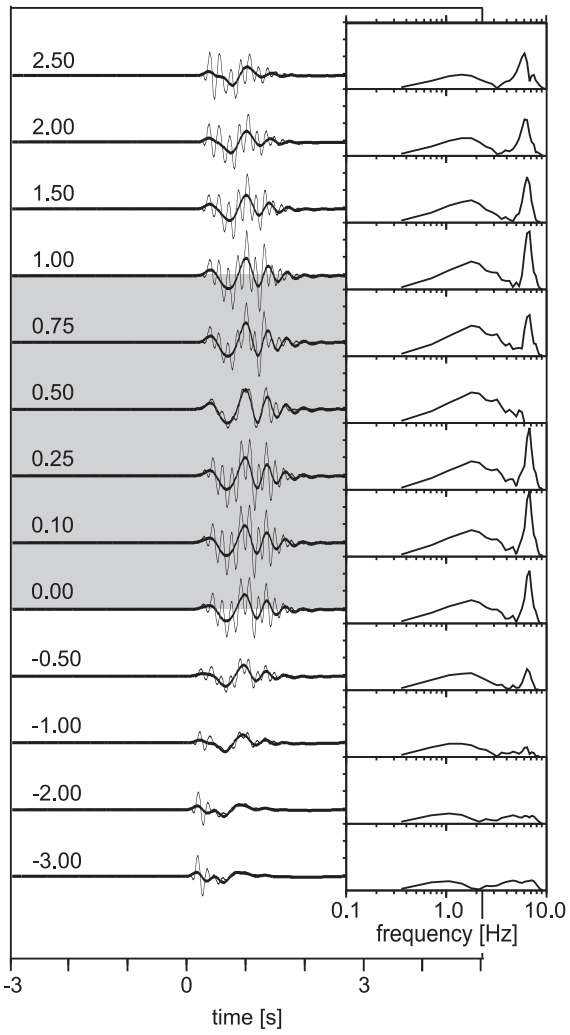

Figure 3.9: Displacement seismograms and spectra for varying source positions relative to the layer (explosive source). Source depth is 200 km. Synthetics are impulse responses low-pass-filtered with 7.5 Hz (thin line) and 3.5 Hz (thick line), respectively. The shaded area in the seismogram section marks the extent of the LVL. Labels on top of each trace indicate normalized distance of the source to the subducted oceanic Moho.

Frequency effects of DC source position and orientation

Expanding the simulations on source position, tests for DC sources of varying orientation are presented. The orientation of DC sources causes shifts in the patterns of guided wave excitation. More precisely, the amount of low- and high-frequency energy generated changes dependent on the direction of P- and S-lobes relative to the layer interfaces i.e. the source dip. Frequency content of onsets does therefore

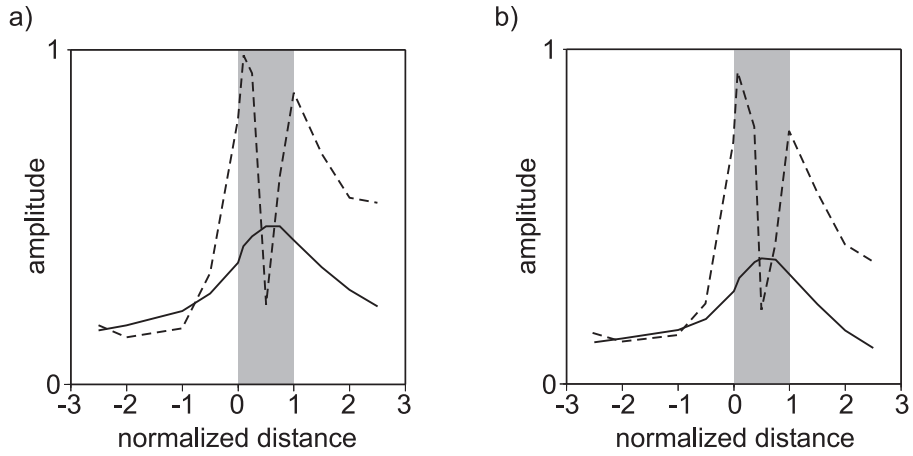

Figure 3.10: Energy versus source position plot for P onsets of explosive sources. The shaded area represents the low-velocity layer. Solid line: Maximum energy in the low-frequency region. Dashed line: Maximum energy in the high-frequency region. a) Layer of 2.0 km width. b) Layer of 4.0 km width.

depend on position and orientation of DC sources and waveforms can vary considerably from those simulated using explosion sources.

To summarize the dependencies of guided waves on source position, a set of 56 simulations is depicted in Figure 3.11. Each graph represents 14 simulations carried out with the same focal mechanism but varying source positions. For explanations on the processing see beginning of this section. Sample seismograms are displayed in Figure 3.12.

We first describe sources with fault planes between 22.5°- 67.5° dip angle (Figure 3.11b - d) analyzing the relative amount of high- to low-frequency energy in each plot. Sources located above the layer can readily be excluded from possible source positions because high-frequency energy prevails (see examples in Figure 3.12a), whereas sources below the layer are potentially favorable for low-frequency onsets (see examples in Figure 3.12b). Sources too far from the layer however, result in sharp direct onsets (see examples in Figure 3.12c) . When sources are placed inside the layer, the link to the dip of the fault plane is most pronounced. The 22.5° sources in the layer are not suited to produce low-frequency first arrivals, high-frequency energy dominates the onset. The sources with fault planes between 45.0°

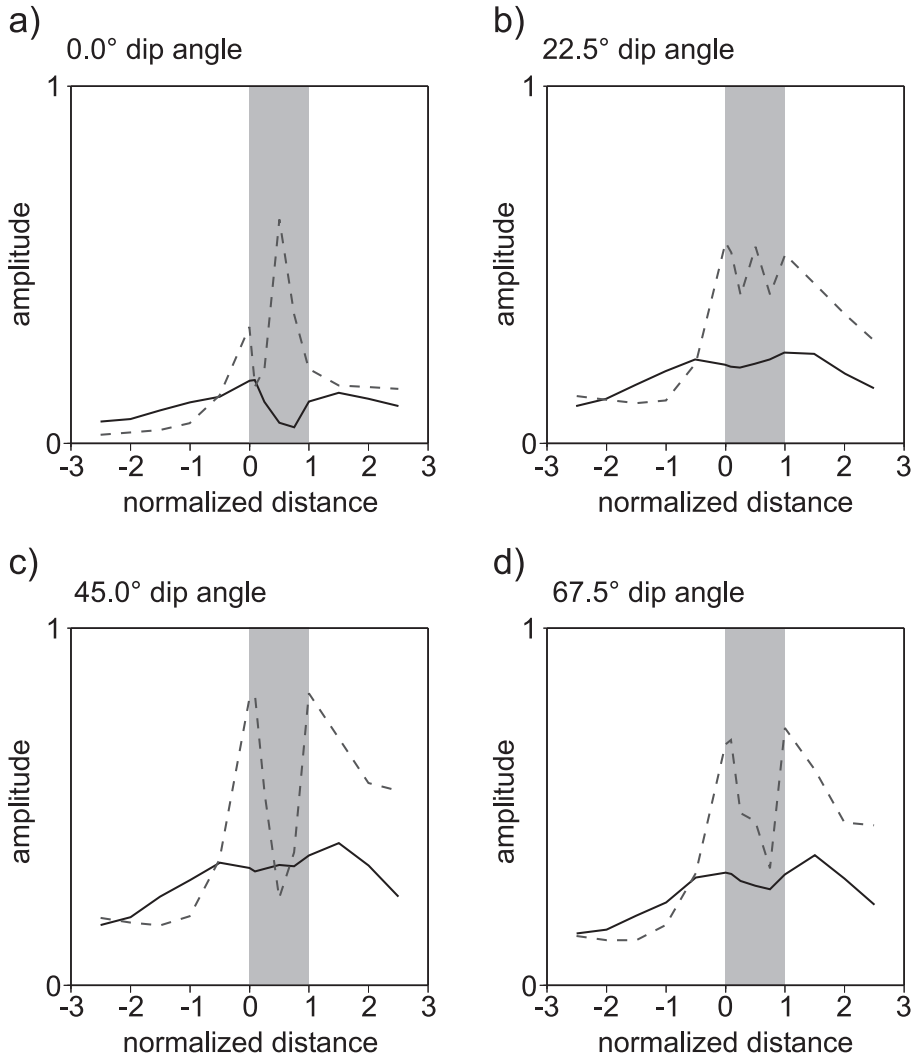

Figure 3.11: Energy versus source position plot for P onsets of DC sources. The shaded area represents the LVL. Solid line: Maximum energy in the 2.0 Hz region. Dashed line: Maximum energy in the 7.0 Hz region. Labels on top of each panel indicate fault plane dip angle relative to the slab surface.

and 67.5° dip angle (Figure 3.11c and d) behave similar to the explosive source: High-frequency energy decreases towards the center of the layer suggesting that the observations are best matched by sources near the center (see examples in Figure 3.12d). The biggest deviations from the explosive sources and in fact all other fault planes tested are present in the onsets of DC sources with the fault plane paralleling the slab (Figure 3.11a, compare to Figure 3.10). The sources in the vicinity of the

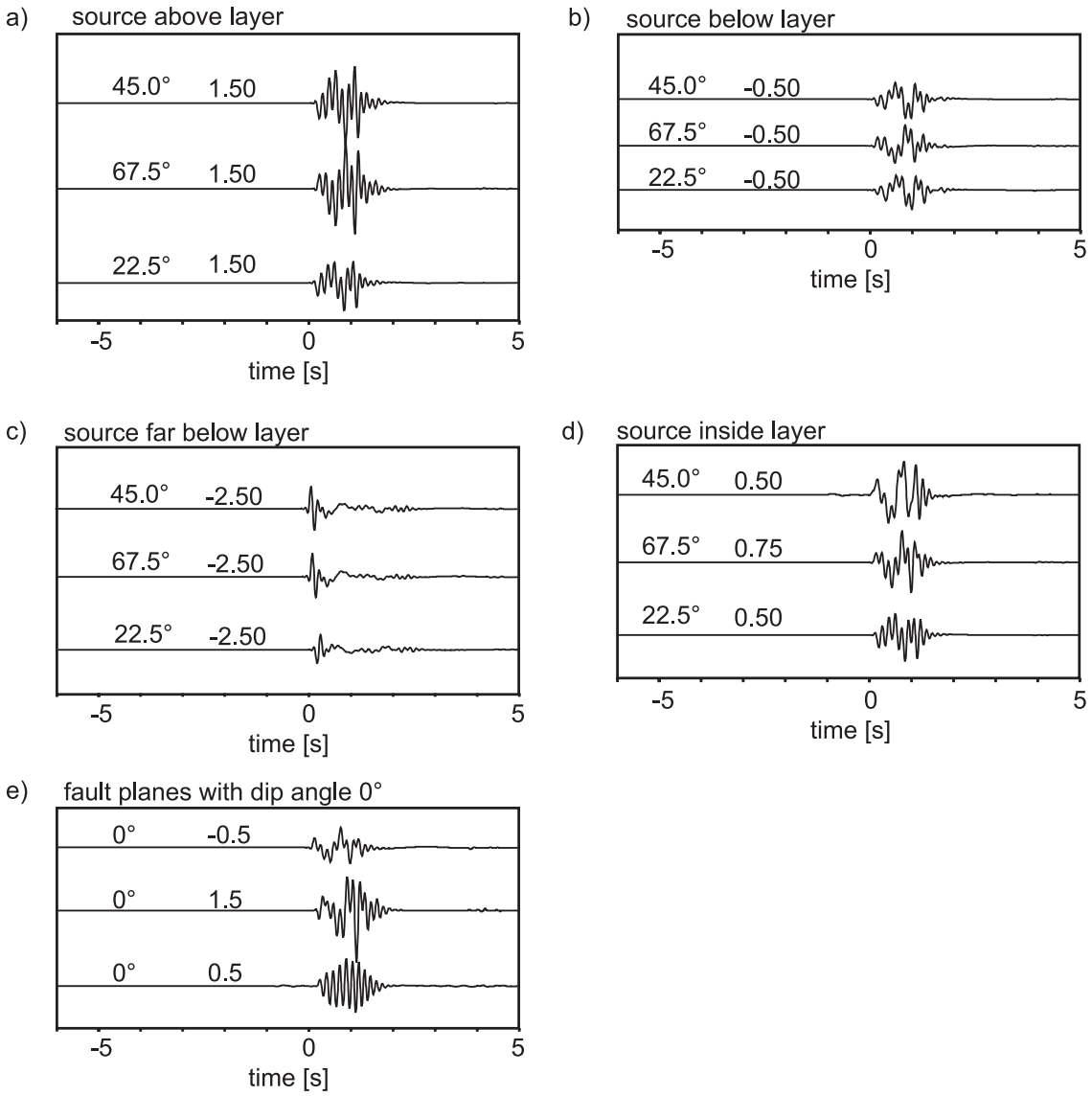

Figure 3.12: Selected displacement seismograms for varying source positions relative to the layer (DC source). Source depth is 200 km. Synthetics are impulse responses low-pass-filtered with 7.5 Hz. Labels above each trace indicate fault plane dip angle and normalized distance to subducted oceanic Moho. a) Sources (dip angle 45°, 67.5°, 22.5°) located 1.5 layer widths above the subducted Moho, b) Sources (dip angle 45°, 67.5°, 22.5°) located 0.5 layer widths below the subducted Moho, c) Sources (dip angle 45°, 67.5°, 22.5°) located 2.5 layer widths below the subducted Moho, d) Sources (dip angle 45°, 67.5°, 22.5°) located inside the LVL (0.5 layer width, 0.75 layer width, 0.5 layer width), e) Source of dip angle 0° located 0.5 layer widths below the subducted Moho, 1.5 layer widths above the oceanic Moho and in the middle of the LVL.

layer boundaries and even above the layer give best results, whereas those inside the layer are carrying too much high frequencies to match the observations (see examples in Figure 3.12e).

We conclude that DC source orientation has to be taken into account when deducing source position. Down-dip extensional sources like those found in Chile at 21°S [*Rudloff*, 1998; *Rietbrock and Waldhauser*, 2004] restrict source positions for low-frequency P onsets to the center of the LVL and a thin stripe below the LVL (not further than 2 layer width from the subducted oceanic Moho). Sources near the LVL boundaries and above the LVL are ruled out. The inferences may however be biased by damping of high frequencies in the overlying mantle which is not accounted for in simulations.

3.2.6 Guided waves in random media

The proposed subduction zone wave guide is predicted to be composed of coarse grained and partially eclogized gabbroic material of the lower subducted crust [*Hacker et al.*, 2003a, b]. Deduced velocities and layer widths favor this interpretation [*Martin et al.*, 2003]. Kinetic hindering is probably causing the crust to remain partially gabbroic i.e. phase transformations do not occur along smooth p-T paths. A crustal wave guide at that depth is thus best approximated by a patchy medium of random velocity undulations rather than a uniform layer used in the tests so far. We therefore add two more refined tests. The first to preclude that a completely different phenomenon causes the low-frequency onsets: testing wave propagation in random media of the same composition and seismic velocity as the mantel. Can mere scattering cause the observed normal dispersion?

The second to verify if the sensitive guided wave mechanism is robust enough to function in an undulating non-homogeneous structure: Testing propagation along an averagely 7 % slow wave guide of undulating velocity. Will strong guided wave energy emerge at the free surface if the wave guide is not uniform?

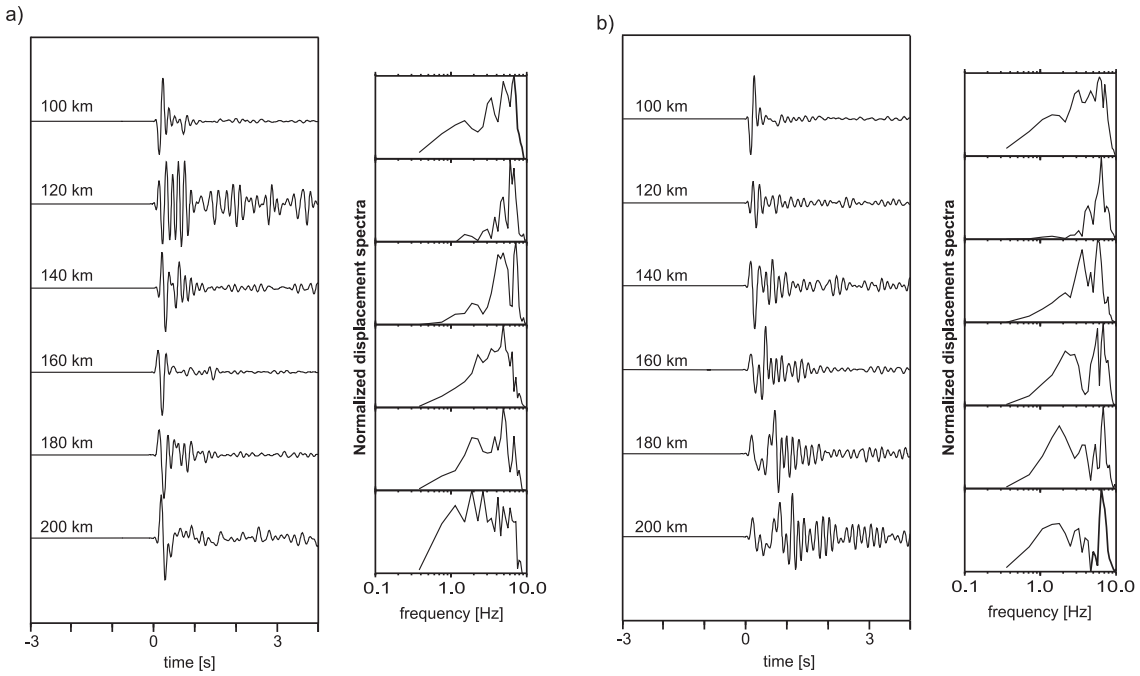

Figure 3.13: Displacement seismograms and spectra for varying source depth (DC source). Source position is 0.5 layer width above subducted Moho, fault plane dip angle is 45°. Synthetics are impulse responses low-pass-filtered with 7.5 Hz. Labels on top of each trace indicate source depth. a) Test 1: Crustal layer of 8.1 km/s average P velocity with random velocity undulations (+/- 5.0 %) of correlation length 1.0 km. b) Test 2: Crustal layer of 7.5 km/s average P velocity with random velocity undulations (+/- 5.0 %) of correlation length 1.0 km.

The pure random medium without reductions in velocity (test 1, Figure 3.13a) generally does not cause the observed effect of systematic distortion in waveforms. Even though spectra of onsets comprise more and more low-frequency energy with increasing source depth, no normal dispersion emerges. Simulated onsets are high in amplitudes and frequency, unlike any of the observations. The layer of reduced velocity (test 2, Figure 3.13b) functions as a wave guide, undulations in velocity do not interfere with the guided wave propagation. Seismograms of sources located deeper than 140 km are dominated by an increasingly strong low-frequency onset (compare to data in Figure 3.2a).

3.2.7 Velocity gradients in wave guides

Subduction zone wave guides stretch out over vertical distances of 100 km and more. With changing p-T conditions, wave guide and host rock properties vary. The resulting seismic velocity structure is sophisticated, including not only gradients conditional upon p-T conditions, but also depth dependent variations of the LVL due to phase transformations and fluids migrating within the slab [*Hacker et al.*, 2003a, b]. The entrapment and guiding of seismic energy requires rather narrow-band conditions regarding velocity contrasts. We therefore test different gradient models based on IASP91 [*Kennett and Engdahl*, 1991] on their ability to propagate guided wave energy to receiver IP. Ultimately the modeling of guided wave onsets may allow to put constraints not only on basic mineral composition of the wave guide but also the transformation rates of crustal material during subduction.

The model generated for the Chile-Peru slab (Figure 3.14a) incorporates the depth dependent P wave velocities as found in IASP91. The relative velocity contrasts of the geological units are those introduced in section 3.2.3 (see Figure 3.1), i.e. the LVL is 7.0 % slow and the slab is 1.25 % fast compared to overlying mantle. The test set derived from this model simulates the fading out of the LVL due to phase transformations. The successive models include LVLs fading from 7.0 % reduced velocity at 80 km depth to 5.0 %, 3.0 %, and 0.0 % reduced velocity at 200 km depth respectively.

The IASP model including a 7.0 % slow layer yields synthetic data comparable to those simulated using the standard model introduced in Figure 3.1. We conclude that guided wave propagation is not disturbed by depth dependent velocity gradients, as long as velocity contrasts relative to the host rock remain constant with depth. Seismograms resulting from the fading low-velocity layers (Figure 3.14b, c, d), however confirm the sensitivity of wave entrapment to changing velocity contrasts. The continuous drop of velocity contrast relative to the host rocks permits guided energy to leak and thus P onsets at IP become more and more high-frequent.

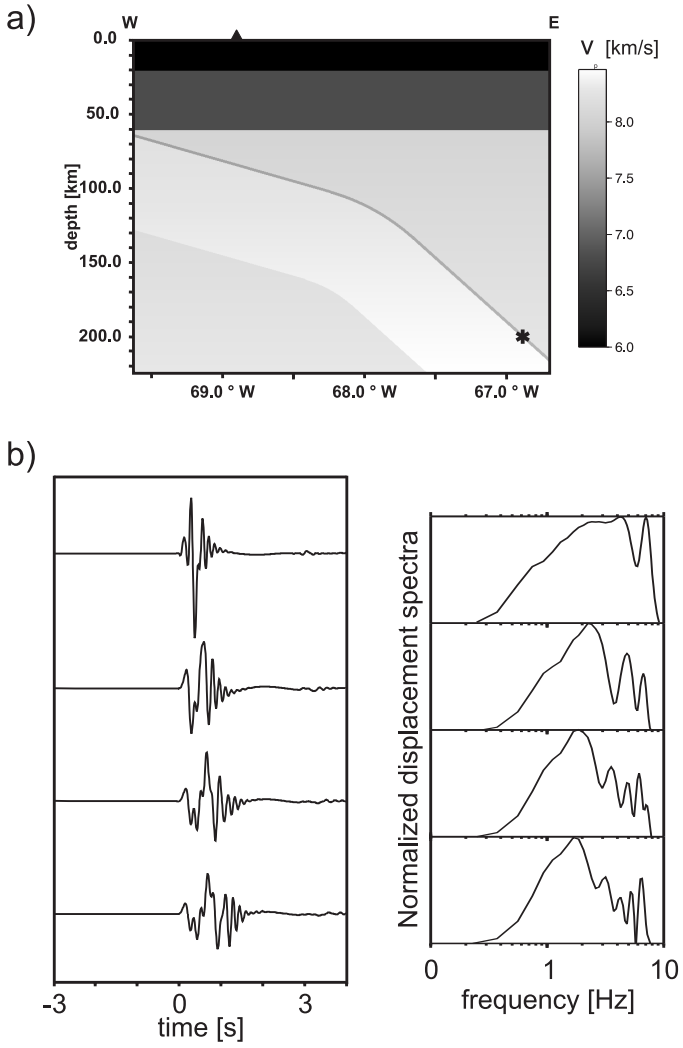

Figure 3.14: a) 2D P velocity model based on IASP91. The asterisk marks the source position, the triangle indicates the receiver position. b) Displacement seismograms and spectra for a fading LVL in the IASP91 model. Source depth is 200 km, synthetics are impulse responses low-pass-filtered with 7.5 Hz. Velocity contrast of the LVL to host rocks is (top to bottom): 7 % at 100 km depth rising to 0 % at 200 km depth, 7 % at 100 km depth rising to 3 % at 200 km depth, 7 % at 100 km depth rising to 5 % at 200 km depth, 7 % (constant).

The seismograms for the LVL fading to 3 % may still be compatible with the observations at IP, but a layer reduced to 0 % velocity contrast at 200 km depth produces onsets completely unlike the recorded low-frequency data.

3.2.8 Conclusions

Exemplary tests using a realistic IASP91 velocity model for the Chile-Peru subduction zone prove the basic feasibility of a crustal wave guide to explain the observations at station AER. The gradual velocity rise along the length of the wave guide has virtually no influence on the wave guide and guided wave propagation is not hindered by depth dependent velocity variations. However, a random medium as opposed to a low-velocity layer, is not suited to explain the distorted P onsets at the Chile-Peru slab. Simulated random velocity undulations in the subducted crust do not match the frequency distortion seen at the employed stations of the ANCORP network, nor can a simple random structure cause the interlinked observations made at stations AER and BOS. Based upon this evidence indicating a wave guide atop the Chile-Peru slab, up-dip subduction zone wave guides were thoroughly investigated in respect to slab geometry, receiver and source positioning.

Decoupling of guided energy from deep subduction zone wave guides is linked to slab geometry. Changes of direction of the wave guide cause a fraction of guided energy to leave the low-velocity structure. For up-dip profiles, energy leaks from the crustal wave guide when subduction angle changes. Surprisingly, even slight changes will cause as much energy leakage as strong changes of direction such as at the Chile-Peru profile. Thus the observation of guided energy from deep events at up-dip stations is expected at any subduction zone, provided a wave guide is present and sources are located favorable.

To make full use of the potential of the guided wave effect, however, receiver positioning is crucial. The arrival times of guided waves depend on receiver position relative to the point of decoupling of guided waves at depth. Only if the slab geome-

try is favorable, guided waves will arrive together with body wave arrivals, otherwise they are preceded by a direct P wave. Thus observed seismograms sometimes resemble two distinct phases [*Fukao et al.*, 1983; *Abers et al.*, 2003; *Abers*, 2005] and the low-frequent arrival of the guided wave may be masked by precursors resulting in overestimation of velocity contrasts. A straight forward analysis of moveout times seems not suitable unless velocity models and ray tracing are very accurate.

The frequency content and pulse shapes of guided wave onsets are variable and also partially depend on slab curvature. Strong low-frequency onsets are dominant at regions where the slab surface is curving gently, fully dispersive pulses including strong late arriving high-frequency energy are caused by sharp kinks in the slab structure or possibly lateral offset of the layer.

Dispersive patterns of guided waves also carry information on fault plane solutions. Simulations of DC sources show that excitation of the guided wave normal mode and higher modes is closely connected to source location and orientation and the higher frequency content in DC simulations differs from simulations using simple explosive sources. For the Chile-Peru subduction zone and the relevant receiver position, we conclude that down-dip extensional sources are most suited to cause guided wave onsets. For this mechanism we exclude those sources situated above the layer because of fast higher-mode high-frequency energy that cannot be matched with the observations and those below the layer that are further than 2 layer widths away from the subducted oceanic Moho. Ultimately, visco-elastic simulations will have to be carried out to reliably match observed onsets with simulations for the high-frequency region relevant for predicting small scale source positioning.

Finally sources situated in a gradually fading low-velocity layer were simulated. The tests show that a rise of wave guide velocities relative to surrounding host rock (e.g. a rise in velocities conditional upon phase transformations in the layer) does influence the observations. Guided wave observations can thus potentially constrain rates of eclogitization in the subducted crust at depth.

Chapter 4

A coherent registration of a guided wave phase at the Chile-Peru subduction zone

4.1 Preface

Going back to the seismological data collected during the SFB 267 campaign (see section 1.4), new and unique indications for a wave guide at the Chile-Peru subduction zone were discovered: A coherent dipping phase was recorded at a refraction line situated nearly 100 km trenchward of the stations investigated so far. This chapter is dedicated to reveal the basic geometry of this shallow wave guide (event depth is 98 km), rounding out the guided wave analysis at this particular region of the Chile-Peru subduction zone.

This further evidence of a wave guide permits us to analyze, where the effect can potentially be observed along the dipping slab in the forearc region. The question points directly to the issue of decoupling of guided energy from the wave guide and another favorable constellation to observe guided waves: A 'leak' in the wave guide caused by equalization of velocities resulting in a refracted guided phase to reach the surface. Supplementary to the decoupling of guided waves due to bending of the slab (investigated in chapter 3), this is another explanation for guided wave observations in the forearc region of subduction zones.

Seismological signals carrying information on low-velocity layering are thus present

at two distinct regions at the free surface. The information obtained may differ regarding depth, propagation distance, width and velocity contrast of the wave guide, since different parts of a - probably connected - low-velocity layer are sampled.

4.2 Forearc decoupling of guided waves in the Chile-Peru subduction zone

(**article to be submitted to** *Geophys. Res. Lett.*: Martin, S., C. Haberland, and A. Rietbrock, Forearc decoupling of guided waves in the Chile-Peru subduction zone.)

4.2.1 Abstract

The structure and alterations of subducted oceanic lithosphere (e.g., thickness and seismic velocity of oceanic crust) can be obtained by analyzing guided seismic waves generated by earthquakes within the slab (Wadati-Benioff zone). In northern Chile prominent secondary phases from intermediate-depth seismicity, observed in the forearc region can be interpreted as guided waves. For the observation of guided waves it is usually required to have stations close to the wave guide, a fact which is not directly given for forearc stations in subduction zone environments. With the help of finite difference simulations we model the decoupling mechanism of guided waves at the contact between the descending oceanic plate and the upper plate crust where the wave guide is opened due to the equalization of seismic velocities. Provided that suited stations are available this mechanism allows the use of intermediate depth seismicity in guided wave studies to study the shallow subduction zone structure ($\leq$ 100 km depth).

4.2.2 Introduction

Guided waves propagating in subducting oceanic slabs provide unique insight into the composition of these thin layered structures at greater depth [e.g., *Fukao et al.*, 1983; *Hori*, 1990; *Abers*, 2000; *Abers et al.*, 2003]. They contribute to still open geoscientific questions such as phase transformations of the slab and its composition, the depth of the gabbro-eclogite transformation during the metamorphosis of the subducting oceanic crust, and the presumably related intermediate depth Wadati-Benioff seismicity [e.g., *Helffrich and Abers*, 1997; *Hacker et al.*, 2003a].

During recent years an increasing number of papers exploited the potential of guided seismic waves propagating in subducted oceanic crust [e.g., *Fukao et al.*, 1983; *Helffrich and Abers*, 1997; *Lin et al.*, 1999; *Abers*, 2000; *Abers et al.*, 2003; *Martin et al.*, 2003; *Martin and Rietbrock*, 2004]. The technique has not only provided evidence for the existence of low-velocity layers at circum-pacific subduction zones but also permitted to predict layer thickness and velocity contrasts at various depth for a number of subduction zones [e.g., *Hori*, 1990; *Abers and Sarker*, 1996; *Abers et al.*, 2003; *Martin et al.*, 2003]. However, results tent to be ambiguous partially owing to the lack of knowledge on the generation, propagation and the prerequisites for observation of guided waves at subduction zones.

In general, guided waves can be produced by sources within or very close to the wave guide, and can only be observed in the wave guide or in its direct vicinity [*Ben-Zion and Aki*, 1990; *Igel et al.*, 1997; *Ben-Zion*, 1998; *Haberland et al.*, 2003]. While in subduction zones the former is usually provided by the Wadati-Benioff seismicity, the latter is not implicitly given and obviously strongly dependent on the forearc structure. The upper plate is usually in-between the forearc seismic stations and the wave guide. Distances of more than 50 km between the recording station and the actual wave guide raise the question, how the guided energy reaches the point of observation. Thus mechanisms to trigger leakage of guided energy are required to explain the guided wave observations conclusively, to allow to locate the exact

portion of the wave guide sampled by the guided wave and ultimately to define receiver positions in the varying wave field.

At least two mechanisms are to be considered for decoupling at subduction zone wave guides.

One is the geometrical bending of slabs and was investigated by *Martin et al.* [2003]. The appearance of low-frequency onsets at the Central Chilean subduction zone associated with a deep up-dip wave guide was explained by changes of subduction angle at greater depth and subsequent decoupling of guided energy.

Fukao et al. [1983] and *Hori* [1990] presented anomalous phases for events at depth < 100 km recorded in the subduction zone of Japan and proposed that these phases are associated with waves guided in the subducted oceanic crust. They invoke another decoupling mechanism at the contact between subducted oceanic and overlying continental crust (oceanic/continental crust, OCC) releasing guided energy due to equal seismic velocities.

Here we present observations of anomalous phases in local earthquake recordings at stations located at the coast line of the Chile-Peru subduction zone in conjunction with finite difference (FD) simulations illustrating the mechanism of decoupling at the OCC contact. This mechanism is likely to be fundamental for many guided wave observations originating from shallow subduction zone wave guides.

4.2.3 An earthquake observation at a dense seismic refraction line

Our observations stem from an accidental recording of a local earthquake along a temporarily deployed refraction line [*Lessel*, 1997; *Schmitz et al.*, 1999]. Stations and earthquake are situated in the subduction zone of northern Chile (see Figure 4.1) where the oceanic Nazca plate subducts beneath the South American continent. Data were recorded with Mark L4 1Hz 3-component seismometers and a sampling interval of 0.01 s.

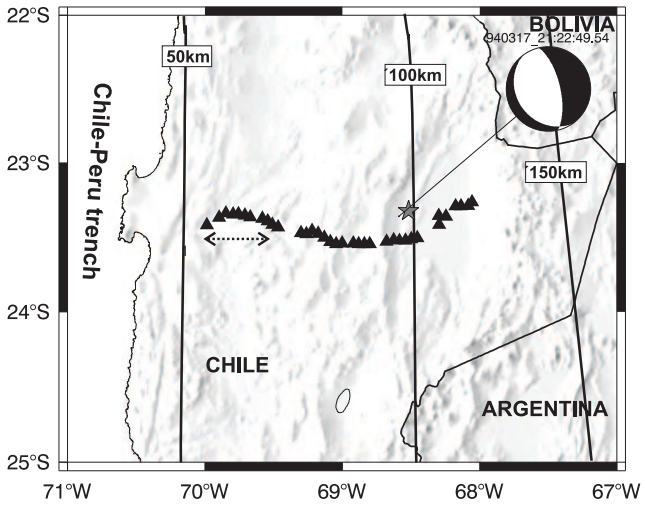

Figure 4.1: Distribution of recording stations of the PISCO refraction line (solid triangles). The local earthquake ($M_l \sim 5.0$, March 17, 1994, 21:22:49.54 GMT, 23° 21.29'S, 68°34.72'W, *depth* = 97.96 km [*Rudloff*, 1998]) is shown by a star. The depicted lower hemisphere of the fault plane solution calculated by the method of *Reasenberg and Oppenheimer* [1985]. Black lines indicate slab depth, the dotted line marks the area of second arrivals.

Since the event was observed by a temporary local seismological network, precise location, fault mechanism, and magnitude are also available [*Rudloff*, 1998; *Graeber and Asch*, 1999]. The small station spacing along the refraction line ($\sim$ 5 km) which is usually not achieved in local studies of subduction zone earthquakes allows the observation of coherent waveforms and the identification of exotic wave groups.

The seismograms (vertical component) are low-pass-filtered (1 Hz) to enhance the strong correlation of the later arrival and aligned on the first onsets (Figure 4.2). At 0 s the direct P wave arrives, and at the westernmost stations (70.°W - 69.5°W) a prominent secondary phase appears with strong amplitudes (often stronger than the first arrivals). This phase dips toward the east relative to the first arrivals.

4.2.4 Simulation

Synthetic seismograms are calculated using a parallel code based on the fourth-order staggered grid FD scheme of *Virieux* [1984, 1986] including a planar free

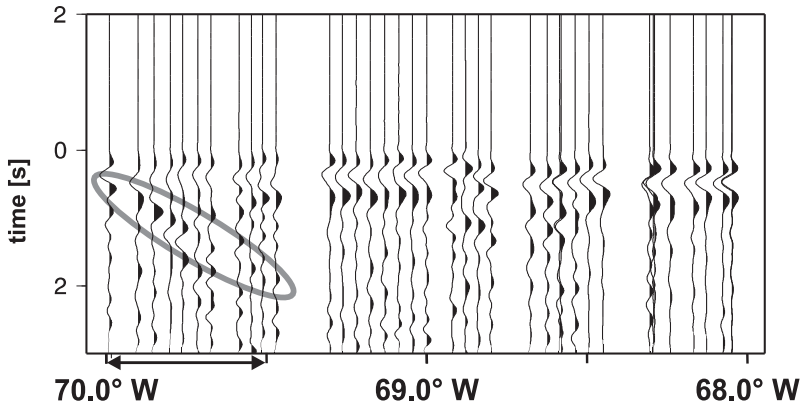

Figure 4.2: Waveforms (velocity seismograms, 1 Hz low-pass-filtered) of a Benioff zone earthquake (see Figure 4.1) recorded on the refraction line and aligned according to the P onset times. The solid line marks the eastward dipping later arrival.

surface condition [*Levander*, 1988]. The method is well suited to simulate 2D P-SV wave propagation up to high frequencies in large models including complicated boundaries such as the laterally varying subduction zone geology and has been used in several other studies [*Martin et al.*, 2003; *Martin and Rietbrock*, 2004]. The small grid spacing guarantees that numerical dispersion is less than 1.0 % even for the highest frequencies of S waves and propagation distances up to 300 km. See more information on the computing details in *Martin et al.* [2003].

We use an explosion source to obtain an unobstructed image of the low-frequency guided wave preventing high-frequency effects due to DC source mechanisms [*Martin and Rietbrock*, 2004]. The earthquake is located in the subducting crust 4.0 km below the slab surface at a depth of 100 km. In order to obtain comparable waveforms, we convolved the simulations (delta impulse) with a 1 Hz Ricker wavelet.

The seismic velocity model studied is based on results from extensive refraction seismics and earthquake studies (tomography, receiver functions) in the region of Central Chile between 24°S and 20°S [*Lessel*, 1997; *Patzwahl et al.*, 1999; *Bock et al.*, 2000; *Yuan et al.*, 2000]. Since we are interested in gaining a conceptual understanding of the process, the model was simplified to highlight the effects of decoupling of the guided wave at the OCC contact. The determining feature of the

velocity model is the area where velocities of the forearc crust and subducted oceanic crust are equal (OCC contact). The depth is 70 km and the average crustal velocity above the OCC contact point is 6 km/s. For simplicity, the continental Moho is assumed to be situated at that constant depth throughout the model. In reality hydration of the forearc mantle may have a mayor influence on the depth of the contact point [*Brocher et al.*, 2003]. The mantle beneath the continental crust and oceanic crust has a velocity of 8.0 km/s and 8.1 km/s respectively. The subducting crust is assigned a P velocity of 7.5 km/s and 7 km width (see Figure 4.3a).

Aside from the direct P wave, a strong phase is developing in the wave guide formed by the subducting oceanic crust (Figure 4.3b). At the base of the OCC contact (at 70 km depth in Figure 4.3a) the wave guide is opened and the prominent, formerly trapped guided energy is refracted towards the surface (Figure 4.3c). In the seismograms it is visible as a strong phase in the westernmost portions of the forearc with a slowness lower than the direct P wave's slowness (Figure 4.3d). Depending on the forearc geometry this phase merges with the direct phase (P) or the wave traveling in the oceanic mantle (P_n), or is a separate phase. The point of occurrence of this phase is defined by the position where the forearc velocity equals that of the velocity of the oceanic crust. The slowness of this phase is controlled by the velocities of the wave guide and the surrounding mantle superposed by the effect of the up-dip propagation of the guided wave phase. Accordingly it is in-between the direct P and P_n slownesses.

4.2.5 Discussion and conclusions

Since most seismic stations located in subduction zone forearcs are not situated directly on top of the wave guide formed by the subducting oceanic crust (but rather offset from it by the forearc lithosphere), appropriate decoupling mechanisms that permit the observation of guided waves in the forearc are bound to exist.

A possible mechanism for decoupling of guided waves from the wave guide is

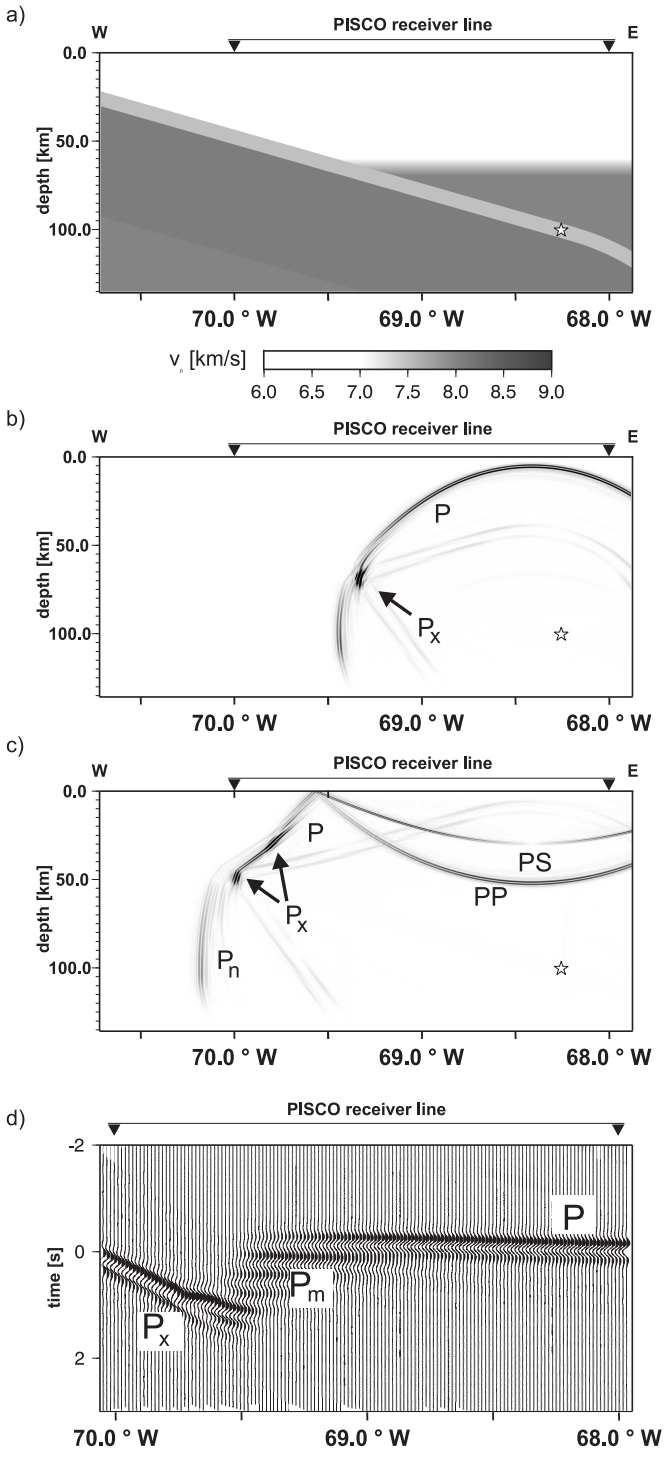

Figure 4.3: FD simulations of the wave field of a typical Benioff zone earthquake at a depth of 100 km. a) P velocity model used in the simulations consisting of continental and oceanic crust, and continental and oceanic mantle lithosphere. The hypocenter is indicated by a star. b) and c) Snapshots of the wave field before and after decoupling at the OCC contact. d) Simulated waveforms (vertical component velocity seismograms, convolved with a 1 Hz Ricker wavelet) at the surface stations after moveout correction. Note the strong phase (P_x) at the westernmost portion of the recording line after the P arrival. The (steep-angle) multiple reflections at the oceanic Moho are labeled P_m.

linked to the OCC contact [*Fukao et al.*, 1983; *Hori*, 1990], where the wave guide velocity is equaled by the low velocities of the forearc crust at a certain depth and the wave guide structure is broken-up. Subsequently a part of the guided wave leaves the low-velocity layer and approaches the surface as a refracted guided wave phase.

The decoupled guided energy appears as a prominent phase with high amplitudes and relatively low frequencies which - dependent on the longitude of the station - distorts the direct or refracted P waves, or can be identified as a distinct phase. The dip of the phase is defined by the velocity contrast of subducted crust towards the host rocks and the subduction angle along the ray path.

Guided waves decoupling in subduction zones by this mechanism are restricted to a narrow area determined by the OCC contact and modified by the direction of propagation. In Central Chile this region is different from the area where guided waves decoupling at slab-bends can be observed [*Martin et al.*, 2003]. For other subduction geometries both ways of decoupling may contribute to guided wave observations in the same region and cause distorted onsets with a different interaction geometry and character, likely originating from different depth regions. Geometrical bending of slabs tends to result in a bigger portion of low-frequency energy [*Martin et al.*, 2003]. The findings suggest to have a close look at the host of observations made at other subduction zones [e.g., *Helffrich and Abers*, 1997; *Abers et al.*, 2003]. On the one hand to determine whether guided waves are refracted or leaking at bends and thus discriminate guided phases probing the wave guide at different depth regions potentially distinctive in composition and width. On the other hand, to utilize phases decoupling at the OCC contact for guided wave studies in the forearc region, thus gaining information on the structure of the lowermost forearc crust and upper mantle wedge as well as depth of the OCC contact. This could be useful to determine whether mantle material on top of the slab is serpentinized or not [e.g., *Bostock et al.*, 2002; *Brocher et al.*, 2003]. The findings on refraction of guided wave phases are also valuable to predict regions where guided wave phases

are to be observed. Due to the strong amplitudes of the guided waves, this might have implications for hazard assessment at coastal regions.

The simulations for the Chile-Peru subduction zone are in accordance with a 7 km thick low-velocity wave guide presumably formed by the subducting oceanic crust, although further modeling is needed to quantitatively asses this issue.

Future seismological experiments which cover the forearc region with a dense station spacing (resulting in coherent waveforms) will allow further analysis of the waves from intermediate depth earthquakes traveling in wave guides related to descending oceanic slabs.

Chapter 5
Discussion and conclusion

Although mineralogical, petrological, thermal and conventional seismological methods at subduction zones are advancing to ever greater accuracy, the evolution of subducted oceanic crust at depth > 60 km is still elusive. The guided wave method can potentially contribute details of immense value regarding the processes near the slab surface, such as layering of subducted lithosphere, source locations of intraslab seismicity and most of all, range and manner of the eclogite transition.

In the foregoing chapters 2 to 4, the guided wave phenomenon was analyzed to gain conceptual knowledge on the processes underlying guided wave propagation and assess its merits and limits. Here, we summarize and discuss the core results of this work. They are compiled in sections regarding the aspects of 1) geometry and 2) wave guide parameters, followed by a short note on guided S waves, a phenomenon closely related to the guided P waves investigated in this thesis. A brief look at guided wave observations at other subduction zones follows and finally mineralogical inferences for the Chile-Peru subduction zone are presented.

5.1 Geometry of subduction zone wave guides and observation of guided phases

Up to now most studies of guided waves in subduction zones have used simplified approaches to infer wave guide parameters, such as analytical solutions for acoustic wave propagation [*Ben-Zion*, 1998] or rather coarse numerical modeling not suited

to resolve the thin wave guide structure [*Igel et al.*, 2002]. Inversion algorithms employed model the observations in terms of planar structures only [e.g., *Abers*, 2000]; i.e. the specific geometry of subduction zones and subsequently the exact receiver position in the complicated wave field resulting from a curved wave guide are not considered. Such simplification of the model eliminates fundamental effects of P wave entrapment. Thus, at present it is not clear how reliable these estimates are, as the effects of leakage of guided waves, variations in receiver position, and geometry of the wave guide on guided phases at subduction zones are not well understood.

The FD simulations presented in the foregoing chapters give a reliable estimate of the areas, where guided waves are observed within an up-dip geometry for the Chile-Peru subduction zone near 21°S. The same approach can be applied for any along-strike or up-dip scenario at other subduction zones, since the general velocity structure in subduction zones and changes in subduction angle are a common feature for subducting slabs [e.g., *Kirby et al.*, 1996; *England et al.*, 2004].

Two distinctive decoupling mechanisms, discussed in chapter 4 and 5, determine the area of observation of guided waves propagating perpendicular to the strike of the subduction zone (Figure 5.1). The first one is leakage of guided waves due to the curved geometry of slab surfaces. Wave guides leak energy when the direction of the low-velocity layer changes and these leaking guided phases are recorded at receivers situated above the slab. In the investigated up-dip geometry, a pronounced bend in the wave guide near 110 km depth results on average in 30 % of guided energy escaping from the wave guide. The impingement point of the ray trajectory determines the center of a region exposing guided wave onsets. The extent of this area increases with increasing width of the wave guide, it is however independent on the sharpness of the bend in the slab structure. The existence of this decoupling mechanism has three direct implications on the interpretation of guided waves. First, guided waves at subduction zones can be observed far away (50 km and more) from

the wave guide they originated in. Second, the waves hold information on the segment of the wave guide stretching from the source location to the next bend in the structure. Finally, pulse shapes of guided waves are influenced by the curvature of the slab. Simulations show that the curving slab has a frequency-selective effect on the guided phases, i.e. parts of the dispersive wave train traveling with velocities of the LVL or slower are reduced in amplitudes after decoupling (see chapter 3).

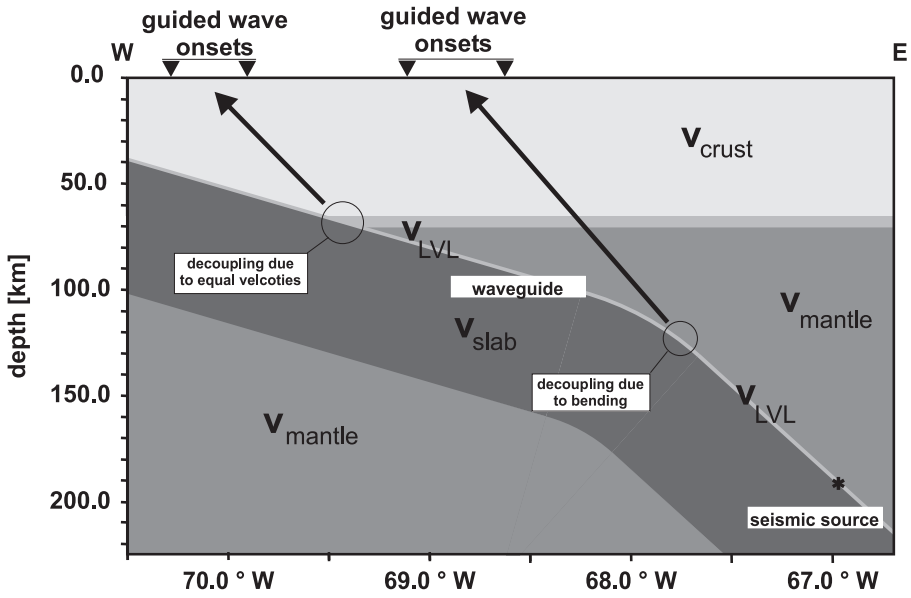

Figure 5.1: Schematic illustration of guided wave decoupling in an up-dip geometry. The seismic source (asterisk) is situated in a low-velocity wave guide at 200 km depth. Arrows indicate the direction of decoupled guided wave energy after leaving the wave guide.

The second mechanism causing guided waves to reach the free surface is the equalization of seismic velocities of the wave guide and the overlying host rocks. This is the case in the forearc region at the Chile-Peru subduction zone at around 60 to 70 km depth, roughly where the continental crust is in contact with the subducting oceanic crust (see Figure 5.1). At that depth, guided energy is refracted to the surface reaching forearc stations [*Fukao et al.*, 1983; *Martin et al.*, 2005]. These 'refracted' phases expose strong amplitudes in the high-frequency region, typically appear close to the region above the mantle wedge, and are also observed for comparatively shallow events (focal depth < 100 km). The wave trains are not as long

as those caused by deep wave guides, since propagation length is shorter and the LVL is thicker at shallow depths [*Abers*, 2005].

The intensity and pulse shape of the guided wave phases observed at the free surface is further dependent on source position and the exact conditions of decoupling (see chapter 3). The center region of guided wave onsets indicated in Figure 5.1 typically exposes guided phases with amplitudes up to 5 times higher than ambient body waves. Simulations underline that 1) leakage of energy is common for subduction zone wave guides, and 2) guided waves at subduction zones may be different in character from those waves predicted for an ideal flat wave guide. Tests also show that the remaining part of guided energy continues to propagate along the wave guide despite bending or refraction, potentially causing guided wave observations at other regions. We therefore picture the low-velocity wave guide as a patchy layer of varying width capable of trapping seismic energy and releasing fractions of these energy at various depth.

We conclude, that the wave field of intraslab events observed in the forearc region is profoundly affected by the slab and particularly by the slow and comparatively small-scale layer at the top of the slab surface. Dependent on receiver position, guided phases distort the direct or refracted P wave or can be identified as distinct phases. Closely positioned receivers even allow to record coherent arrivals associated with the subduction zone wave guide in the forearc region of the Chile-Peru subduction zone (compare chapter 4).

Applying inversion methods based on normal-mode methods [*Abers*, 2005] or analytical solutions for plain layers [*Ben-Zion*, 1998; *Haberland et al.*, 2003] after assessing the interaction geometry of guided phases with the wave guide will yield the best estimates of wave guide structure. Failure to account for interaction geometry can bias wave guide thickness and velocity contrasts. At the Chile-Peru subduction zone, failure to account for decoupling at bends leads to overestimation of propagation distance in the wave guide of $\sim$ 80 km and subsequently underestimation of

velocity contrasts by up to 5%. Also, deep wave guide observations may be mapped to shallow regions if decoupling at slab bends is not accounted for. Even misinterpretation of the entire observation is possible, e.g. mistaking fast phases refracted at the subducted Moho for part of the dispersed guided wave phase.

5.2 The utility of guided waves for imaging slab low-velocity layering

A several kilometer thick low-velocity channel causes strong seismic guided wave phases that distort P onsets at forearc stations. Observations at the Chile-Peru subduction zone presented here as well as observations at several other circum-pacific subduction zones show such signals. They indicate that the top of the down-going plate remains coherent and a seismically slow layer is located near the slab surface. A host of information on that layer can be extracted from the guided phases if analyzed carefully.

The waveforms of guided waves are composed of the interference of many different components and are sensitive to small changes in the interference conditions. These waveforms potentially allow to resolve small details of structure and source location. However, due to a number of strong tradeoffs between propagation distance along the structure, layer width, velocity contrast, source location and attenuation (Q values), interpretation is not straight forward.

We give an overview of fundamental wave guide parameters in the context of subduction zones. The range of parameters is restricted to values feasible for the subduction zone setting, i.e. layering is assumed to be of less than 10 km width [e.g., *Helffrich*, 1996], possible velocity contrasts are in the range of 0 % to 15 % [*Kirby et al.*, 1996], and propagation distances in the wave guide for up-dip geometries typically range from 0 to 300 km. Quality factors in the low-velocity layer are assumed to be higher than 400. No areas of high attenuation were imaged in

the Chile-Peru, or other subducted slabs [*Hashida*, 1989; *Haberland and Rietbrock*, 2001], and temperatures in the slab are low such that Q values are expected to be comparatively high. We also exclude the possibility that pore fluids cause high attenuation in the subducted plate, since pumping of fluids caused by a seismic wave and subsequent attenuation does not seem plausible at the high confining pressures involved. Therefore the influence of attenuation is neglected, noting that the issue can not ultimately be discussed since Q factors at such small spatial scales can up to now not be resolved. Only Q factors as low as 100 would be low enough to affect guided wave characteristics [*Ben-Zion*, 1998].

A variety of approaches were taken to interpret guided waves [*Hori et al.*, 1985; *Ben-Zion*, 1998; *Lin et al.*, 1999; *Abers*, 2000, 2005]. Varying observation geometries and length scales ask for different suitable methods, ranging from direct interpretation of velocities of second arrivals [*Hori*, 1990], ray-geometrical approaches [*Lin et al.*, 1999], waveform modeling based on analytical solutions for fault zone guided waves [*Ben-Zion et al.*, 1992; *Peng et al.*, 2000] to dispersion analysis for a number of subduction zone wave guides [*Abers*, 2005]. The intensive 2D FD simulations for the Chile-Peru subduction zone wave guide indicate that the frequency spectrum of guided wave onsets is the most significant quantity to infer wave guide parameters and source positioning. Spectra are easy to measure and capture the guided wave effect including possible higher-mode excitation. Body wave contamination is marginal since guided wave energy typically dominates the onsets. On the one hand, peak frequency values of the guided wave fundamental mode are associated with a certain combination/triplet of layer width, velocity contrast, and propagation distance in the wave guide. On the other, the excitation of the guided wave fundamental-mode frequency and higher-mode frequencies is associated with source position and orientation relative to the layer. We will discuss both aspects independently in the following paragraphs.

The issue of foremost importance regarding mineralogical interpretations is the

inference of the coupled parameters velocity contrast and layer width. The effect of these parameters on the peak frequency of the guided wave fundamental mode is illustrated in Figure 5.2 for a typical propagation distance in the wave guide of approximately 110 km. Propagation distance in the range of interest (40 to 160 km) is only weakly linked to the frequency content. However, an upper limit of layer width together with an upper limit of velocity contrast restrict the range of models resulting in a continuous wave train. If the layer width is too big and the velocity contrast too high, the onsets resemble a series of pulses rather than a coherent wave train. For a propagation distance of 110 km, the limits are 10 % low velocity and 4 km width (compare Figure 5.2).

The frequency values presented in Figure 5.2 are independent of source position or orientation provided sources are located close to the layer ($<$ 2 layer widths). Fundamental-mode peak frequencies are stable and only shift slightly ($<$ 0.5 Hz) to lower values for sources outside of the layer (compare chapter 3). Thus, for a given geometry, low-frequency peaks are dependent on layer width and velocity contrasts alone, and inversion regarding these parameters seems feasible.

The second major aspect of information content in guided wave onsets is that of source position and orientation. The tests undertaken corroborate the hypothesis that distorted P onsets with significant low-frequency content can only be caused by sources close to the layer. In the investigated subduction zone setting, DC sources are only capable of exciting guided waves if located inside the LVL or within a distance of roughly two layer widths of the LVL. Within this range of source locations, P onsets vary significantly regarding the ratio of low- to high-frequency energy (see chapter 3). These variations are due to higher-mode excitation causing fast, high-frequency energy to appear in onsets. Due to the directional focus of P and S energy of DC sources, even a small change in source dip or position can cause profound changes in interference patterns and subsequently in the amount of high-frequency energy present in the onsets. The relative amount of high- and low-

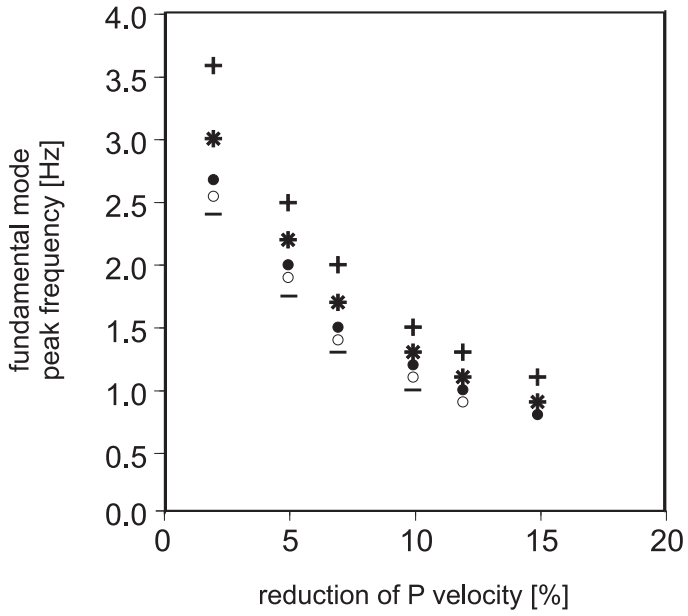

Figure 5.2: Guided wave peak frequencies and interdependencies of velocity contrast and layer width. The seismic explosion source is centered in the layer at 200 km depth. Layer widths are 2.0 km (cross), 2.5 km (asterisk), 3.0 km (solid circle), 3.5 km (open circle) and 4.0 km (dash). Wave guides of width $\geq$ 4 km do not cause frequency distortion for the given propagation distance and velocity contrasts $>$ 10 %.

frequency energy potentially serves to discriminate source locations and orientation. Provided source mechanisms are known exactly, source position can be derived at sub-kilometer scale.

First inferences based on intensive simulations using DC sources are made assuming that the majority of source mechanisms of intermediate depth seismicity are down-dip extensional [*Rudloff*, 1998]. The simulated frequencies for this class of events indicate, that sources situated above the low-velocity layer produce large amounts of high-frequency higher-mode energy and thus do not match the observations. The same is the case for sources located very close to the subducted oceanic Moho. Only sources in the center of, or slightly below the layer show clear low-frequency onsets.

Finally, the simulations of the foregoing chapters also point to complications to be taken into account when interpreting guided waves at subduction zones. Higher-

mode high-frequency effects make the interpretation of guided wave onsets more complicated than was assumed by studies looking at fundamental-mode dispersion only [e.g., *Ben-Zion*, 1998; *Abers*, 2000], particularly when DC sources are taken into account. We conclude that the normal dispersion of guided wave onsets may be contaminated by high-frequency energy of guided wave higher modes rendering dispersion analysis unreliable. The dispersive character of guided waves can provide unique and independent information on velocity contrasts and layer width. At the moment, however, we are not aware of a feasible technique to measure dispersion in such a complex wave field including higher-mode excitation. Analysis based on frequency peaks in spectra of first onsets seems at this stage of research a simple and powerful method to infer constraints on subduction zone wave guides.

5.3 On P and S guided waves at subduction zones

The topics discussed in the above sections are equally relevant for P and S guided waves. In fact, studies at fault zones have widely employed and modeled S guided waves [*Ben-Zion and Aki*, 1990; *Li et al.*, 1990; *Li and Leary*, 1990]. Most observations in the context of subduction zones, however, are based on P guided phases, combined P and S wave measurements were conducted only recently [*Abers*, 2000, 2005].

Wave guide geometry and dependencies on wave guide parameters are similar for S and P guided waves. Subduction zone wave guides potentially cause distorted S waves at the same surface region where distorted P onsets are observed. Moreover S guided wave amplitudes are up to 5 times higher than P guided wave amplitudes because leakage due to P-S conversion does not apply. Wave guide parameters, such as width of the wave guide and contrast in S velocities can be inferred in a similar manner as for P waves, however, peak frequencies are shifted to lower values.

The issue of excitation of guided waves by DC sources points to one important distinction between the observation of P and S guided waves: Sources that result in

high levels of P guided energy produce only small amounts of S guided energy and vice versa.

Source orientation does play a major role in excitation of guided waves and simulations show the exact opposite correlation of source orientation and guided wave excitation for P and S waves. E.g., down-dip extensional sources situated slightly below the oceanic Moho are better suited to inject P wave energy into the LVL than S wave energy. Thus P and S guided wave observations differ in intensity and pulse shapes even for identical source-receiver geometries and source mechanisms. Since slabs at intermediate depth are usually in down-dip extension [*Chen et al.*, 2004], source mechanisms are more favorable for the excitation of P guided waves than S guided waves. The combined analysis of S and P guided waves can provide valuable information on Poisson's ratios in the wave guide and thus constrain the type of mineral assemblage in the LVL.

5.4 Evaluating guided wave observations at circum-pacific subduction zones

Since the pioneering studies on subduction of oceanic crust [*Fukao et al.*, 1983; *Matsuzawa et al.*, 1986], more and more seismological data was gathered on slab structure of circum-pacific subduction zones [e.g., *Iidaka and Obara*, 1993; *Gubbins et al.*, 1994; *Abers and Sarker*, 1996; *Oda and Douzen*, 2001; *Martin et al.*, 2003]. Many of the studies are based on guided wave analysis and the presented simulations permit to set a number of these observations in perspective.

The majority of early observations stem from shallow sources and thus rather shallow wave guides (depth < 60 km) [*Fukao et al.*, 1983; *Oda et al.*, 1990; *Hori*, 1990]. The observations are often described as consisting of two distinct phases rather than one dispersed wave. More studies dealing with sources located deeper in the subducted slab followed and many of them report on dispersive guided waves

[e.g., *Abers and Sarker*, 1996; *Abers*, 2000; *Abers et al.*, 2003; *Martin et al.*, 2003; *Abers*, 2005]. The propagation distances and inferred widths of the wave guides for depth less than 60 km are not sufficient for the waves to form dispersive onsets and two separate phases are observed. The second arrivals are attributed to a direct or critically reflected wave propagating in the subducted crust, whereas the first phase is regarded as a direct or refracted wave traveling in the fast mantle [*Fukao et al.*, 1983; *Hori*, 1990]. Dispersion is only observed where propagation distances in the layer are long and the widths of these low-velocity layers are generally thinner than the 8 km proposed for subducted crust. The interference pattern forming a guided wave can then fully develop and continuous dispersion in the time series can be observed [e.g., *Martin et al.*, 2003].

A recent study of *Abers* [2005] distinguishes between different slab segments located at different depth. This was long due because there is evidence that the wave guide is not constituted by one and the same structure at different depth [*Tatsumi et al.*, 1994; *Hacker et al.*, 2003a, b]. In fact, shallow wave guide studies most likely imaging intact subducted crust are to be separated from observations of deep wave guides that probably consist of a fragment of the crust or a different layer entirely.

Subsuming the studies regarding the structure of the upper slab region at circum-pacific subduction zones, a comparatively consistent picture arises. Mode-converted, reflected, and dispersed body wave phases have shown that the upper few kilometers of subducted slabs contain sharp interfaces or layering [e.g., *Helffrich and Stein*, 1993; *Gubbins et al.*, 1994; *Helffrich*, 1996; *Yuan et al.*, 2000]. Results for wave guide parameters vary between 2 to 8 km for thickness and 3 % to 15 % for velocity contrasts. Velocity contrasts and layer widths are always reported to be largest for shallow depths. The depth extent of low-velocity layers for different subduction zones varies, but a minimum depth of 140 km has been inferred at eight different circum-pacific slabs.

We conclude with comments on two exceptions in the work published on subducted oceanic crust so far. Both are to be reconceived against the background of this study. Exception one is the Tonga-Kermadec subduction zone, where a layer of high velocity, as opposed to reduced velocity, at the top of the slab is predicted [*Gubbins and Snieder*, 1991; *Gubbins et al.*, 1994]. The second is the Nicaragua slab which was only recently investigated [*Abers et al.*, 2003]. It exposes large lag times in guided wave observations (approximately 1.5 times higher than at other subduction zones) and is therefore predicted to feature a layer of extremely low velocity.

The main difference in the setting at the Tonga-Kermadec subduction zone is the much larger propagation distance of the signals (several times larger than those at other slabs [*Gubbins et al.*, 1994]). Very long propagation distances in a slow layer of appropriate width and velocity contrast atop the slab would result in very low fundamental-mode frequencies (< 1 Hz). Subsequently, higher-mode frequencies are already present near 3 Hz (compare to 6 Hz at the Chile-Peru slab). The inference of a high-velocity layer at Tonga-Kermadec causing anormal dispersion in *Gubbins and Snieder* [1991] is based on dispersion analysis from 1.0 Hz to 6.0 Hz. We call attention to the possibility that the lowest frequencies of the fundamental mode are cut off due to processing, i.e. original normal dispersion including higher modes may be masked due to band passing. Careful analysis of new broad-band data should be carried out to survey, if fast arriving low-frequency energy (< 1 Hz) is present in the data. This could lead to a unified interpretation of subduction zone wave guides worldwide.

The simulations and data of the Chile-Peru slab also give cause to a critical view of recent results at the Nicaragua slab [*Abers et al.*, 2003]. Based on extreme time delays observed between low- and high-frequency arrivals, a rather high velocity contrast was deduced for the Nicaragua slab. However, failure to account for the exact position of the recording station possibly resulted in a misinterpretation of two separate phases as one dispersed phase leading to oversimplified deductions.

The concerns are based on simulations for the Chile-Peru study that can easily be transferred to the Nicaragua subduction zone. At the Chile-Peru slab, stations AER and BOS (separated by less than 1.5°) expose variations in time delay of low- and high-frequency arrivals of up to 2 seconds for one and the same event. Clearly, dispersion analysis of each station would give different results. The key to understanding this discrepancy is the exact position of the station relative to the slab. At the location of station BOS, guided waves are preceded by a fast refracted wave traveling at slab velocities, whereas at AER the onset is formed solely by the dispersive guided wave. Simulations confirm that station AER is due to fortunate coincidence located ideally to register guided wave first onsets for the events used.

Since only one station is presented in the study of the Nicaragua slab we pose the question, if this station may not be located in such a fortunate way. Thus, the first break could actually be formed by a fast wave refracted at the subducted Moho similar to those at station BOS at the Chile-Peru subduction zone. The observation that onsets sometimes resemble two phases and measured time delay of high-frequency phases is larger than at other slabs for comparable distances [*Abers et al.*, 2003] supports this hypothesis.

Reinterpreting the data published so far and excluding the Tonga-Kermadec subduction zone which has to be revisited, we see a concise picture causing the following effects at eight circum-pacific subduction zones: 1) Fast refracted or direct phases can be observed at stations above the slab. These phases reflect the rise in seismic velocities caused by the fast, cool slab. 2) Seismic energy of intraslab events located near the slab surface is trapped in a low-velocity layer at the top of the slab. If conditions are favorable, frequency distortion and comparably high amplitudes due to energy entrapment are created. Dependent on receiver location, the dispersive guided wave may form the P onset but is likely preceded by a faster phase traversing the slab.

5.5 Mineralogical inferences for the Chile-Peru subduction zone

The results of chapters 2 and 3 put a number of constraints on the mineralogical evolution with depth of the Chile-Peru subduction zone near 21°S. Above all, a layered structure persists at the top of the subducted plate to depths in excess of 160 km. The wave guide is imaged at depths of 100 km to 250 km, we are thus investigating a deep wave guide. The observed guided waves stem from a comparatively thin layer and velocity contrasts are in the range of 7 %. Tradeoffs in velocity contrasts and widths allow for variation in these two parameters, but an upper limit of 3 km for layer width can reliably be inferred from simulations. We also deduce that sources are located inside the layer or at least not further than 6 km below it.

Helffrich et al. [1989] showed that neither temperature nor bulk-compositional difference alone or in combination can generate velocity contrasts as large as those observed. Thus mineralogical changes appear to dominate velocity contrasts and layering near the slab surface. The above findings put narrow limits on possible mineralogical-petrological interpretations of the LVL at the Chile-Peru subduction zone. The possibility of intact subducted gabbroic crust ($\sim$ 8 km thick) causing the guided wave effect is immediately excluded. A layer of this thickness does not produce any effect of comparable quality for the propagation distances involved. Moreover, the guided wave signals are linked to the deep wave guide structure and the majority of mineralogical models predict oceanic crust at least to be altered at that depth [*Kirby et al.*, 1996]. The possibility of a completely eclogized layer (oceanic crust after gabbro-eclogite transition) causing the effect is excluded for an equally straight forward reason: The velocity of eclogite is at least equal to anhydrous mantle peridotite [*Gubbins et al.*, 1994], i.e. non of the multitude of observed reflected, converted and guided phases could be explained.

At present there are a number of other candidate explanations for the deep wave guide structure suggested by e.g., *Helffrich et al.* [1989], *Helffrich* [1996], *Peacock* [2001], and *Hacker et al.* [2003a, b]. Namely three phenomena that facilitate low seismic velocities near the slab surface are currently in focus of debates. 1) Serpentinized mantle located above the slab surface or below the subducted Moho (serpentinite hypothesis), 2) hydrous phases in the subducted crust at great depth causing the low velocities (HCrust hypothesis), or 3) dry gabbroic crust persisting metastably to depth because the gabbro-eclogite transformation is hindered (DCrust hypothesis).

We first compare the Serpentinite hypothesis with our inferences. The layer velocity derived is compatible with the hydrous mineral assemblages and the simulations put restrictions on the location of the layer. Hydrous phases can potentially be situated in a layer of serpentinized upper mantle within the plate [*Peacock*, 2001; *Rüpke et al.*, 2002; *Ranero et al.*, 2003] or hydrated mantle immediately above the down-going crust [*Tatsumi*, 1986; *Davies and Stevenson*, 1992; *Tatsumi et al.*, 1994]. To conform with our results, the serpentinized layer can only be situated in the slab mantle. Serpentinized continental mantle above the slab surface would be too far offset ($\sim$ 10 km) in respect to earthquake sources located beneath the subducted Moho to inject sufficient energy for guided wave excitation [*Rietbrock and Waldhauser*, 2004]. The proposition by *Ranero et al.* [2003] of a layer of serpentinized slab mantle located directly beneath the subducted Moho carrying low velocities does not disagree with the findings for the Chile-Peru slab. There is, however, no evidence for the zone of serpentinization to form a continuous or at least clearly defined layer at all.

The HCrust hypothesis predicts that the LVL is formed by the subducted oceanic crust and constituted of hydrous metabasalt facies present in the subducted crust at depth [*Peacock*, 1993; *Helffrich and Abers*, 1997]. The results at the Chile-Peru slab contradict the HCrust hypothesis, since the layer width of 2 - 3 km deduced at

the Chile-Peru subduction zone is much smaller than the typical 8 km thick oceanic crust. Even though the velocity contrasts for HCrust (7 % slow to surrounding mantle [*Helffrich*, 1996]) are in accordance with our results, we conclude, that the deep wave guide in Chile-Peru (depth $>$ 100 km) cannot be explained by hydrous oceanic crust.

A refinement of the third hypothesis, the DCrust hypothesis is favored among the mineralogical explanations of the Chile-Peru data. It assumes that anhydrous gabbroic crust exists metastably to great depth [*Hacker et al.*, 2003a]. The model includes different evolutions for upper and lower crust, suggesting that only within the lower crust are conditions sufficiently dry for metastable gabbro to prevail and that the gabbro-eclogite transition is triggered at shallow depth but completes only partially until beyond the volcanic arc. This hypotheses predicts a partially eclogized layer of 2 to 4 km width (the lower crust) carrying reduced velocities dependent on the degree of eclogitization. Our tests show comparable velocity contrasts and the restriction of the wave guide to the lower crust explains the comparatively thin layer detected at the Chile-Peru slab. In accordance with simulations, sources are expected to be located within or closely below the layer.

If metastable gabbro causes the low velocities, it is likely that the sluggish transformation produces patches of gabbro surrounded by eclogite resulting in an inhomogeneous velocity distribution in the layer. Would this undermine the wave guide effect? Remarkably, tests conducted in chapter 3 regarding velocity undulations show that changes of +/- 5 % in an averagely 7 % slow layer do not cause noteworthy effects on the guided wave propagation.

The kinetically hindered anhydrous gabbro-eclogite transformation is therefore a likely explanation of the guided wave effect observed in the Chile-Peru subduction zone. The percentage of eclogitization could then be measured directly in terms of guided wave peak frequency. A completely gabbroic layer would result in 15 % low velocity, the 7 % slow layer in Chile-Peru points to partial eclogitization of 40 % at

the most.

5.6 Outlook

At the present stage of research, a number of possibilities regarding the deep wave guide at the Chile-Peru subduction zone are already excluded, such as serpentinization of mantle rock above the slab, as well as any very thin (sediment) layer, or thick (> 3 km) layer causing the effect. Ultimately we aim to distinguish between the serpentinite hypothesis and DCrust hypothesis (both could form a layer of ~ 2 km thickness). Modeling of P and S guided waves would allow to place constraints on the Poisson's ratio of the material in the layer and thus the discrimination of serpentinite carrying unusually high Poisson's ratios.

To put tighter limits on layer width and percentage of velocity reduction in a realistic slab section using the frequency method, we will conduct tests using velocity models derived from petrological-mineralogical models calculated for the Chile-Peru slab. In addition, taking advantage of the extensive station coverage at the Chile-Peru slab, we also seek to deploy P wave data collected at further stations above the slab (see stations in Figure 1.3). Combined interpretation of frequency content, pulse shapes and time delays at each station will allow to eliminate tradeoffs associated with guided wave interpretation and to derive layer velocity, layer width and source position independently.

Finally, more detailed information on event locations (obtained by relative relocalization) can be incorporated in simulations. This would allow to confirm the connection of high-frequency effects seen in the data with source position relative to the wave guide. Strong constraints on source position are the key, not only to gain knowledge on the guided wave effect in subduction zones, but also to test, whether the mechanism of dehydration embrittlement is suited to ultimately explain intermediate depth seismicity.

Acknowledgements

First and foremost I would like to express my gratitude to Dr. Andreas Rietbrock - secret supervisor of this PhD project - for putting so much energy in this work and providing assistance not only regarding scientific issues but also many other career-related aspects of my life!

I am grateful to Prof. Frank Scherbaum for his supervision and the opportunity to undertake this PhD project at the University of Potsdam. I thank Dr. Christian Haberland and Dr. Frank Krüger for fruitful discussions and great contributions to this work. Furthermore thanks are due to Prof. Nick Kusznir for providing the opportunity to research at the great Department of Earth Sciences of Liverpool University.

As always, everything is possible with the support of my family.

Bibliography

Abers, G. A., Hydrated subducted crust at 100-250 km depth, *Earth Planet. Sci. Lett.*, *176*, 2000, doi:10.1029/2002GL015649.

Abers, G. A., Seismic low-velocity layer at the top of subducting slabs: observations, predictions, and systematics, *Phys. Earth Planet. Inter.*, *149*, 7–29, 2005.

Abers, G. A., and R. Sarker, Dispersion of regional body waves at 100-150 km depth beneath Alaska: In situ constraints on metamorphism of subducted crust, *Geophys. Res. Lett.*, *23*, 1171–1174, 1996.

Abers, G. A., T. Plank, and B. R. Hacker, The wet Nicaraguan slab, *Geophys. Res. Lett.*, *30*, 323–330, 2003.

Ahrens, T. J., and G. Schubert, Gabbro-eclogite reaction rate and its geophysical significance, *Rev. Geophys.*, *13*, 383–400, 1975.

Amundsen, L., and A. Reitan, The relationship between 2-D and 3-D wave propagation, *64th Annual Internat. Mtg., Soc, Expl. Geophys., Expanded Abstracts*, *94*, 1378–1381, 1994.

ANCORP Working Group, Seismic reflection image revealing offset of Andean subduction-zone earthquake locations into oceanic mantle, *Nature*, *397*, 341–344, 1999.

Ansell, J. H., and D. Gubbins, Anomalous high-frequency wave propagation from the Tonga-Kermadec seismic zone to New Zealand, *Geophys. J. R. Astron. Soc.*, *85*, 93–106, 1986.

Barazangi, M. B., B. Isacks, and J. Oliver, Propagation of seismic waves through and beneath the lithosphere that descends under the Tonga island arc, *J. Geophys. Res.*, *77*, 952–958, 1972.

Ben-Zion, Y., Properties of seismic fault zone waves and their utility for imaging low velocity structures, *J. Geophys. Res.*, *103*, 12,567–12,585, 1998.

Ben-Zion, Y., and K. Aki, Seismic radiation from an *SH* line source in a laterally heterogeneous planar fault zone, *Bull. Seismol. Soc. Am.*, *80*, 971–994, 1990.

Ben-Zion, Y., S. Katz, and P. Leary, Joint inversion of fault zone head waves and direct p arrivals for crustal structure near major faults, *J. Geophys. Res.*, *97*, 1943–1951, 1992.

Ben-Zion, Y., Z. Peng, D. Okaya, L. Seeber, J. G. Armbruster, N. Ozer, A. J. Michael, S. Baris, and M. Aktar, A shallow fault zone structure illuminated by trapped waves in the Karadere-Duzca branch of the North Anatolian Fault, western Turkey, *Geophys. J. Int.*, *152*, 699–717, 2003.

Bock, G., B. Schurr, and G. Asch, High-resolution image of the oceanic Moho in the subducting Nazca plate from P-S converted waves, *Geophys. Res. Lett.*, *27*, 3929–3932, 2000.

Bostock, M. G., R. Hyndman, S. Rondenay, and S. M. Peacock, An inverted continental Moho and serpentinization of the forearc mantle, *Nature*, *417*, 2002.

Brocher, T. M., T. Parsons, A. M. Trehu, C. M. Snelson, and M. A. Fischer, Seismic evidence for widespread serpentinized forearc upper mantle along the Cascadia margin, *Geology*, *31*, 2003.

Brune, J. N., Tectonic stress and the spectra of seismic shear waves from earthquakes, *J. Geophys. Res.*, *75*, 1970.

Brune, J. N., Correction, *J. Geophys. Res.*, *76*, 1971.

Carcione, J. M., Seismic modelling in viscoelastic media, *Geophysics*, *581*, 1993.

Cassidy, J. F., and F. Waldhauser, Evidence for both crustal and mantle earthquakes in the subducting Juan de Fuca plate, *Geophys. Res. Lett.*, *30*, 1095, 2003, doi:10.1029/2002GL015511.

Chen, P., C. R. Bina, and E. A. Okal, A global survey of stress orientations in subducting slabs as revealed by intermediate-depth earthquakes, *Geophys. J. Int.*, *159*, 721–733, 2004.

Christensen, D. H., and L. Ruff, seismic coupling and outer rise earthquakes, *J. Geophys. Res.*, *93*, 13,421–13,444, 1988.

Coutant, O., J. Virieux, and A. Zollo, Numerical source implementation in a 2D finite difference scheme for wave propagation, *Bull. Seismol. Soc. Am.*, *85*, 1507–1512, 1995.

Davies, D., and D. P. McKenzie, Seismic travel-time residuals and plates, *Geophys. J. R. Astron. Soc.*, *18*, 51–63, 1969.

Davies, H., The role of hydraulic fractures and intermediate-depth earthquakes in generating subduction zone magmatism, *Nature*, *398*, 142–145, 1999.

Davies, J., and D. Stevenson, Physical model of source region of subduction zone volcanics, *J. Geophys. Res.*, *97*, 2037–2070, 1992.

DeMets, C., R. Gordon, D. Argus, and S. Stein, Current plate motions, *Geophys. J. Int.*, *101*, 425–478, 1990.

England, P., R. Engdahl, and W. Thatcher, Systematic variation in the depth of slabs beneath arc volcanoes, *Geophys. J. Int.*, *156*, 377–408, 2004, doi:10.1111/j.1365-246X.2003.02132.x.

Fohrmann, M., H. Igel, G. Jahnke, and Y. Ben-Zion, Guided waves from sources outside faults: An indication for shallow fault zone structure?, *Pure and Applied Geophysics*, *161*, 2125–2137, 2004.

Fuchs, K., and G. Müller, Computation of synthetic seismograms with the reflectivity method and comparison with observations, *Geophys. J. R. Astron. Soc.*, *23*, 417–433, 1971.

Fukao, Y., K. Kanjo, and I. Nakamura, Deep seismic zone as an upper mantle reflector of body waves, *Nature*, *272*, 606–608, 1978.

Fukao, Y., S. Hori, and M. Ukawa, A seismological constraint on the depth of basalt-eclogite transition in a subducting oceanic crust, *Nature*, *303*, 413–415, 1983.

Graeber, F. M., Seismische Geschwindigkeiten und Hypozentren in den Südlichen Zentralen Anden aus der simultanen Inversion von Laufzeitdaten des seismologischen Experiments PISCO '94 in Nordchile, Ph.D. thesis, GeoForschungszentrum Potsdam, 1997.

Graeber, F. M., and G. Asch, Three-dimensional models of P wave velocity and P-to-S velocity ratio in the southern central Andes by simultaneous inversion of local earthquake data, *J. Geophys. Res.*, *104*, 20,237–20,256, 1999.

Gubbins, D., and R. Snieder, Dispersion of p-waves in subducted lithosphere: evidence for an eclogite layer, *J. Geophys. Res.*, *96*, 6321–6333, 1991.

Gubbins, D., A. Barnicoat, and J. Cann, Seismological constraints on the gabbro-eclogite transition in subducted oceanic crust, *Earth Planet. Sci. Lett.*, *122*, 89–101, 1994.

Gudmundsson, O., and M. Sambridge, A regionalized upper mantle (rum) seismic model, *J. Geophys. Res.*, *103*, 7121–7136, 1998.

Haberland, C., and A. Rietbrock, Attenuation tomography in the Western Central Andes: A detailed insight into the structure of a magmatic arc, *J. Geophys. Res.*, *106*, 11,151–11,167, 2001.

Haberland, C., A. Agnon, R. El-Kelani, N. Maercklin, I. Qabbani, G. Ruempker, T. Ryberg, F. Scherbaum, and M. Weber, Modelling of seismic guided waves at the Dead Sea Transform, *J. Geophys. Res.*, *108*, 2003, doi:10.1029/2002JB002309.

Hacker, B. R., S. M. Peacock, G. A. Abers, and S. D. Holloway, Subduction factory, 1, Theoretical mineralogy, densities, seismic wave speeds and H_20 contents, *J. Geophys. Res.*, *108(B1)*, 2003a, doi:10.1029/2001JB001127.

Hacker, B. R., S. M. Peacock, G. A. Abers, and S. D. Holloway, Subduction factory, 2, Are intermediate-depth earthquakes in subducting slabs linked to metamorphic dehydration reactions?, *J. Geophys. Res.*, *108(B1)*, 2003b, doi:10.1029/2001JB001129.

Hashida, T., 3-Dimensional seismic attenuation structure beneath the Japanese islands and its tectonic and thermal implications, *Tectonophysics*, *159*, 163–180, 1989.

Helffrich, G., Subducted lithospheric Slab Velocity Structure: Observations and Mineralogical Inferences, in *Subduction Top to Bottom*, edited by G. E. Bebout, D. W. Scholl, S. H. Kirby, and J. P. Platt, Geophysical Monograph 96, pp. 215 – 222, The AGU Books Board, 1996.

Helffrich, G., and G. A. Abers, Slab low-velocity layer in the eastern Aleutian subduction zone, *Geophys. J. Int.*, *130*, 640–648, 1997.

Helffrich, G., S. Stein, and B. J. Wood, Subduction zone thermal structure and mineralogy and their relationship to seismic wave reflections and conversions at the slab/mantle interface, *J. Geophys. Res.*, *94*, 753–763, 1989.

Helffrich, G. R., and S. Stein, Study of the structure of the slab mantle interface using reflected and converted seismic waves, *Geophys. J. Int.*, *115*, 15–40, 1993.

Hori, S., Seismic waves guided by untransformed oceanic crust subducting into the mantle: The case of the Kanto district, central Japan, *Tectonophysics*, *176*, 355–376, 1990.

Hori, S., H. Inoue, Y. Fukao, and M. Ukawa, Seismic detection of the untransformed basaltic oceanic crust subducting into the mantle, *Geophys. J. R. Astron. Soc.*, *83*, 169–197, 1985.

Hough, S. E., Y. Ben-Zion, and P. C. Leary, Fault-zone waves observed at the southern Joshua Tree earthquake rupture zone, *Bull. Seismol. Soc. Am.*, *84*, 761–767, 1994.

Hurukawa, N., and M. Imoto, Subducting oceanic crusts of the Phillipine Sea and Pacific Plates, *Geophys. J. Int.*, *109*, 693–652, 1992.

Husen, S., E. Kissling, E. Flueh, and G. Asch, Accurate hypocenter determination in the seismogenic zone of the subducting Nazca plate in Northern Chile using a combined on-/offshore network, *Geophys. J. Int.*, *138*, 687–701, 1999.

Igel, H., Y. Ben-Zion, and P. C. Leary, Simulation of $SH-$ and P-SV-wave propagation in fault zones, *Geophys. J. Int.*, *128*, 533–546, 1997.

Igel, H., T. Nissen-Meyer, and G. Jahnke, Wavepropagation in 3D spherical sections: effects of subduction zones, *Phys. Earth Planet. Inter.*, *132*, 219–234, 2002.

Iidaka, T., and K. Obara, The upper boundary of the subducting Pacific plate estimated from ScSp waves beneath the Kanto region, *Japan, J. Phys. Earth*, *41*, 103–108, 1993.

Jahnke, G., H. Igel, and Z. Ben-Zion, Three-dimensional calculations of fault-zone-guided waves in various irregular structures, *Geophys. J. Int.*, *151*, 416–426, 2002.

Kennett, B. L. N., and E. R. Engdahl, Traveltimes for global earthquake location and phase identification, *Geophys. J. Int.*, *105*, 429–465, 1991.

Kirby, S., E. R. Engdahl, and R. Denlinger, Intermediate-depth intraslab earthquakes and arc volcanism as physical expressions of crustal and uppermost mantle metamorphism in subducting slabs, in *Subduction Top to Bottom*, edited by G. E. Bebout, D. W. Scholl, S. H. Kirby, and J. P. Platt, Geophysical Monograph 96, pp. 195 – 214, The AGU Books Board, 1996.

Lay, T., and T. C. Wallace, *Modern Global Seismology*, Academic Press, London, 1995.

Lessel, K., Die Krustenstruktur der zentralen Anden in Nordchile (21-24°S), abgeleitet aus 3D-Modellierungen refraktionsseismischer Daten, Ph.D. thesis, Freie Universität Berlin, 1997.

Levander, A. R., Fourth order finite difference P-SV-seismograms, *Geophysics*, *53*, 1425–1436, 1988.

Li, Y.-G., and P. C. Leary, Fault zone trapped waves, *Bull. Seismol. Soc. Am.*, *80*, 1245–1271, 1990.

Li, Y.-G., and J. E. Vidale, Low-velocity fault-zone guided waves: Numerical investigations of trapping efficiency, *Bull. Seismol. Soc. Am.*, *86*, 371–378, 1996.

Li, Y.-G., P. Leary, K. Aki, and P. Malin, Seismic trapped modes in the Oroville and San Andreas fault zones, *Science*, *249*, 763–766, 1990.

Lin, C. H., B. S. Huang, and R. J. Rau, Seismological evidence for a low-velocity layer within the subducted slab of southern Taiwan, *Earth Planet. Sci. Lett.*, *174*, 231–240, 1999.

Martin, S., and A. Rietbrock, Guided waves at subduction zones: Dependencies on slab geometry, receiver locations and earthquake sources, *Geophys. J. Int.*, 2004, submitted.

Martin, S., A. Rietbrock, C. Haberland, and G. Asch, Guided waves propagating in subducted oceanic crust, *J. Geophys. Res.*, *108*, 2003, doi:10.1029/2004GL019610.

Martin, S., C. Haberland, and A. Rietbrock, Forearc decoupling of guided waves in the Chile-Peru subduction zone, *Geophys. Res. Lett.*, 2005, to be submitted.

Matsuzawa, T., N. Umino, A. Hasegawa, and A. Takagi, Upper mantle velocity structure estimated from PS-converted wave beneath the north-eastern Japan Arc, *Geophys. J. R. Astron. Soc.*, *86*, 767–787, 1986.

Matsuzawa, T., N. Umino, A. Hasegawa, and A. Takagi, Estimation of thickness of a low-velocity layer at the surface of the descending oceanic plate beneath the north-eastern Japan arc by using synthesized PS-wave, *Thoku Geophys. J.*, *31*, 19–28, 1987.

Meade, C., and R. Jeanloz, Deep-focus earthquakes and recycling of water into the earth's mantle, *Science*, *252*, 68–71, 1991.

Michael, A. J., and Y. Ben-Zion, Inverting fault zone trapped waves with genetic algorithms, *EOS Trans. AGU*, *79*, S11C–16, 1998.

Mitronovas, W., B. L. Isacks, C. Meade, and R. Jeanloz, Seismic velocity anomalies in the upper mantle beneath the Tonga-Kermadec island arc, *J. Geophys. Res.*, *76*, 7154–7180, 1971.

Oda, H., and T. Douzen, New evidence for a low-velocity layer on the subducting Phillipine Sea plate in southwest Japan, *Tectonophysics*, *332*, 347–358, 2001.

Oda, H., T. Tanaka, and K. Seya, Subducting oceanic crust on the Philippine sea plate in southwest Japan, *Tectonophysics*, *172*, 175–189, 1990.

Patzwahl, R., Plattengeometrie und Krustenstruktur am Kontinentalrand Nord-Chiles aus weitwinkelseismischen Messungen, Ph.D. thesis, Freie Universität Berlin, 1998.

Patzwahl, R., J. Mechie, A. Schulze, and P. Giese, 2-D-velocity models of the Nazca plate subduction zone between 19.5°S and 25°S from wide-angle seismic measurements during the CINCA 95 project, *J. Geophys. Res.*, *104*, 7293–7317, 1999.

Peacock, S. M., The importance of blueshist - eclogite dehydration in subducting oceanic crust, *Geol. Soc. Am. Bull.*, *105*, 684–694, 1993.

Peacock, S. M., Thermal and Petrological Structure of Subduction Zones, in *Subduction Top to Bottom*, edited by G. E. Bebout, D. W. Scholl, S. H. Kirby, and J. P. Platt, Geophysical Monograph 96, pp. 119 – 133, The AGU Books Board, 1996.

Peacock, S. M., Are the lower planes of double seismic zones caused by serpentine dehydration in subducting oceanic mantle?, *Geology*, *29*, 293–302, 2001.

Peng, Z., Y. Ben-Zion, and A. Michael, Quantitative inversion of seismic fault zone waveforms in the rupture zone of the 1992 Landers earthquake for structural properties at depth, *EOS Trans. AGU*, *82*, S32E–09, 2000.

Randal, C. J., Absorbing boundary condition for the elastic wave equation: velocity stress formulation, *Geophysics*, *54*, 1141–1152, 1989.

Ranero, C., P. Morgan, K. Mcintosh, and C. Reichert, Bending-related faulting and mantle serpentinization at the Middle America trench, *Nature*, *425*, 367–373, 2003.

Reasenberg, P. A., and D. Oppenheimer, Fpfit, fpplot, and fppage: Fortran computer programs for calculating and displaying earthquake fault-plane solutions, *Open-File Rep. 85-739*, U.S. Geol. Surv., 1985.

Rietbrock, A., and C. Haberland, ANCORP'96: Das passive seismologische Experiment, in *Berichtsband für die Jahre 1996 bis 1998*, pp. 470 – 479, Sonderforschungsbereich 267: Deformationsprozesse in den Anden, 1998.

Rietbrock, A., and F. Waldhauser, A narrowly spaced double-seismic zone in the subducting Nazca plate, *Geophys. Res. Lett.*, *31*, 2004, doi:10.1029/2004GL019610.

Rietbrock, A., G. Asch, G. Chong, and P. Giese, ANCORP '96 - seismicity along the ANCORP traverse in northern Chile, *AGU*, 1997.

Ringwood, A. E., Phase transformations and mantle dynamics, *Earth Planet. Sci. Lett.*, *14*, 233–241, 1972.

Rudloff, A., Bestimmung von Herdflächenlösungen und detaillierte Spannungsinversion aus ausgewählten Ereignissen des seismologischen Netzes PISCO '94 (Nord-Chile), *Sci. Tech. Rep. STR98/01*, GeoForschungsZentr. Potsdam, Potsdam, Germany, 1998.

Rüpke, L. H., J. Phipps-Morgan, M. Hort, and J. A. D. Connolly, Are the regional variations in Central American arc lavas due to differing basaltic versus peridotitic slab sources of fluids?, *Geology*, *30*, 1035–1038, 2002.

Schmidt, M. W., and S. Poli, Experimentally based water budgets for dehydrating slabs and consequences for arc magma generation, *Earth Planet. Sci. Lett.*, *163*, 361–379, 1998.

Schmitz, M., et al., The crustal structure beneath the central Andean forearc and magmatic arc derived from seismic studies - the PISCO 94 experiment in northern Chile (21°-23° s), *J. South Am. Earth Sci*, *12*, 237–260, 1999.

Schurr, B., G. Asch, A. Rietbrock, R. Trumbull, and C. Haberland, Complex patterns of fluid and melt transport in the central Andean subduction zone revealed by attenuation tomography, *Earth Planet. Sci. Lett.*, *215*, 105–119, 2003.

Seno, T., and Y. Yamanaka, Double seismic zones, compressional deep trench-outer rise events, and superplumes, in *Subduction Top to Bottom*, edited by G. E. Bebout, D. W. Scholl, S. H. Kirby, and J. P. Platt, Geophysical Monograph 96, pp. 347–355, The AGU Books Board, 1996.

Snoke, J. A., I. S. Sacks, and H. Okada, Determination of the subducting lithosphere boundary by use of converted phases, *Bull. Seismol. Soc. Am.*, *67*, 1051–1060, 1978.

Tatsumi, Y., Formation of the volcanic front in subduction zones, *Geophys. Res. Lett.*, *13*, 717–720, 1986.

Tatsumi, Y., K. Ito, and A. Goto, Elastic wave velocities in isochemical granulite and amphibolite: Origin of a low-velocity layer at the slab/mantle wedge interface, *Geophys. Res. Lett.*, *21*, 17–20, 1994.

Tessmer, E., and D. Kosloff, 3-D elastic modeling with surface topography by a Chebychev spectral method, *Geophysics*, *59*, 464–373, 1994.

Van der Hilst, R., and R. Snieder, High-frequency precursors to P wave arrivals in New Zealand: implications for slab structure, *J. Geophys. Res.*, *101*, 8473–8488, 1996.

Virieux, J., SH-wave propagation in heterogeneous media: velocity stress finite difference method, *Geophysics*, *49*, 1933–1957, 1984.

Virieux, J., P-SV-wave propagation in heterogeneous media: velocity stress finite difference method, *Geophysics*, *51*, 889–901, 1986.

Wang, R., A new wavenumber integration algorithm for synthesizing high-precision seismograms, *Geophys. J. Int.*, *129*, 345–356, 1997.

Wang, R., A simple orthonormalization method for stable and efficient computation of Green's functions, *Bull. Seismol. Soc. Am.*, *89*, 733–741, 1999.

Yuan, X., S. V. Sobolev, R. Kind, O. Oncken, and Andes Seismology Group, Subduction and collision processes in the Central Andes constrained by converted seismic phases, *Nature*, *408*, 958–961, 2000.